

**EXPERIMENTAL STUDY OF THE BEHAVIOR OF
FIBER REINFORCED POLYMER DECK SYSTEM**

by

Wahyu Yulisma

B.S. in Civil Engineering, Institut Teknologi Bandung, 1986

M.S. in Civil Engineering, University of Kentucky, 1991

Submitted to the Graduate Faculty of

the School of Engineering in partial fulfillment

of the requirements for the degree of

Doctor of Philosophy

University of Pittsburgh

2005

UNIVERSITY OF PITTSBURGH
SCHOOL OF ENGINEERING

This dissertation was presented

by

Wahyu Yulimana

It was defended on

April 13, 2005

and approved by

Dr. Jeen-Shang Lin, Associate Professor
Department of Civil and Environmental Engineering

Dr. Julie M. Vandenbossche, Assistant Professor
Department of Civil and Environmental Engineering

Dr. Jeffrey S. Vipperman, Assistant Professor
Department of Mechanical Engineering

Dr. Christopher J. Earls, Associate Professor
Department of Civil and Environmental Engineering
Dissertation Director

ABSTRACT

EXPERIMENTAL STUDY OF THE BEHAVIOR OF FIBER REINFORCED POLYMER DECK SYSTEM

Wahyu Yulismana

University of Pittsburgh, 2005

The deterioration of the transportation infrastructures in the United States is proceeding at an alarming rate. Therefore, it becomes increasingly urgent to determine the feasibility of utilizing high performance composite materials for the fabrication of new structures as well as for the retrofitting of existing ones. It was estimated that almost 30 percent of 600,000 highway bridges in the US are either structurally deficient or functionally obsolete and repair costs are estimated to start at \$90 billion [Dunker, KF and Rabbat, BG, 1993]. In 1997, Salim et al. reported that 42 percent of the nation's bridges are considered deficient.

Fiber Reinforced Polymer (FRP) bridge decking holds out great promise for partially ameliorating this unsatisfactory condition. However, to be properly used in modern bridge decking application, FRP decks must be made to act compositely with underlying stringers (this work focuses on steel stringers). To behave compositely, a sufficiently robust shear transfer interface at the FRP to steel transition zone is required. While some efforts to achieve such interfacial shear transfer have been undertaken current understanding is weak and existing theories inadequate. The current research aims to contribute to our evolving understanding of this complex and important interface.

The research reported herein find that FRP deck and the underlying steel beam on both specimens tested as part of this work are interacting in a partially composite way at large load; as evidence by the discontinuity in strain at the FRP-to-steel interface. This result means that there was observed to be significant slip between FRP deck and underlying steel beam. It is also noted that at service load (e.g. 0-30 kips), even though the strain variations are relatively small, the FRP deck and steel beam are not acting in a fully composite fashion. It appears from the results presented herein that effective width approaching 75% of beam spacing (the overall width of the FRP deck).

TABLE OF CONTENTS

PREFACE.....	xiv
1.0 INTRODUCTION AND BACK GROUND	1
1.1 INTRODUCTION	1
1.2 RESEARCH MOTIVATION	6
1.3 PREVIOUS WORKS.....	6
1.4 RESEARCH OBJECTIVES and SCOPES.....	8
1.5 DISSERTATION OVERVIEW.....	9
2.0 MATERIAL TESTING of FRP DECK.....	10
2.1 INTRODUCTION	10
2.2 STRAIN GAGE TECHNOLOGY.....	11
2.2.1 Surface Preparation.....	14
2.2.2 Strain Gage Bonding.....	16
2.3 COMPRESSIVE TEST	17
2.3.1 Experiment Procedure.....	17
2.3.2 Results and Discussions.....	21
2.4 TENSILE TEST.....	25
2.4.1 Experimental Procedure.....	26
2.4.2 Results and Discussions.....	28
3.0 SHEAR STUD CONNECTION.....	32
3.1 INTRODUCTION	32

3.2	EXPERIMENTAL PROCEDURE	36
3.3	RESULTS and DISCUSSION	43
4.0	CONTINUOUS COMPOSITE DECK TESTING	55
4.1	INTRODUCTION	55
4.2	EXPERIMENTAL PROCEDURE	58
4.3	RESULTS and DISCUSSION	63
5.0	ULTIMATE STRENGTH COMPOSITE BEAM	67
5.1	INTRODUCTION	67
5.2	EXPERIMENTAL PROCEDURE	71
5.2.1	Test Set-up	71
5.2.2	Instrumentation	74
5.3	RESULTS and DISCUSSION	80
6.0	CR 46 BRIDGE: A COMPARATIVE STUDY	103
6.1	INTRODUCTION	103
6.2	STRUCTURE DESCRIPTION	103
6.3	INSTRUMENTATION & TESTING PROCEDURE	104
6.4	MEASURED STRAIN	106
6.5	RESULTS and DISCUSSION	107
7.0	CONCLUSIONS, RECOMMENDATION for FUTURE WORK	118
7.1	CONCLUSIONS	118
7.2	RECOMMENDATION for FUTURE WORKS	122
	APPENDIX A	123
	MATERIAL SAFETY DATA SHEET	123

BIBLIOGRAPHY..... 127

LIST OF TABLES

Table 2-1 Compressive Strength 0° Direction	22
Table 2-2 Compressive Strength 90° Direction	24
Table 2-3 Tensile Strength 0° Direction	29
Table 2-4 Tensile Strength 90° Direction	31
Table 3-1 Results of Push-off Testing	43
Table 3-2 Shear Stud Test Results	54
Table 5-1 Grout Cube Test Results.....	72
Table 5-2 Calculated Neutral Axis Beam Specimen #1	86
Table 5-3 Calculated Neutral Axis Beam Specimen #2	95
Table 5-4 Transformed Area Method	96
Table 5-5 Effective Width	97
Table 5-6 Elastic Section Properties	98
Table 5-7 Effective Width (Bernoulli-Navier Theorem).....	102
Table 5-8 Effective Width FRP Deck (Both Method).....	102
Table 6-1 Description of CR 46 Bridge Structure	104
Table 6-2 Average Exterior Beam N.A	109
Table 6-3 Average Interior Beam N.A	113
Table 6-4 Transformed Area Method	115
Table 6-5 Exterior and Interior Beam Effective Width	115
Table 6-6 Effective Width (LRFD/AASHTO)	117

Table 6-7 Measured Effective Width..... 117

LIST OF FIGURES

Figure 1-1 Pultrusion Schematic.....	3
Figure 1-2 FRP Panel Deck	5
Figure 1-3 High Bay Testing Facility	9
Figure 2-1 Universal Testing Machine	18
Figure 2-2 Coupon Specimen under Loading System	19
Figure 2-3 Failed Compressive Specimen (0°)	20
Figure 2-4 Failed Compressive Specimen (90°)	20
Figure 2-5 Compressive Test 0° Direction.....	21
Figure 2-6 Compressive Test 90° Direction.....	23
Figure 2-7 Preparation of Tensile Specimens.....	27
Figure 2-8 Tensile Specimens.....	27
Figure 2-9 Tensile Test 0° Direction.....	28
Figure 2-10 Tensile Test 90° Direction.....	30
Figure 3-1 Comparison of Deflected Beam	33
Figure 3-2 Preparation to Install Shear Stud.....	35
Figure 3-3 Grout Pocket after Stud Installation.....	35
Figure 3-4 Specimen #1	38
Figure 3-5 Specimen #2	39
Figure 3-6 Specimen #3	40

Figure 3-7 Specimen #4	41
Figure 3-8 Specimen in Loading Frame	42
Figure 3-9 Failed Specimen	43
Figure 3-10 Failed Studs - Specimen #1 - Bad Stud Installation.....	44
Figure 3-11 Failed Specimen #1	45
Figure 3-12 Load - Deformation Specimen #1	46
Figure 3-13 Failed Specimen #2	47
Figure 3-14 Load - Deformation Specimen #2	48
Figure 3-15 Failed Specimen #3	49
Figure 3-16 Load - Deformation Specimen #3	50
Figure 3-17 Failed Specimen #4.....	51
Figure 3-18 Load - Deformation Specimen #4	52
Figure 4-1 Dimensioned Cross Section of a Single MMC DuraSpan 500 FRP Tube	58
Figure 4-2 Continuous Panel Specimen.....	60
Figure 4-3 Elevation of Composite Deck (un-scaled)	61
Figure 4-4 Instrumentation Set Up (not to scale).....	61
Figure 4-5 Continuous Decks on the Load Frame	62
Figure 4-6 Tire Contact Areas	63
Figure 4-7 Deformation of Deck Section #1.....	64
Figure 4-8 Deformation of Deck Section #2.....	64
Figure 4-9 Deformation of Deck Section #3.....	65
Figure 5-1 FRP Beam Composite Specimen	70
Figure 5-2 Typical Specimen FRP Composite Beam in the Load Frame.....	71

Figure 5-3 Grout Cube Samples	73
Figure 5-4 Spreader Beam	74
Figure 5-5 Elevation & Cross Section of Composite Beam	78
Figure 5-6 Plan View of Composite Deck	79
Figure 5-7 Strain Variation in Composite Beam	80
Figure 5-8 Strain Variation Section C-C Specimen #1	81
Figure 5-9 Strain Variation Section D-D Specimen #1	81
Figure 5-10 Strain Variation Section E-E Specimen #1	82
Figure 5-11 Strain Variation Section F-F Specimen #1	82
Figure 5-12 Slip between Deck and Beam Test #1	83
Figure 5-13 Slip between Deck and Beam Test #1	83
Figure 5-14 Strain Variation at Service Load	84
Figure 5-15 Strain Variation at Service Load	85
Figure 5-16 Strain Variation at Service Load	85
Figure 5-17 Strain Variation at Service Load	86
Figure 5-18 Typical FRP Composite Beam Specimen	88
Figure 5-19 Typical Specimen FRP Composite Beam in the Load Frame	88
Figure 5-20 Failed Specimen #2 (note: web side-sway buckling followed after interfacial bond failure)	89
Figure 5-21 Strain Variation Section C-C Specimen #2	90
Figure 5-22 Strain Variation Section D-D Specimen #2	90
Figure 5-23 Strain Variation Section E-E Specimen #2	91
Figure 5-24 Strain Variation Section F-F Specimen #2	91
Figure 5-25 Slip between Deck and Beam Specimen #2	92

Figure 5-26 Slip between Deck and Beam Specimen #2.....	92
Figure 5-27 Strain Variation at Service Load.....	93
Figure 5-28 Strain Variation at Service Load.....	93
Figure 5-29 Strain Variation at Service Load.....	94
Figure 5-30 Strain Variation at Service Load.....	94
Figure 5-31 Typical Cross Section Composite Beam.....	96
Figure 6-1 Instrumentation & Test Plan	105
Figure 6-2 Load Configuration of Test Truck	105
Figure 6-3 CR 46 Bridge, Salmon River, Lewis County, NY	106
Figure 6-4 Strain Variation G1, Path Y2	107
Figure 6-5 Strain Variation G7, Path Y1	108
Figure 6-6 Strain Variation G7, Path Y2	108
Figure 6-7 Strain Variation G2, Path Y2	109
Figure 6-8 Strain Variation G3, Path Y1	110
Figure 6-9 Strain Variation G3, Path Y2	110
Figure 6-10 Strain Variation G4, Path Y1	111
Figure 6-11 Strain Variation G4, Path Y2	111
Figure 6-12 Strain Variation G5, Path Y1	112
Figure 6-13 Strain Variation G5, Path Y2	112
Figure 6-14 Strain Variation G6, Path Y1	113
Figure 6-15 Transformed Area Section	114

PREFACE

“Praise be to Allah, The Cherisher and Sustainer of the world.”

Completion of this dissertation certainly has increased my understanding and knowledge in conducting experimental studies. This work has been made possible partly by the support of many persons. I would like to express my deep gratitude to my academic advisor, Dr. Christopher J. Earls. He has been patiently giving me guidance and support throughout my graduate academic studies. My thanks to him are endless.

Special thanks are due to Dr. Lin, Dr. Vandebossche and Dr. Viperman for their feedback and suggestions.

I would also like to thank all the students and colleagues who provided support, inspirations, ideas, kindness and friendship. Jonathan Moses is one of them.

Nevertheless, this work probably would have taken a harder journey without continuous moral support from my mother and all the people I love. This dissertation is dedicated to them.

1.0 INTRODUCTION AND BACK GROUND

1.1 INTRODUCTION

The deterioration of the infrastructures in the United States is proceeding at an alarming rate. Therefore, it becomes increasingly urgent to determine the feasibility of utilizing high performance composite materials for the fabrication of new structures as well as for the retrofitting of existing ones. It was estimated that almost 30 percent of 600,000 highway bridges in the US were either structurally deficient or functionally obsolete and repair costs were estimated to start at \$90 billion [Dunker, KF and Rabbat, BG, 1993]. In 1997, Salim et al. reported that 42 percent of the nation's bridges were considered deficient.

The Civil Engineering Research Foundation (CERF) has recommended the use of high performance materials and construction systems, citing potentially substantial cost savings due to lower volumes of materials needed, reduced maintenance and longer lifetimes [CERF Executive Report, 1993].

One innovative material that has received much interest in the construction industry, especially infrastructure application, is fiber reinforced polymer (FRP) composites. In this context, innovative refers to materials that extend service life, reduce maintenance cost, and improve life-cycle cost efficiency. However, the use of FRP composites in construction has been limited due partly to a lack of knowledge among designers and engineers concerning the behavior of these materials. Each FRP manufacturer has different products, processes, and geometric shapes. The Engineer needs to analyze each system on an individual basis. In the US

there are more than six competitive supplier of FRP, and each uses one of three basic manufacturing methods:

- Pultrusion (e.g. Martin Marietta Composites)



- Vacuum Assisted Resin Transfer Molding (e.g. Hardcore Composites)



- Open Mold Hand Lay-up (e.g. Kansas Structural Composites)



FRP shapes are produced primarily by pultrusion. Within the last two decades, the pultrusion process has emerged as the dominant manufacturing process in the industry. Using pultrusion, high strength, light weight and maintenance free products and structures have been designed and built. Pultrusion is a continuous molding process using fiber reinforcement in polyester or other thermosetting resin matrices. Pre-selected reinforcement materials are drawn through a resin bath in which all material is thoroughly soaked with a liquid thermosetting resin. The wet out fiber is formed to the required geometric proportions and pulled into a heated steel die. Once inside the die, the resin cure is initiated by controlling precise elevated temperatures. The laminate solidifies in the exact cavity shape of the die, as it is continuously pulled by the pultrusion machine (Figure 1-1).

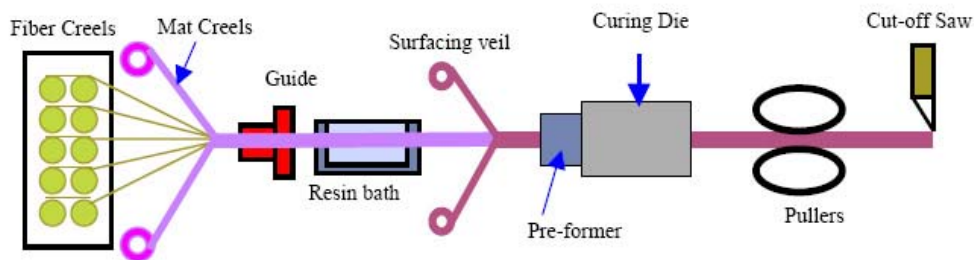


Figure 1-1 Pultrusion Schematic

Although the cross sectional shapes of FRP members are similar to those of other construction materials (i.e. steel, conventional concrete, etc), the structural behavior of an FRP section can be quite different from its conventional counterpart; mainly because an FRP section usually consists of thin-walled panels with distinct fiber architectures leading to material anisotropy. Due to the complexity of composite materials, the analytical and design tools

developed for members made from conventional materials cannot be readily applied to FRP shapes.

Pultruded sections, such as wide flanges, box, and other shapes, consist typically of arrangement of flat walls or panels. Usually, the reinforcement employed is E-glass fiber, and the resin, or matrix, is either vinylester or polyester. Although pultruded FRP shapes are not laminated structures in an exact sense, they are pultruded with material architectures that can be simulated as laminated configurations.

A typical pultruded section may mainly include the following three types of layers [Davalos JF.et al.,1996]:

- a. continuous (or chopped) strand mats (CSM) of different weights consisting of continuous (or short) randomly oriented fibers;
- b. stitched fabrics (SF) with different angle orientations;
- c. roving layers that contain continuous unidirectional fiber bundles which contribute the most to the stiffness and the strength of a section.

Each discrete layer maybe conceived as being homogeneous, linearly elastic, and generally orthotropic material. In order to evaluate its properties, the information provided by the material producer and pultrusion manufacturer are used to compute the stiffness coefficients of laminated composite elements [Lopez-Anido et al.,1995]

FRP materials are non-corrosive and posses the necessary property of high tensile strength that make them attractive as structural reinforcement for concrete. However, unlike steel reinforcement, there is no yielding or ductility with this material [Yost and Schmeckpeper, 2001]. As such, in uni-axial tension, FRP materials, which are brittle, respond linearly elastic until failure.

As conventional concrete bridge decks are concerned, length and depth dimensions vary little. That is, the local Department of Transportation typically has deck design detail sheets that specify concrete strength, deck thickness, and the amount of reinforcement as a function of effective girder spacing. As a result of the prescriptive design environment, wherein the required shear and flexural strength are provided by these standard detail sheets, strength and serviceability must be experimentally investigated so that the feasibility of using FRP deck is objectively demonstrated in an empirical sense.

As mentioned above, the use of FRP laminated plates in advanced engineering application has expanded rapidly and created a need for improved failure analysis capabilities. The mechanical properties of such materials show a high degree of variability due to the heterogeneous make-up of the constituent elements and the subjective nature of the highly proprietary production processes involved.

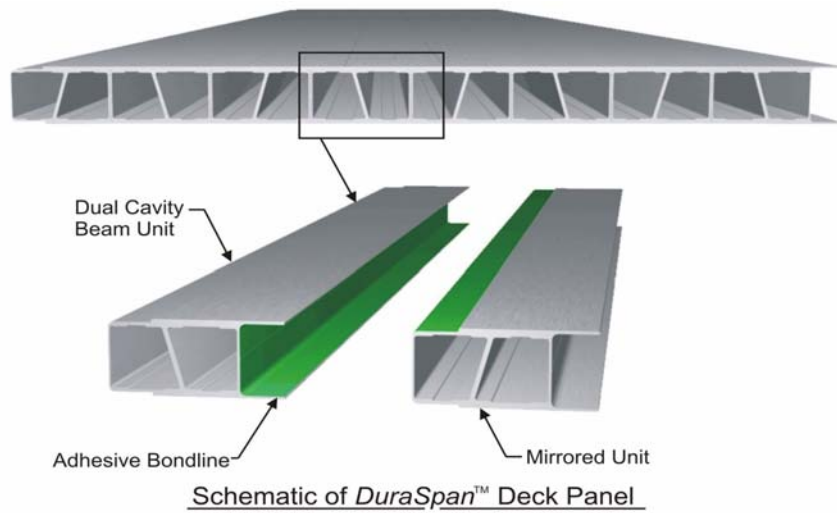


Figure 1-2 FRP Panel Deck

1.2 RESEARCH MOTIVATION

To be properly used in modern bridge decking application, FRP decks must be made to act compositely with underlying stringers (this work focuses on steel stringers). To behave compositely, a sufficiently robust shear transfer interface at the FRP to steel transition zone is required. While some efforts to achieve such interfacial shear transfer have been undertaken current understanding is weak and existing theories inadequate. The current research contributes to our evolving understanding of this complex and important interface.

1.3 PREVIOUS WORKS

This research was motivated by previous studies done on Fiber Reinforced Polymer (FRP) bridge decks. A series of push-out tests were performed by Wood et al. (2001) to study shear connection behavior between FRP decks and prestressed concrete girders. Similar push-out tests also were performed by Moon et al. (2002) to study shear connection behavior between FRP decks and steel girders. In this study, Moon et al. used two different deck sections to test their design concept. The first connection was tested in concert with the MMC (Martin Marietta Composite) Gen3 deck while the second and third connections were tested with the MMC Gen4 deck. Gen3 deck has 35% thicker face sheets than Gen4 deck. Their study (Moon et al., 2002) concluded that approximately 60–70% of the capacity of a longitudinal connection in a continuous concrete deck was developed. This decreased capacity was due to failure modes related to the discrete nature of FRP decks. As a result, an expression was proposed for the determination of longitudinal capacity for shear stud connections employed in FRP decks. Moon et al. (2002) suggested a new relationship be used for developing the capacity of a shear stud as follows:

$$Q_n = t_{fs} d_{sc} F_{frp} \leq A_{sc} F_u$$

Equation 1-1

where: Q_n = the nominal shear capacity of one stud;
 t_{fs} = thickness of the bottom face sheet;
 d_{sc} = diameter of shear connector;
 F_{frp} = compressive strength of composite material;
 A_{sc} = area of shear connector;
 F_u = ultimate shear stress of connector.

Turner and Harries (2002) also performed a series of tests on shear stud connections between FRP decks and steel girders. Two specimens were designed and constructed using 8-in MMC Deck (DuraSpan 766). The panels of 8-in FRP deck were attached to W12x106 section steel girder and were placed in a testing frame. A 300-kip capacity hydraulic ram was used to apply load to the specimens. Turner and Harries (2002) concluded that the shear studs were unable to achieve their normal capacity; vis-à-vis concrete deck. There was no evidence of bearing failure within the grout pocket around the stud.

Kumar et al. (2002) presented fatigue and strength experimental qualifications performed for all-composite deck. The materials used for the fabrication were 3 inch pultruded square hollow glass and carbon FRP tubes of varying lengths. These tubes were bonded using an epoxy adhesive and mechanically fastened together using screws in seven different layers to form the bridge deck with tubes running both longitudinal and transverse to the traffic direction. The cross section of the deck was in the form of four identical I-beams running along the length of the bridge. The loads for these tests were computed so as to meet AASHTO H-20 truckload requirement based on strength and maximum deflection. The specimen was subjected to 2 million service load cycles at a nominal frequency of 4 Hz. The conclusions of this research were that the design of bridges using readily available pultruded FRP tubes for decking can meet the necessary strength and deflection design criteria as defined in the AASHTO specifications. The

failure load of 30 kips was almost four times the design wheel load of 8 kips for the quarter section of the bridge deck.

There are many technical papers related to the effective compression flange width present within concrete deck – steel girder composite flexural systems (ASCE 1979). Ahmadi (1996) wrote a technical report on the effective compression flange width in concrete filled steel deck acting compositely with steel girders in a bridge in West Virginia. This technical report is relevant to the current research effort focusing on FRP decks because both FRP decks and concrete filled steel decks are categorized as orthotropic plates. Their strong direction is most frequently oriented normal to the steel girder longitudinal axis. However, there are no references available that relate to the specific case of compression flange effective width in FRP deck – steel girder composite designs at ultimate load or at service load. The lack of research in this particular area needs to be addressed if FRP is to be properly used in bridge applications and therefore was a strong motivation to conduct this current research.

1.4 RESEARCH OBJECTIVES and SCOPES

The objective of this research is to perform a series of laboratory based experimental tests to primarily evaluate the interfacial shear performance of the Fiber Reinforced Polymer (FRP) deck when mechanically attached to steel stringer(s) as required in the bridge deck system. An additional and important outcome is to provide guidelines for computation of effective flange widths that should be employed in engineering calculation used in the design of FRP deck system.

To support this research four types of tests are conducted in the Watkin-Haggart Structural Engineering Laboratory at the University of Pittsburgh: Compressive and Tensile

Material Testing, Push-off Testing, Continuous Panel Testing, and Ultimate Strength Composite Beam Testing.



Figure 1-3 High Bay Testing Facility

1.5 DISSERTATION OVERVIEW

This dissertation is divided into 7 Chapters that describe the experimental study/research performed. The first chapter is an introduction to Fiber Reinforced Polymer and overview of previous research done on Fiber Reinforced Polymer bridge deck. Chapter 2 is a description of material testing of Fiber Reinforced Polymer bridge deck using compressive and tensile coupon specimens. Chapter 3 evaluates the capacity of grout embedded stud connection used between FRP deck and steel girder in the composite beam bridge system. Chapter 4 discusses the deck deflection of continuous FRP deck panels under a load system that simulates HS25-44 ASSHTO design truck. Chapter 5 evaluates and determines the neutral axis on a full scale composite beam loaded monotonically to failure. Chapter 6 will describe a comparative study of Fiber Reinforced Polymer deck bridge system. Chapter 7 presents the conclusions of the research and recommendation for future work.

2.0 MATERIAL TESTING of FRP DECK

2.1 INTRODUCTION

Composite materials have many mechanical behavioral characteristics that are different from those of more conventional engineering materials. Some characteristics are merely modifications of conventional behavior; others are totally new and require new analytical and experimental procedures.

Most common engineering materials are both homogeneous and isotropic. A homogeneous body has uniform properties throughout, i.e., the properties are independent of position of the body. An isotropic body has material properties that are the same in every direction at a point in the body, i.e., the properties are independent of orientation at a point in the body.

In contrast, composite materials are often both non-homogeneous and non-isotropic (orthotropic or, more generally, anisotropic). An orthotropic material has properties that are different in perpendicular directions at a point in the body. The properties depend on orientation at a point in the body.

Because of the obviously heterogeneous nature of composite materials, it is convenient to study mechanical response from two points of view: micromechanics and macromechanics. Micromechanics is the study of composite material behavior wherein the interaction of the constituent materials is examined on microscopic scale to determine their effect on properties of the composite material. On the other hand, macromechanics is the study of composite material behavior wherein the material is presumed homogeneous and the effects of the constituent

materials are detected only as averaged apparent macroscopic properties of the composite material.

For isotropic materials, application of normal stress causes extension in the direction of the stress and contraction in the perpendicular directions, but no shearing deformation. Also, application of shear stress causes only shearing deformation. Only two material properties, Young's modulus (the extensional modulus or slope of the material's uniaxial stress-strain curve) and Poisson's ratio (the ratio of lateral contraction strain to axial extensional strain caused by axial extensional stress), are needed to determine the deformations.

For orthotropic materials, like isotropic materials, application of normal stress in a principal direction results in extension in the direction of the stress and contraction perpendicular to the stress. The magnitude of the extension in one direction under normal stress in that direction is different from the extension in another direction under the same normal stress in that other direction. Thus, different Young's moduli exist in the different principal directions.

Information concerning the material properties can be obtained by using experimental methods. Common experimental methods used to obtain that information include coupon testing of FRP coupons in a universal testing machine with strain gages bonded to the coupon. Selection of the proper strain gage is one of the first steps toward a successful test.

2.2 STRAIN GAGE TECHNOLOGY

In 1856 Lord Kelvin reported that resistance of copper and iron wires increased when subjected to a tensile strain [Dally and Riley, 1978]. This basic discovery has ultimately led to the development of the modern resistance foil strain gage. The underlying concept of resistance strain gages is very simple. In essence, an electrically conductive wire is securely bonded to a

structure of interest, and the resistance of the wire is measured before and after the structure is loaded. Since the wire is firmly bonded to the structure, strains induced in the structure are also induced in the wire. This results in a change in wire resistance, which serves as an indirect measure of the strain induced in the structure.

Although the underlying concept is simple, there are several sources of error which may lead to erroneous strain measurements if not properly accounted for. These sources of error can be loosely grouped into the following six categories [Tuttle, 1998]:

- a. The wire must be firmly bonded to the structure, so that the deformation of the wire is an accurate reflection of the deformation of the structure,
- b. The wire must not locally reinforce the structure, otherwise the strain field in the vicinity of the wire will be disturbed and an inaccurate measure of strain will be obtained,
- c. The wire must be electrically insulated from the structure,
- d. The change in wire resistance per unit micro-strain is very small; however this small change in resistance must be measured accurately if an accurate measure of strain is to be obtained,
- e. The structure (as well as the wire) may be deformed by mechanism other than an applied load,
- f. The resistance of the wire may be changed by mechanisms other than physical deformation.

The most common strain gages used in experimental testing are foil strain gages which are produced from a metal foil using a photo-etch process. The foil gage is normally bonded to a thin polymeric backing material, and the entire assembly (i.e., the strain gage) is adhesively bonded to the test structure.

Calibration of strain gage is performed by the manufacturer, and is reported to the user in the form of four gage characteristics: gage resistance, gage factor, transverse-sensitivity coefficient, and self-temperature-compensation (STC) number. These parameters are measured for a statistically significant number of gages from each lot produced, and the measured values are included with each strain gage package purchased from a given manufacturer.

Other parameters to be considered in using strain gages are: specimen geometry and surface contours, thermal expansion and thermal conductivity properties of the test material, test environment, test duration, expected strain level and strain gradients, required level of accuracy and stability, and simplicity the system.

Gage selection for composites is not generally more difficult than for other materials, but the following characteristics of composites should be remembered:

- The strain field of a composite exhibits local strain variations due to both the non-homogeneity and the surface texture of the material,
- Composites are poor thermal conductors,
- Principal strains and stresses may not be coaxial due to the anisotropic nature of composites,
- The effective coefficient of thermal expansion of a composite varies both with direction and with the previous load and thermal history of the specimen,
- Composites are not commonly utilized in hostile environments which would damage most strain gages.

Most practical engineering experience is based upon the familiar behavior of homogeneous isotropic materials. In contrast, advanced composites are highly heterogeneous and orthotropic. Consequently composites can exhibit surprising and unusual behavior, which would

not be expected based upon experience with isotropic materials. In some cases, these surprises can lead to erroneous interpretation of experimental results. Some specific examples of this are errors due to slight gage misalignment, the enhancement of transverse sensitivity errors due to orthotropic material properties, and strain measurement near a free edge.

2.2.1 Surface Preparation

Strain gages can be bonded satisfactorily to almost any solid material if the material surface is properly prepared. There are many surface preparation techniques available, the specific procedures and techniques that were used in this current research were ideal for M-Bond 200 Adhesive System (Vishay Micro-Measurements, Inc).

The purpose of surface preparation is to develop a chemically clean surface having a roughness appropriate to gage installation requirements, a surface alkalinity of the correct pH, and visible gage layout lines for locating and orienting the strain gage. There are five basic operations to prepare the surface of the samples, as follows:

- solvent degreasing,
- surface abrading,
- application of gage lines,
- surface conditioning,
- neutralizing

To ensure maximum cleanliness and best results, the following should be avoided in all steps: touching the surface with fingers, wiping back and forth or reusing swabs or sponges, dragging contaminants into the cleaned area from the un-cleaned boundary of that area, allowing a cleaning solution to evaporate on the surface, and allowing partially prepared surface to sit between steps in the preparation process or a prepared surface to sit before bonding.

Degreasing is performed to remove oils, greases, organic contaminants, and soluble chemical residues. Degreasing should always be the first operation. Degreasing can be accomplished using a solvent such as CSM-1 Degreaser (Vishay Micro-Measurements, Inc.) Spray applicators are preferred to avoid back-contamination of the parent solvent. Use a clean gauze sponge to clean the entire specimen.

The surface is abraded to remove any loosely bonded adherents (scale, rust, paint, coatings, oxides, etc), and to develop a surface texture suitable for bonding. For most specimens a suitable surface can be produced with silicon-carbide paper of the appropriate grit. Place a liberal amount of M-Prep Conditioner A (Vishay Micro-Measurements, Inc.) in the gauging area and wet-lap with clean 220/320-grit silicon-carbide paper. Add Conditioner A as necessary to keep the surface wet during the lapping process. Wipe the surface dry with a clean gauze sponge. A clean surface of the gauze should be used with each wiping stroke. A sufficiently large area should be cleaned to ensure that contaminants will not be dragged back into the gauging area during the steps to follow. Repeat the above step, using 320/400-grit silicon-carbide paper.

The desired location and orientation of the strain gage on the test surface should be marked. All residues from the marking should be removed in the following step.

After the layout lines are marked, Conditioner A should be applied repeatedly, and the surface scrubbed with cotton-tipped applicator until a clean tip is no longer discolored by scrubbing. The surface should be kept constantly wet with conditioner A until the cleaning is completed. When clean, the surface should be dried by wiping through the cleaned area with a single slow stroke of a gauze sponge. The stroke should begin inside the cleaned area to avoid dragging contaminants in from the surrounding area. Throw the used gauze away. With fresh gauze, make a single slow stroke in the opposite direction. Throw the second gauze away.

To provide optimum alkalinity for strain gage adhesives, the cleaned surfaces must be neutralized. This can be done by applying M-Prep Neutralizer 5A (Vishay Micro-Measurements, Inc.) liberally to the cleaned surface, and scrubbing the surface with a clean cotton-tipped applicator. The cleaned surface should be kept completely wet with Neutralizer 5A throughout this operation. When neutralized, the surface should be dried by wiping through the cleaned area with a single slow stroke of a clean gauze sponge. Throw the gauze away and with another fresh piece, make a single slow stroke in the opposite direction. Always begin within the cleaned area to avoid recontamination from the un-cleaned boundary.

2.2.2 Strain Gage Bonding

The electrical resistance strain gage is capable of making accurate and sensitive indication of strains on the surface of the test part. Its performance is absolutely dependent on the bond between strain gage and the test part. The procedures should be followed carefully to ensure satisfactory bond. No further cleaning is necessary if contamination of the prepared surface is avoided during handling. The bonding surface of the strain gages should never be touched with the hands.

Remove the strain gage from its acetate envelope and apply M-200 Catalyst (Vishay Micro-Measurements, Inc.) cautiously in a thin uniform coat. Wipe the brush against the lip of the bottle approximately fifteen times to remove most of the catalyst. Set the brush down on the gage and swab the gage backing by sliding the brush over the entire gage surface. Allow the catalyst to dry at least one minute under normal ambient laboratory conditions.

Holding the gage in fixed position, apply one or two drops of M-Bond 200 Adhesive at the junction of the gage and specimen surface. Apply firm thumb pressure to the gage and terminal area and hold it for at least one minute.

2.3 COMPRESSIVE TEST

A compression test helps to quantify the behavior of materials under crushing load. The specimen is compressed and the subsequent deformation, at various loads, is recorded. Axial compression testing is a useful procedure for measuring the plastic flow behavior and ductile fracture limits of material. Measuring the plastic flow behavior requires frictionless (homogeneous compression) test conditions. Axial compression testing is also useful for measurement of elastic and compressive failure properties of brittle or low-ductility materials (e.g. FRP).

The determination of the compressive response of fiber composite materials has been a particularly difficult and continuing challenge since the beginning of their development. Even with long term interest and much research, compression testing of composite materials is still one of the least understood areas of mechanical properties characterization. This is evident from the numerous test fixtures and test specimen configurations that have been developed over the past years [Adam, 1995].

It is difficult to define the compressive failure strength of a composite material because of elastic instabilities in-various scale ranges from column buckling of the entire coupon to the buckling of individual fibers within the surrounding matrix material on a more local scale. Which failure mode actually occurs is strongly dependent on the specific specimen geometry and constraints imposed.

2.3.1 Experiment Procedure

Coupon specimens for this compressive test were prepared and tested in accordance with ASTM D695 (Standard Test for Compressive Properties of Rigid Plastics) and ASTM D3410 (Standard Test Method for Compressive Properties of Polymer Matrix with Unsupported Gage Section by

Shear Loading). The specimens were cut from the face sheet of fiber reinforced polymer deck panels of MMC (Martin Marietta Composites) DuraSpan 500.

The coupon compressive specimens were machine cut into rectangular prisms 1” long, 0.5” wide and 0.5” thick. A uni-axial strain gage FLA-6-11 (Texas Measurements, Inc.) was installed at the center of each specimen using Measurement Group M-bond 200. This test had 5 specimens for each direction: 0° (parallel to the direction of pultrusion) and 90° (perpendicular to the direction of pultrusion). All the specimens were tested in the Baldwin Universal Testing Machine (UTM). (Figure 2-1)



Figure 2-1 Universal Testing Machine

To verify successful strain-gage installation, the gage was checked with a digital strain indicator P-3500, from Vishay Measurements Group. A steady strain reading from the P-3500 strain indicator signals a successful installation.

The P-3500 strain indicator was also used to read the strain of each coupon specimen loaded monotonically to failure.



Figure 2-2 Coupon Specimen under Loading System

Figure 2-2 shows how the coupon specimen was oriented under the applied load. Each coupon specimen was tested to failure.



Figure 2-3 Failed Compressive Specimen (0°)



Figure 2-4 Failed Compressive Specimen (90°)

Figure 2-3 and Figure 2-4 show the failed compressive specimens in both directions 0° (parallel to the direction of pultrusion) and 90° (perpendicular to the direction of pultrusion).

2.3.2 Results and Discussions

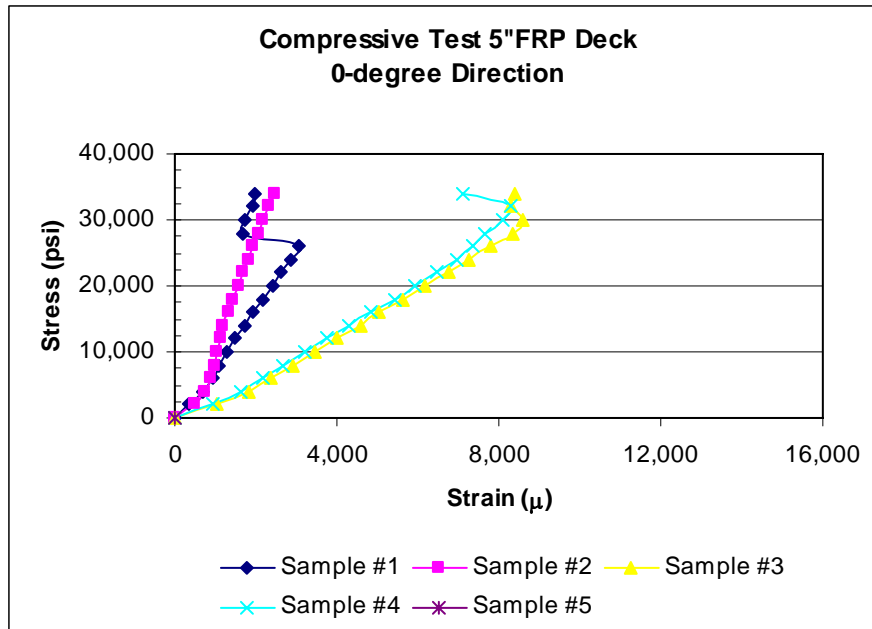


Figure 2-5 Compressive Test 0° Direction

The strain data obtained from sample #5 cannot be included in stress analysis (and thus is not plotted with the other results), because strain gages failed to perform properly. However, the ultimate strength of sample #5 was still valid. Figure 2-5 shows that coupon samples did not respond uniformly under the same test. It also shows that sample #1 and sample #2 were stiffer than sample #3 and sample #4. From observation during the test, delaminating occurred slower on sample #1 and #2 than sample #3 and #4.

Stress analysis results for coupon specimens' 0° direction can be shown in the table below:

Table 2-1 Compressive Strength 0° Direction

	Sample 1	Sample 2	Sample 3	Sample 4	Sample 5
Ultimate Strength (lbs)	8.76E+03	9.02E+03	9.39E+03	8.54E+03	6.93E+03
Ultimate Stress (psi)	3.50E+04	3.61E+04	3.76E+04	3.42E+04	2.77E+04
Ultimate Stress (ave) (psi)	3.41E+04				
Standard Deviation (psi)	3.79E+03				
Modulus Elasticity (psi)	7.13E+06	7.62E+06	2.68E+06	2.92E+06	N/A
Modulus Elasticity (ave) (psi)	5.09E+06				
Standard Deviation (psi)	2.65E+06				

Average ultimate strength of coupon specimens for compressive testing in the 0° direction was 3.41E+04 psi with 3.79E+03 psi standard deviation.

Average modulus of elasticity of these coupon specimens was 5.09E+06 psi with 2.65E+06 psi standard deviation. Conventionally, if only sample #3 and #4 were considered to determine modulus of elasticity, gave a result of 2.80E+02 with 1.76E+05 psi standard deviation.

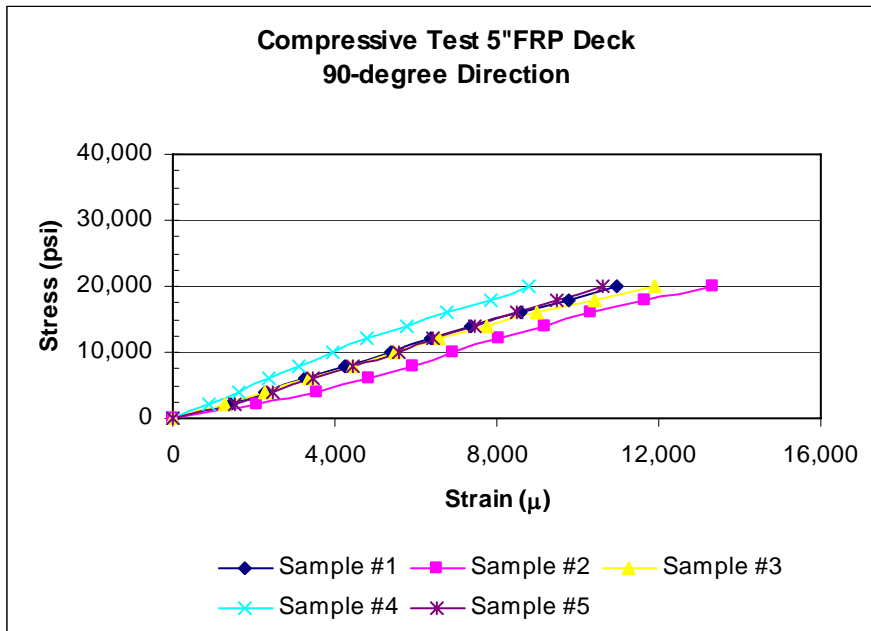


Figure 2-6 Compressive Test 90° Direction

On the other hand, coupon specimens 90° gave more uniform result comparing to the specimens 0°, shown on Figure 2-6. Delaminating of all samples occurred more or less at the same rate.

Stress analysis results for coupon specimens whose fibers were oriented in the 90° direction can be shown in the table below:

Table 2-2 Compressive Strength 90° Direction

	Sample 1	Sample 2	Sample 3	Sample 4	Sample 5
Ultimate Strength (lbs)	5.86E+03	5.75E+03	5.87E+03	5.40E+03	5.50E+03
Ultimate Stress (psi)	2.34E+04	2.30E+04	2.35E+04	2.16E+04	2.20E+04
Ultimate Stress (ave) (psi)	2.27E+04				
Standard Deviation (psi)	8.58E+02				
Modulus Elasticity (psi)	1.83E+06	1.33E+06	1.80E+06	2.53E+06	1.75E+06
Modulus Elasticity (ave) (psi)	1.85E+06				
Standard Deviation (psi)	4.34E+05.				

Average ultimate strength of coupon specimens for compressive test 90° direction was 2.27E+04 psi with 8.58E+02 psi standard deviation.

Average modulus of elasticity of these coupon specimens was 1.85E+06 psi with 4.34E+05 psi standard deviation.

2.4 TENSILE TEST

Tensile testing embraces various procedures by which modulus, strength, and ductility can be assessed. Tests specifically designed to measure phenomena as varied as creep, stress relaxation, stress rupture, fatigue, and impact resistance can all be classified as tensile tests provided that the stress system is predominantly tensile. However by common usage the term “tensile test” is usually taken to mean a test in which a specimen is extended uniaxially at a uniform rate. Ideally, the specimen should be slender, of constant cross section over a substantial gage length, and free to contract laterally as it extends; a tensile stress then develops over transverse plane sections lying within the gage region and the specimen extends longitudinally and contracts laterally; a procedure was initially developed for tests on metals but was subsequently adopted and adapted for tests on rubbers, fibers, and plastics.

Practical tensile testing often conforms to one of several standard methods or to a code of practice, with variants dictated by local circumstances. Most of the conditions set out in the standardized practices embody the collective wisdom of earlier tensile-test practitioners and fall into four distinct groupings:

1. Conditions relating to a specimen-machine system,
2. Conditions relating to the derivation of excitation-response relationship from the raw data,
3. Conditions relating to the precision of the data,
4. Conditions relating to the physical interpretation of the data.

The conditions in the first group are the primary ones because, unless the specimen-machine system functions properly, no worthwhile data can be generated. The conditions in the other three groups are supplementary but are nevertheless essential in that they enable the

outcome of the specimen-machine interaction to be translated progressively into mechanical-properties data for the specimen under investigation.

In one particular respect, tensile testing suffers from a fundamental and obvious deficiency that is common to many types of mechanical tests: the experimenter has no option but to measure force and deformation, whereas the physical characteristics of the specimen and the material should be expressed in terms of stress and strain. The translations of force into stress and deformation into strain are sources of errors and uncertainties.

Tensile testing of fiber reinforced composite materials is performed for the purpose of determining uniaxial tensile strength and Young's modulus relative to principal material directions. The unidirectional lamina provides the basic building block of the multi-directional laminate. Therefore, characterization of lamina material properties allows predictions of the properties of laminates. In actual practice, considerable success has been demonstrated in predicting laminate effective modulus or Poisson's ratio from ply properties. However, prediction of laminate strength properties from lamina strength data has proved more difficult.

2.4.1 Experimental Procedure

Coupon specimens for this tensile test were prepared and tested in accordance with ASTM D3039 (Standard Test for Tensile Properties of Polymer Matrix Composite Materials). The specimens were cut from the face sheet of fiber reinforced polymer deck panel MMC (Martin Marietta Composites) DuraSpan 500.

The coupon tensile specimens were machine cut into rectangular prism 8.0" long, 2.0" wide and 0.5" thick (with end tabs). A uni-axial strain gage FLA-6-11 (Texas Measurements, Inc.) was installed at the center of each specimen using Measurement Group M-bond 200. This test had 5 specimens for each direction: 0° (parallel to the direction of pultrusion) and 90°

(perpendicular to the direction of pultrusion). All the specimens were tested in the Baldwin Universal Testing Machine (UTM). (Figure 2-1)



Figure 2-7 Preparation of Tensile Specimens



Figure 2-8 Tensile Specimens

The same procedure applied to coupon specimens for compressive testing was used to verify successful strain-gage installation: the gage was checked with a digital strain indicator P-3500 from Vishay Measurements Group. A steady strain reading from the P-3500 strain indicator signals a successful installation

The P-3500 strain indicator was also used to read the strain of each coupon specimen loaded monotonically to failure.

2.4.2 Results and Discussions

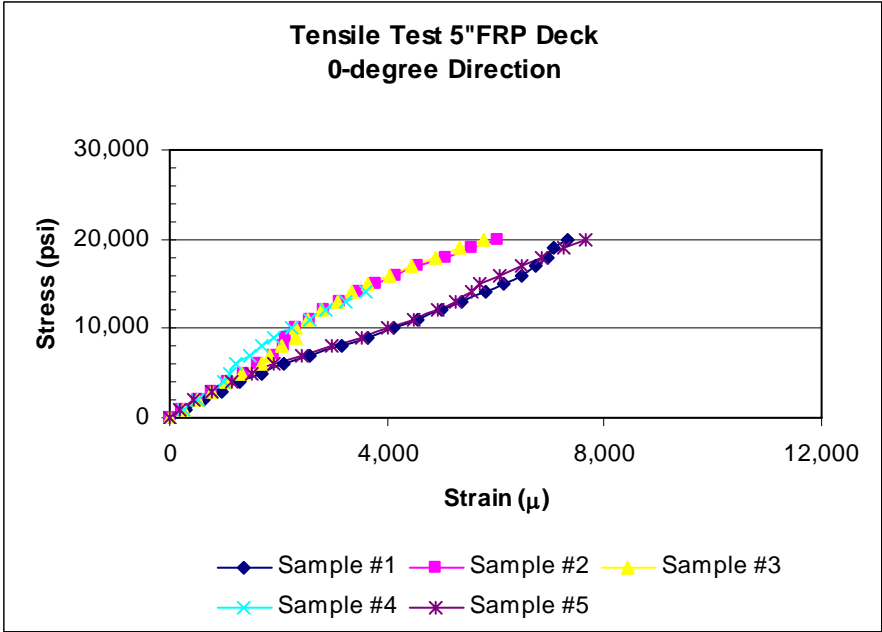


Figure 2-9 Tensile Test 0° Direction

Figure 2-9 shows that coupon specimens' 0° direction for tensile test has better results than those for 0° direction for compressive test. It also shows that, unlike steel reinforcement, there is no yielding or ductility with this material. FRP materials respond linearly elastic until failure under uni-axial tension.

Stress analysis results for coupon specimens' 0° direction can be shown in the table below:

Table 2-3 Tensile Strength 0° Direction

	Sample 1	Sample 2	Sample 3	Sample 4	Sample 5
Ultimate Strength (lbs)	2.06E+04	3.39E+04	3.29E+04	1.46E+04	2.16E+04
Ultimate Stress (psi)	2.19E+04	3.60E+04	3.49E+04	1.55E+04	2.29E+04
Ultimate Stress (ave) (psi)	2.89E+04				
Standard Deviation (psi)	8.86E+03				
Modulus Elasticity (psi)	3.57E+06	4.03E+06	4.09E+06	4.23E+06	4.02E+06
Modulus Elasticity (ave) (psi)	3.99E+06				
Standard Deviation (psi)	2.46E+05				

Average ultimate strength of coupon specimens for tensile test 0° direction was 2.89E+04 psi with 8.86E+03 psi standard deviation.

Average modulus of elasticity of these coupon specimens was 3.99E+06 psi with 2.46E+05 psi standard deviation.

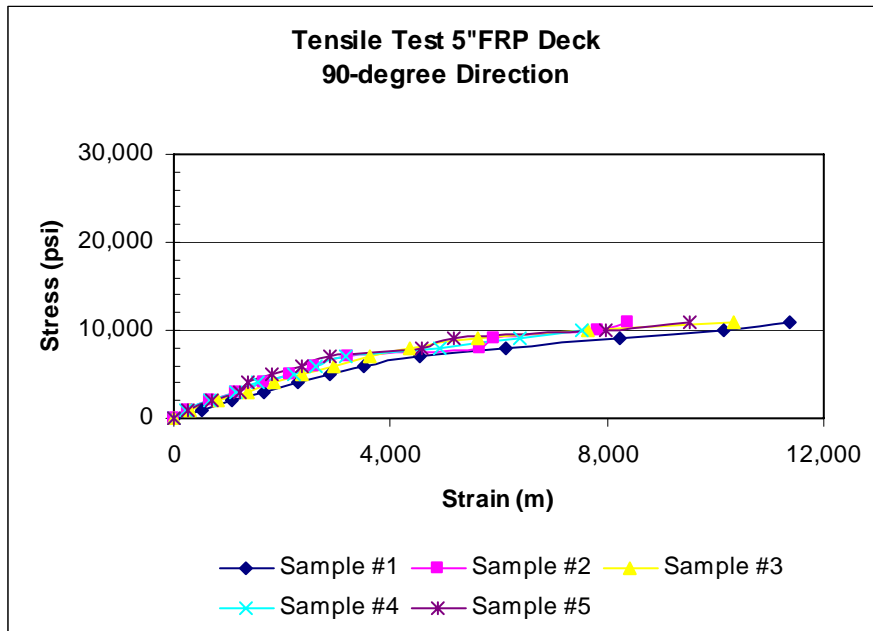


Figure 2-10 Tensile Test 90° Direction

Figure 2-10 shows the stress-strain relationship for coupon specimens' 90° direction for tensile test. All samples whose response is displayed in the figure responded consistently. Based on the tensile responses shown in the foregoing figures, it is shown that FRP material that is the focus of the current research is brittle in nature.

Stress analysis results for coupon specimens' 90° direction can be shown in the table below:

Table 2-4 Tensile Strength 90° Direction

	Sample 1	Sample 2	Sample 3	Sample 4	Sample 5
Ultimate Strength (lbs)	1.14E+04	1.13E+04	1.14E+04	1.09E+04	1.18E+04
Ultimate Stress (psi)	1.21E+04	1.20E+04	1.15E+04	1.16E+04	1.24E+04
Ultimate Stress (ave) (psi)	1.19E+04				
Standard Deviation (psi)	3.74E+02				
Modulus Elasticity (psi)	1.91E+06	2.72E+06	2.23E+06	2.80E+06	2.91E+06
Modulus Elasticity (ave) (psi)	2.51E+06				
Standard Deviation (psi)	4.29E+05				

Average ultimate strength of coupon specimens for tensile test 90° direction was 1.19E+04 psi with 3.74E+02 psi standard deviation.

Average modulus of elasticity of these coupon specimens was 2.51E+06 psi with 4.29E+05 psi standard deviation.

3.0 SHEAR STUD CONNECTION

3.1 INTRODUCTION

An important consideration when utilizing an all composite deck for use in a bridge system is type and capacity of the deck-to-girder connection. Full composite action has been designed and used on conventional concrete slab on steel girder bridges with sufficient connections so as to develop either the compressive capacity of the slab/deck or the tensile capacity of the girder cross section. In a design context, the consideration of composite construction (whether concrete to steel or FRP to steel) is predicated on a well understood interfacial shear transfer response between the components being joined compositely (see Figure 3-1). The current chapter discusses work carried out as part of the current investigation that is aimed specifically at enhancing the understanding of the complex interfacial response between steel stringers and FRP composite deck systems.

In the case of FRP deck, the deck dead load is decreased (as compared with conventional concrete slab decks) thus reducing the presence of interfacial friction as a means for enhancing the mechanical bond between the stringer and deck. Furthermore, in an FRP to steel stringer scenario, more of the moment capacity of the girder is assigned to the resistance of live load and superimposed dead load moments as a result of the relatively low modulus of the FRP relative to the steel. As a result of these interesting differences, FRP to steel stringer composite construction represents a departure from more conventional scenarios for composite construction. Universal to all composite construction is the need for a connection capable of developing some degree of composite action is required. However, the current situation that exists in the state-of-the-art

requires that the quantification of the degree of composite action required must be determined on a case-by-case basis.

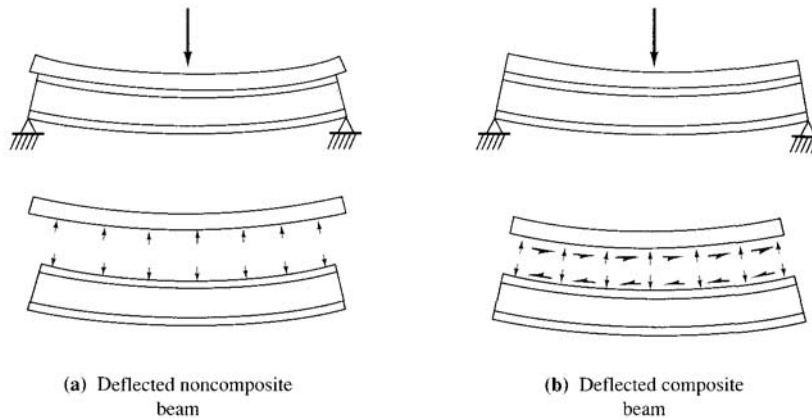


Figure 3-1 Comparison of Deflected Beam

One importance difference between a conventional concrete deck and a FRP deck, other than obvious differences in material properties, is that an FRP deck typically uses discrete cores whereas a conventional concrete deck is continuous. The MMC (Martin Marietta Composites) DuraSpan 500 deck consists of pultruded hollow box-like elements bonded together to form a trapezoidal-core structure. This type of deck configuration results in a more economical and lighter structure. However, this deck also requires a very careful analysis to study the development of the deck-to-girder connection. The important factor in composite action is that the bond between the deck and steel girder remain unbroken (i.e. interfacial force transfer is maintained with only modest slip being manifest).

Since composites may not perform well when subjected to localized loads as a result of artifacts in the composite architecture, developing a system that transfers load from relatively thin face sheets into a steel girder without creating any stress concentrations that exceed the

capacity of the deck, on a local scale, is not simple. As a result of this, it is essential to study the behavior of mechanical shear connectors within the context of the large composite system. The shear connectors are called on to provide the interaction necessary for the deck and the girder to act as a unit. Ideally, to obtain a fully composite section the shear connectors should be stiff enough to provide the interfacial strain compatibility required for complete composite interaction. This requires that the connectors be infinitely rigid and that the adjacent FRP deck be noncompliant as well. Furthermore, from an elementary consideration of the mechanic at work, it is clear that theoretically, that more shear connectors are required near the ends of the span where the shear is high than near the midspan where the shear is low.

While it is that FRP deck to steel stringer systems rely heavily on the integrity of the mechanism for interfacial shear transfer, in the form of shear stud, the nature of the deck system itself may hamper good installation practice while at the same time interfering with standard inspection techniques. A significant difference in the erection of FRP deck bridge systems, compared to other forms of bridge systems, is that the headed shear studs used for mechanical shear transfer between FRP deck and steel stringer(s) are installed onto the stringer(s) through a stud pocket opening; after the deck is in place. Once installed, the shear studs cannot be properly inspected since the studs cannot be bent over to one side as it typically done in concrete deck installation prior to concrete placement. Figure 3.2 shows how shear studs are installed onto the stringer using stud gun when FRP deck systems are employed. The hollow core decks are dammed up using styrofoam blocks that control the flow of non-shrink grout which is injected into the pockets and around the headed shear studs. The haunches formed as a by-product of the grout injection into the pockets are also studied as part of this research because the overall durability of the FRP deck installation depends on the integrity of these haunches.



Figure 3-2 Preparation to Install Shear Stud



Figure 3-3 Grout Pocket after Stud Installation

As a means for quantifying the interfacial capacity and response, a typical concrete to steel test (known as the “push-off” test) is adapted for the work undertaken herein. Specifically, the push-off test is performed to arrive at a practical connection capable of developing the ultimate capacity of the shear stud between steel girder (W21x62) and the MMC DuraSpan 500 FRP deck. Load deflection curves are plotted and the shear stud behavior is observed.

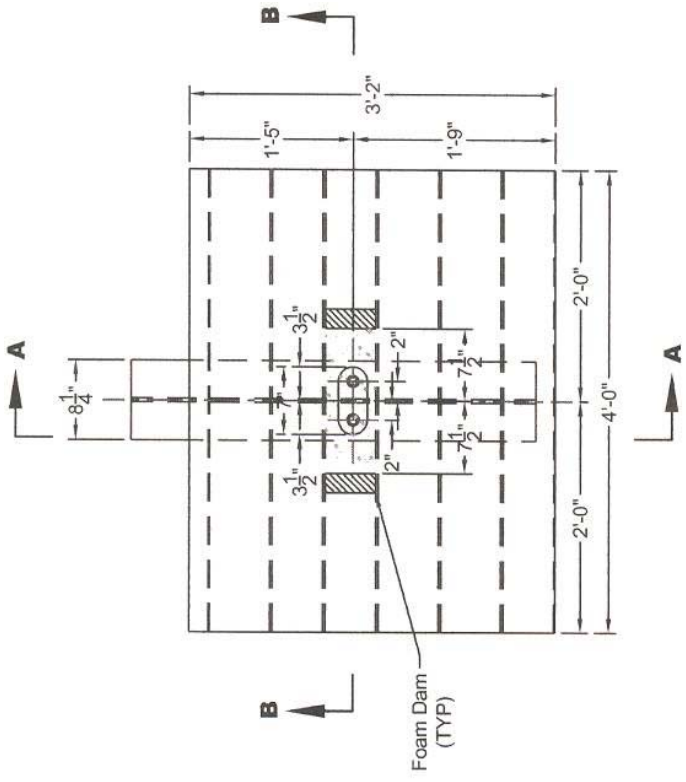
3.2 EXPERIMENTAL PROCEDURE

Four different specimens were constructed in the Watkins-Haggart Structural Engineering Laboratory at the University of Pittsburgh. Martin Marietta Composite Inc. provided all the FRP decks panels used in the specimens tested.

Each specimen (e.g., specimen #1 and specimen #2) used two (2) panels measuring 48” long, 38-1/8” wide, 5” thick (extended module deck – two deck sections bonded together). Specimen #3 and specimen #4 used 2 panels measured 48” long, 26-1/2” wide, 5” thick (one module deck).

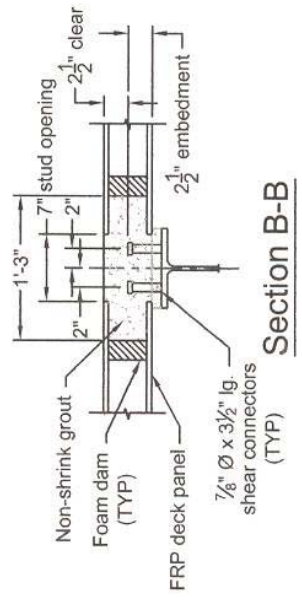
The girders used for these tests were W21x62 sections 42” in length (specimen #1 and specimen #2) and W21x62 sections 30-1/2” in length (specimen #3 and specimen #4), with 2 shear studs installed, side by side, across the flange of the beams at the stud installation location. The W21x62 steel beam sections were recommended by Martin-Marietta as a reasonable design choice given the known properties of the DuraSpan 500 system. At the stud installation location a one inch grout haunch is created between the beam section and FRP decks by providing wooden spacers that also acted as a formwork to contain the grout slurry during pumping. SikaGrout212, a non-shrink material, was used to fill the haunch and stud pocket area. To simulate, to some degree, the dead load of the deck acting on the interfacial bond between the

FRP deck and the steel stringer, a clamping system was used to keep the push-off specimen together. See Figure 3-4, Figure 3-5, Figure 3-6, and Figure 3-7 (respectively).

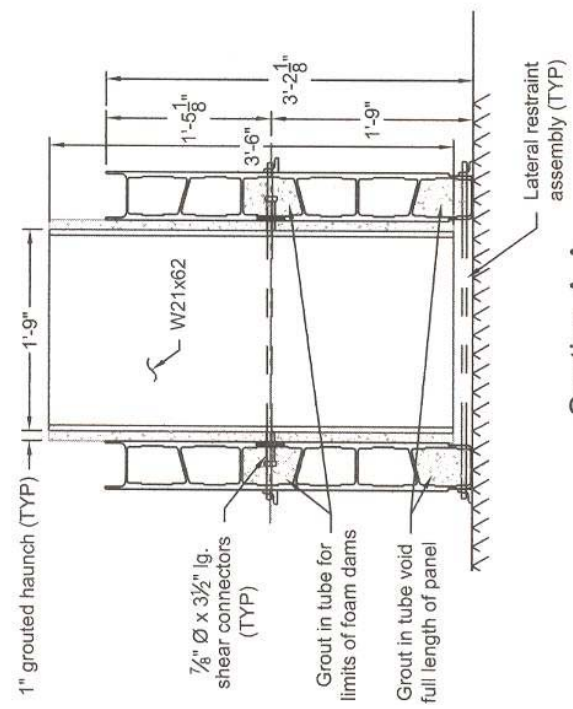


Elevation of Test Fixture

Lateral restraint assemblies not shown.



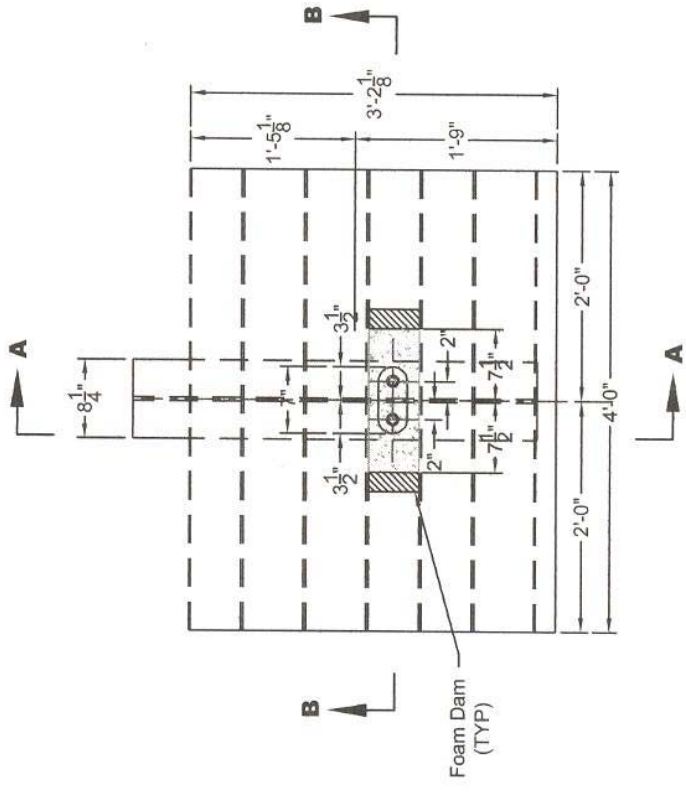
Section B-B



**Section A-A
Through Test Fixture**

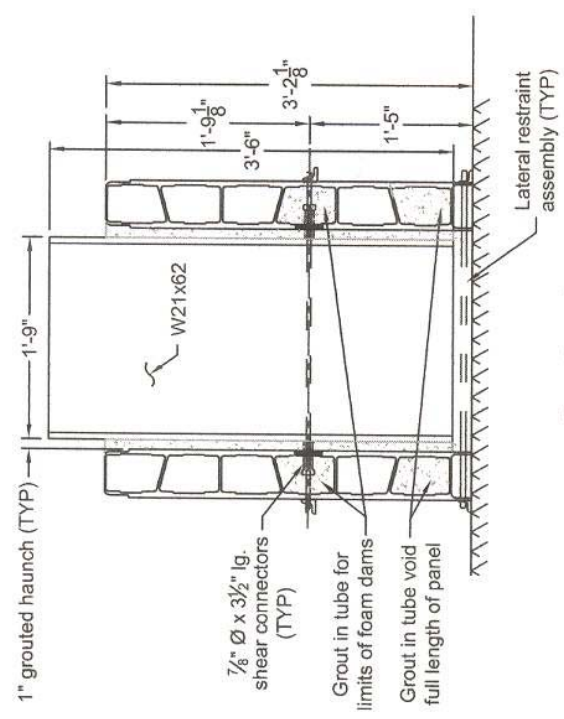
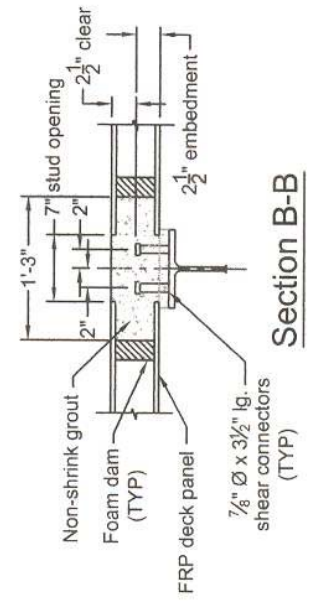
Sample 1

Figure 3-4 Specimen #1



Elevation of Test Fixture

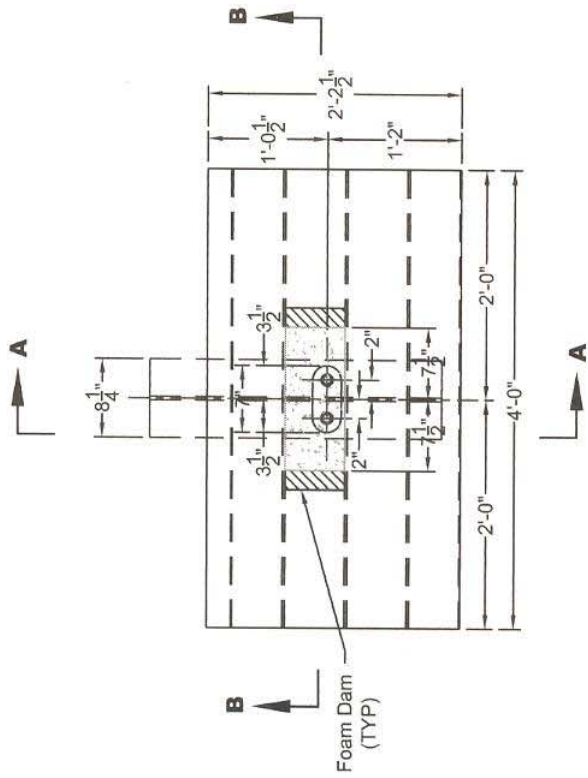
Lateral restraint assemblies not shown



**Section A-A
Through Test Fixture**

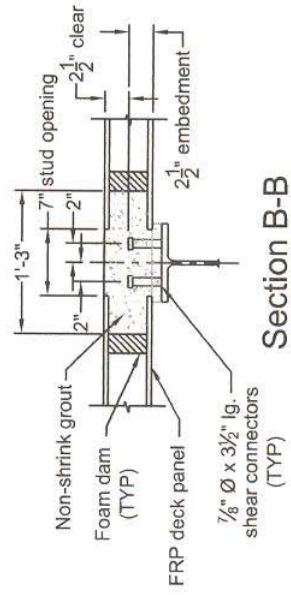
Sample 2

Figure 3-5 Specimen #2

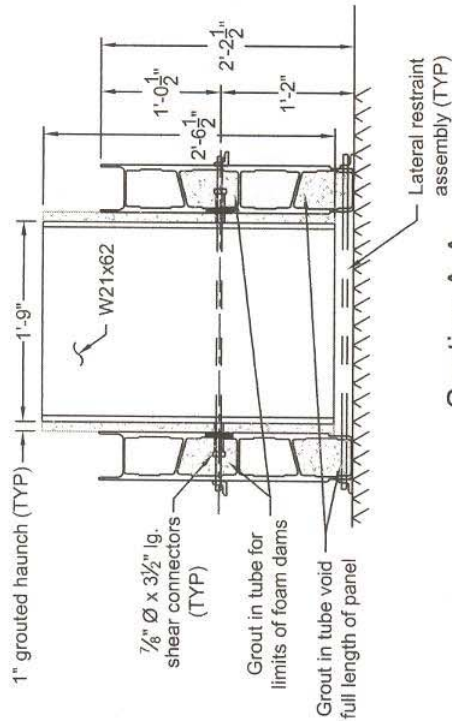


Elevation of Test Fixture

Lateral restraint assemblies not shown



Section B-B

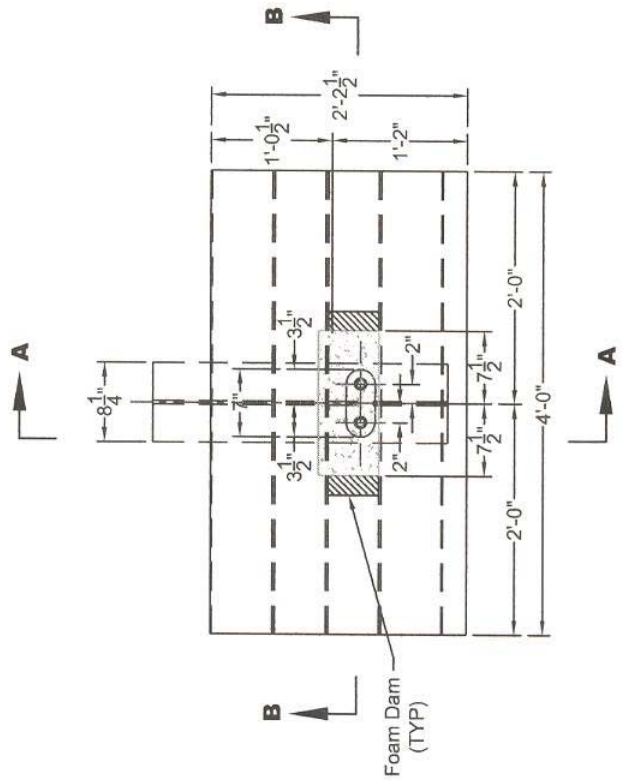


Section A-A

Through Test Fixture

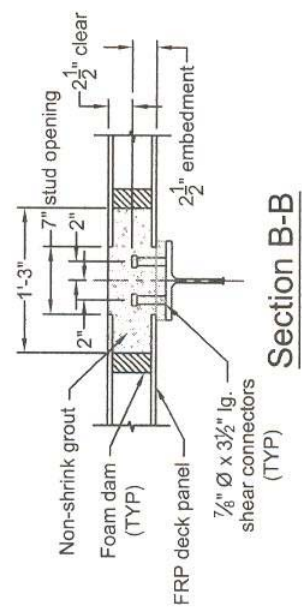
Sample 3

Figure 3-6 Specimen #3

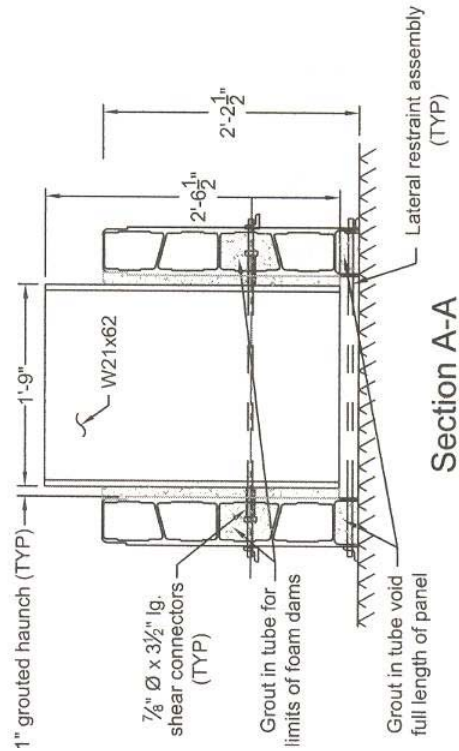


Elevation of Test Fixture

Lateral restraint assemblies not shown



Section B-B



Section A-A

Through Test Fixture

Sample 4

Figure 3-7 Specimen #4

Each specimen then was placed in a testing frame that consisted a thin grout pad (to ensure that the supported end of the specimen was engaging a flat surface) at one end and a three (3) inch thick steel plate with a roller at the other end (extending over the entire steel section, but not touching the grout or FRP deck). A single 200 kip hydraulic actuator applied a force to the roller through a foot attached to a fatigue rated 220 kip StrainSert load cell. An MTS 458 micro-profiler and micro-console were used to control the test in load control mode. Two DCDTs (Direct Current Displacement Transducer), LDC500C model, were used to record the deflection/deformation of the MMC DuraSpan 500 FRP deck relative to the steel girder. The specimens were tested with the standard push through arrangement.



Figure 3-8 Specimen in Loading Frame



Figure 3-9 Failed Specimen

3.3 RESULTS and DISCUSSION

The results of all specimens can be seen in the following table. Load deflection curves are also shown.

Table 3-1 Results of Push-off Testing

Sample	Stud Diameter (in.)	Ultimate Strength (kips)	Strength per Stud (kips)	Stress per Stud (ksi)	Initial Stiffness (kips/in.)
Sample #1 extended deck vertical web	0.875	79.80	19.95	33.10	1.83E+05
Sample #2 extended deck diagonal web	0.875	77.82	19.46	32,37	2.75E+03
Sample #3 one module vertical web	0.875	83.80	20.95	34.86	2.22E+05
Sample #4 one module diagonal web	0.875	74.44	18.61	30.96	1.70E+04

Specimen #1 failed at an ultimate load of 19.95 kips per stud (79.80 kips total). This specimen exhibited a failure of the grout due to diagonal tension near the head of the stud. Two studs in the southern panel (referring to the laboratory layout) failed due to an apparently faulty shear stud installation. There were signs that welding was not appropriately done (see Figure 3-10) In this figure, rusty patches are visible as small crescents facing in, towards one another (and the depicted centerline on the deck). These patches could only have arrived from incomplete welding of the stud to the flanges thus reducing the effective net area in shear present between the flange and the stud shank.

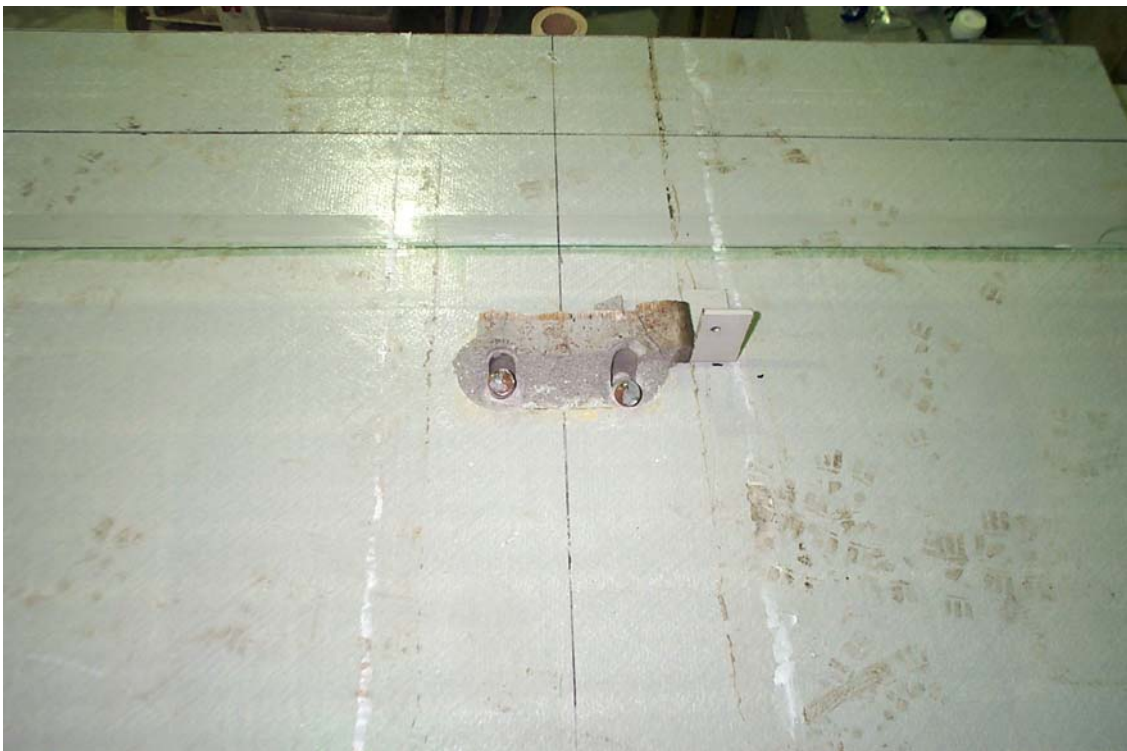


Figure 3-10 Failed Studs - Specimen #1 - Bad Stud Installation



Figure 3-11 Failed Specimen #1

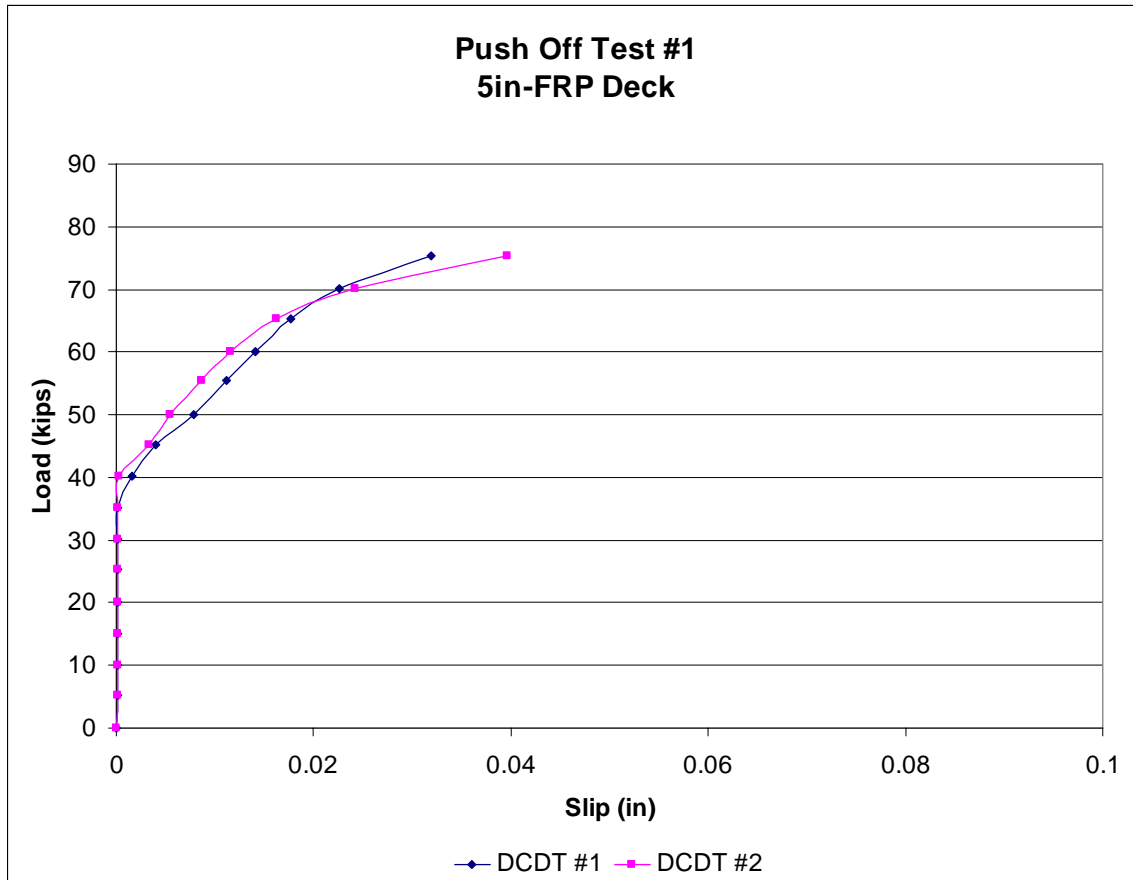


Figure 3-12 Load - Deformation Specimen #1



Figure 3-13 Failed Specimen #2

Specimen #2 failed at an ultimate load of 19.46 kips per stud (77.82 kips total). This specimen displayed the failure of the grout pocket.

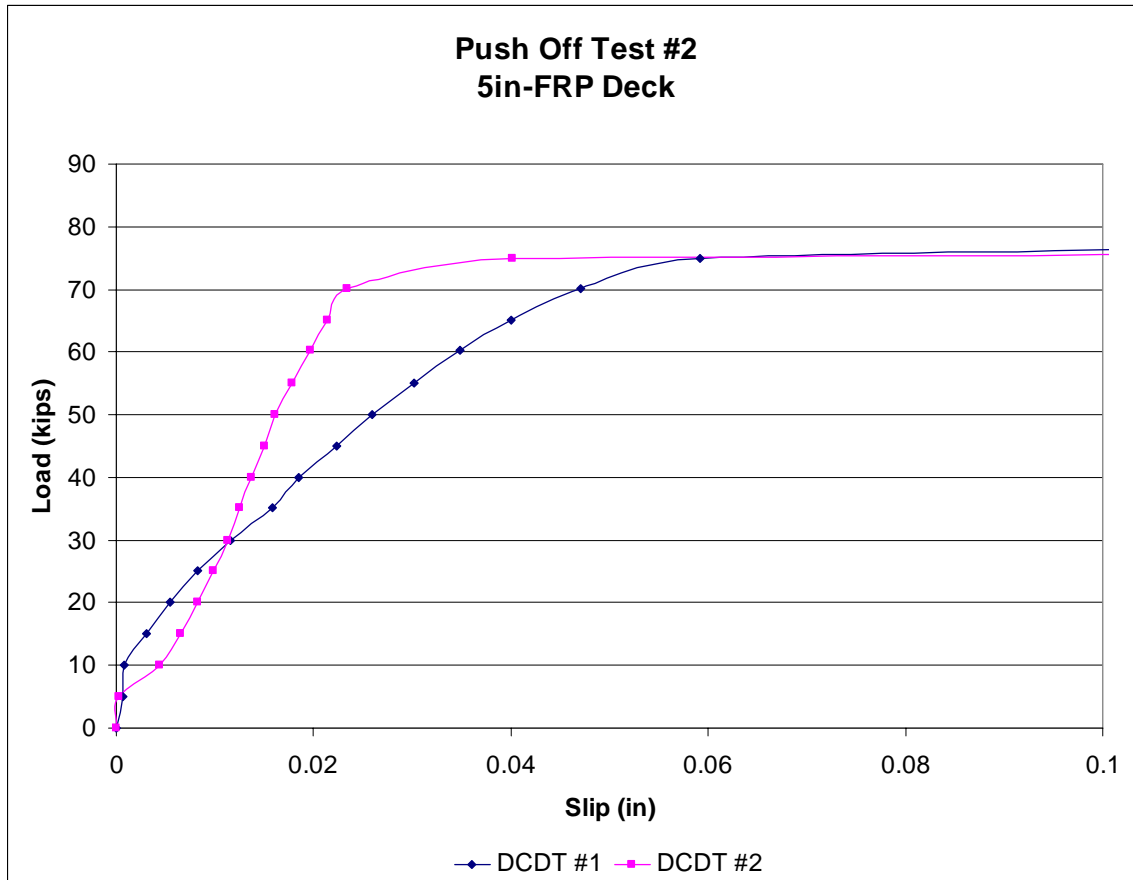


Figure 3-14 Load - Deformation Specimen #2



Figure 3-15 Failed Specimen #3

Specimen #3 failed at an ultimate load of 20.95 kips per stud (83.80 kips total). This specimen showed that the failure of the grout pocket.

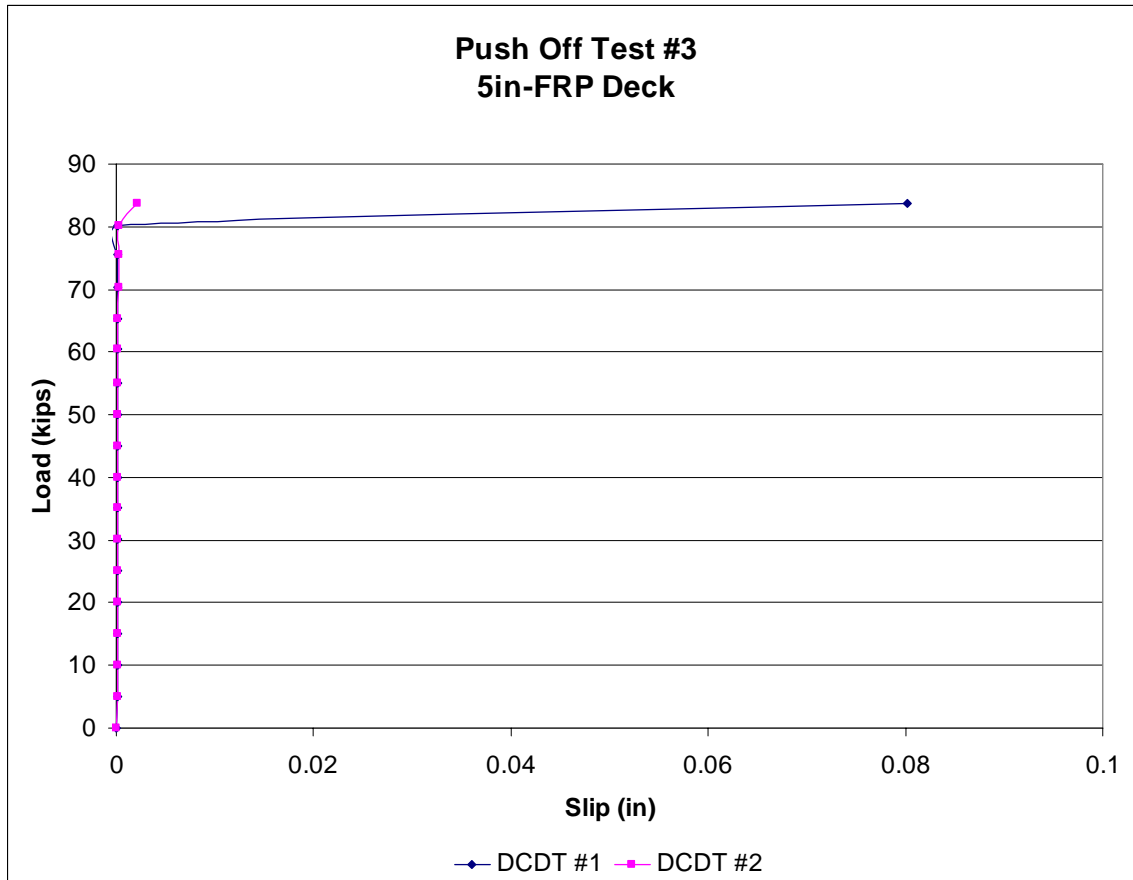


Figure 3-16 Load - Deformation Specimen #3



Figure 3-17 Failed Specimen #4

Specimen #4 failed at an ultimate load of 18.61 kips per stud (74.44 kips total). This specimen showed that the failure of the grout pocket.

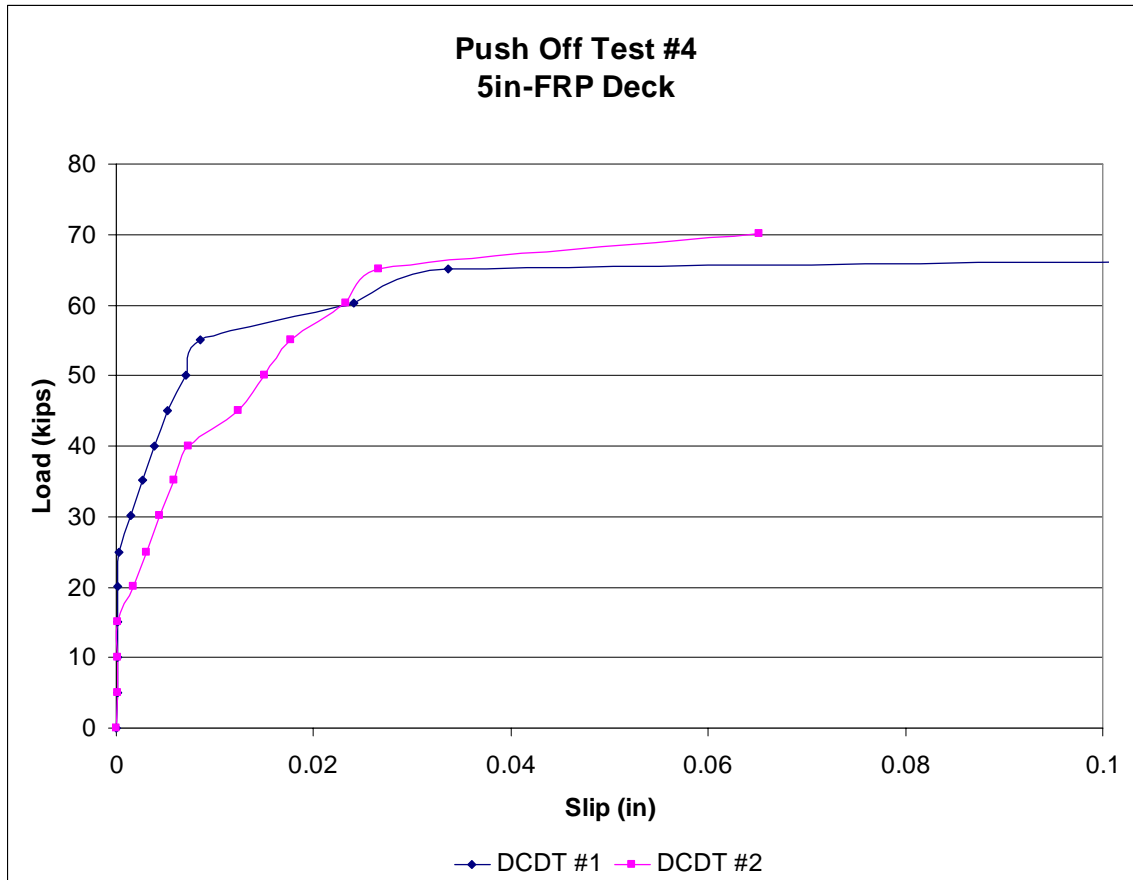


Figure 3-18 Load - Deformation Specimen #4

Except the failed shear studs in the southern panel location of specimen #1, all shear studs deformed without any stud failures. It is interesting to note that some of the specimens appear to deform immediately upon loading, while other specimens seem to exhibit no slip prior to attaining nearly all of the connection capacity. It appears that this is the case since in some specimens the brittle adhesive bond between grout, steel, and FRP remains intact through the start of testing; these are the specimens exhibiting no slip prior to failure. Conversely, the specimens experiencing slip are likely ones that experience some degree of damage to the brittle adhesive bond and thus began slipping almost immediately. Irrespective of intact or damaged adhesive bonding, the ultimate capacity of the specimens remains unchanged since it is the mechanical action of the shear studs (in the plastic range) that determine the connection capacity of the FRP-to-steel composite system.

The AASHTO (American Association of State Highway and Transportation Officials) uses the equation below to calculate nominal horizontal shear capacity of the 7/8" shear stud.

$$Q_n = 0.5A_{sc}\sqrt{f'_c E_c} \leq A_{sc}F_u$$

Equation 3-1

Nominal shear capacity of a single stud (7/8" diameter) is 36 kips ($= A_{sc} F_u$, where A_{sc} = area of shear connector, F_u = ultimate shear stress of connector).

From the result of push-off testing it can thus be said that the shear studs were unable to reach their nominal capacity, as predicted by the AASHTO equation for studs installed in concrete deck (52% - 58% of nominal stud capacity).

Table 3-2 Shear Stud Test Results

No.	Specimens	Push-off Testing (5 in.)
1	Observed Failure Load (kips/stud)	19.95
	Failure Mode	Grout pocket failure, 2 studs at the southern panel failed due to faulty installation weld
2	Observed Failure Load (kips/stud)	19.46
	Failure Mode	Grout pocket failure. All 4 studs deformed without stud failure
3	Observed Failure Load (kips/stud)	20.95
	Failure Mode	Grout pocket failure. All 4 studs deformed without stud failure
4	Observed Failure Load (kips/stud)	18.61
	Failure Mode	Grout pocket failure. All 4 studs deformed without stud failure

Specimen #1 and specimen #3 (both were in the same panel orientation, see Figure 3.2.1 and Figure 3.2.3) were stiffer than specimen #2 and specimen #4 (both were in the same panel orientation, see Figure 3.2.2 and Figure 3.2.3).

Moon et al. (2002) suggested a relationship to account for diagonal web to face sheet delamination failure as following equation:

$$Q_n = t_{fs} d_{sc} F_{frp} \leq A_{sc} F_U$$

Equation 3-2

Applying this equation to the test s presented here would yield a nominal design capacity of 22.00 kip per stud. Push-off test specimens failed at 85% to 95% of the value suggested by Moon et al.

4.0 CONTINUOUS COMPOSITE DECK TESTING

4.1 INTRODUCTION

Maintenance of transportation infrastructure, especially bridges, is a universal increasing interest. The deteriorating condition of bridges has been documented by several researchers [Aref and Parsons, 1996] and recognized by highway agencies [Zureick, 1995] as one of the most multifaceted problems in transportation infrastructure. Fiber Reinforced Polymers (FRPs) are being used in infrastructure as an alternative materials to conventional materials (i.e. conventional concrete) partially as a result of the promise that they hold for long service lives.

While FRP decking has been shown to useful in development to new construction in a demonstration project context, much remains to be done in terms of proving the worth of FRP in the long term, and within a mainstream production context.

To develop economical, efficient, and durable FRP deck systems, a great deal of additional research is required (among other things – such as industry standardization). Analyzing an FRP bridge deck system requires full knowledge of the geometric properties and the material properties. The geometric properties are obtained in the design stage of the deck system. The material and mechanical properties of FRP decks are obtained through experimental characterization of the mechanical properties at the coupon, component, and full deck scale levels.

The first FRP deck research programs conducted in the U.S. [Henry, 1985; Ahmad and Plecnic, 1989] were limited to the development of conceptual design procedures. The results of this early works indicated that the design of FRP deck systems was always controlled by the

deflection limit state (serviceability limit state) rather than the strength limit states. AASHTO (The American Association of State Highway and Transportation Officials) limits the deflection of the deck bridge system as a function of the stringer spacing. Flexural members of the bridge structures are currently required by AASHTO to be designed to have adequate stiffness to limit any deformations that may adversely affect the strength or serviceability of the structure at service load. The deflection limit promulgated by AASHTO in this regard is $L/800$ (where L is the stringer spacing, i.e., the center-to-center distance between decks supports).

Along these lines, a major obstacle to the design of FRP bridge deck is the lack of simplified structural analysis and design approaches. A systematic structural analysis of the deck system will ensure the serviceability of the deck system and build confidence to simplify/optimize the deck structure to reduce the fabrication cost. However, current analytical and design tools developed for conventional materials cannot be directly used for FRP shapes due to the orthotropic of FRP materials.

Although there are no generally accepted principles for current FRP bridge deck design, the general philosophy is that the designed FRP system must have high stiffness and strengths to guarantee appropriate performance and safety with due consideration of the expected life of the structure under a set of defined environmental conditions. In addition, the deck system must be designed to avoid catastrophic failure under impact, collision, or fire and other factors that affect directly to the bridge deck system [Ganga Rao et.al., 1999].

In general, the Fiber Reinforced Polymer (FRP) deck systems are more flexible than conventional reinforced concrete and pre-cast concrete deck systems. The deck rotations over the bridge stringers are larger than typical and as a result haunch durability is a concern as a result of the potential for increased mechanical action degrading the corner of the haunch over time.

Up to now, no official specifications have been proposed for FRP bridge deck design specifically. However, the design load and tire contact area specified in AASHTO Standard Specifications for Highway Bridges [AASHTO, 1996] and the AASHTO LRFD Bridge Design Specification [AASHTO, 1998] have been used for laboratory testing by most FRP deck researchers.

According to AASHTO Standard Specification for Highway Bridges, when designing the bridge deck (the word “deck” is used in a generic sense), the specified loads are applied in critical locations to produce the maximum load effect. The load that produces the largest stress is considered to be the design load. The design engineers can apply the design wheel load over a finite surface area of the deck in computing the load effects in a reinforced concrete deck. This area is defined as the tire contact area and the equation used to compute it is given in the specification based on multiple practical considerations.

The AASHTO Standard Specification provides that a tire contact area shall be assumed as a rectangle with an area in square inches equal to $0.01 P$, and a ratio of length in direction of traffic to width of the tire of 1 to 2.5, in which P is wheel load in pounds.

Although the AASHTO’s specifications provisions are anticipated to be used for reinforced concrete bridge decks, many researchers have used this method to analyze and test FRP decks. Since there are no provisions related to FRP decks in the AASHTO specifications, some researchers used the HS20 truck load and others have chosen the equivalent of an HS25 design truck when applying load to FRP decks [Temeles, 2001]. An HS25 design truck is the same as an HS20 truck except that all loads have been increased by 25%. For example: an HS20-44 truck has a 32 kip rear axle loading 16 kips on each wheel; whereas for an HS25-44 truck, the corresponding load is 40 kips on the rear axles; 20 kips on each wheel.

It was decided that a tire contact area consistent with an AASHTO HS25-44 design truck was a reasonable choice for the current research effort, and thus the tire contact area used herein is 10 inches by 20 inches.

4.2 EXPERIMENTAL PROCEDURE

A full-scale FRP deck (MMC DuraSpan 500, 17' long, 6'-2.5" wide and 5" thick) to underlying steel stringer system was constructed and installed in a specially configured self-reacting load frame. This particular deck system weights about 13 psf and Figure 4.1 shows the dimensioned cross section of a single FRP tube.

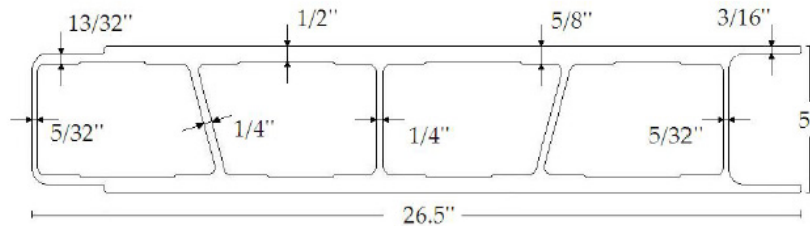


Figure 4-1 Dimensioned Cross Section of a Single MMC DuraSpan 500 FRP Tube

The deck was transversely supported by four W21x62 Grade50 steel beams set 5 ft. on center (the beam size and spacing represented the manufacturers best guess as to a limiting practical design case). The 6'-2.5" wide x 17' lengths of FRP deck were attached to the steel beams with 2, 7/8" headed shear studs spaced 2' on center along the longitudinal axis of the steel beams (see Figure 4-2). A two point concentrated force system was spaced at a 6' interval to simulate the axle of an AASHTO HS25-44 design truck with a tire contact area of 10 inches by 20 inches (see Figure 4-3). The load was monotonically increased until the failure is observed

through the used of two (2) 200kip hydraulic actuators coupled to two (2) separate StrainSert 220 kip load cells (i.e. one per actuator) acting through rollers set against three (3) inch thick steel plates (10" by 20"). The test was run in load control using a MTS 458 Micro-console and Micro-profiler to drive the actuators using a ramp loading function. The back-plane on the Micro-console was split in order that both load cards received the same command signal. The individual cards (one per actuator) then generated valve drive signals based on the individual DC error in each of the two actuators. In this way, good control characteristics were maintained during the testing in order than even loading on both sides of the "axle" where maintained at all the time.

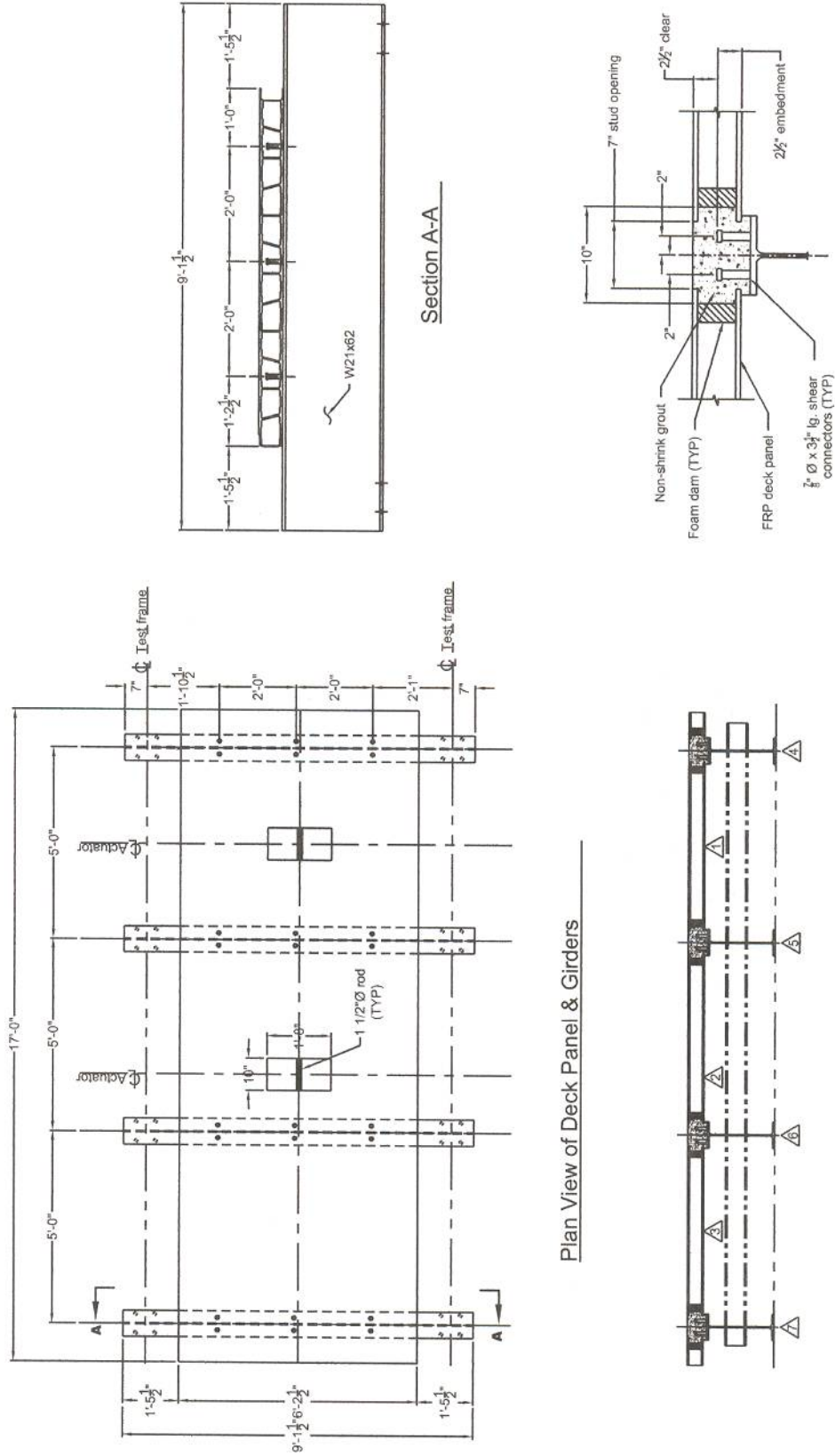


Figure 4-2 Continuous Panel Specimen

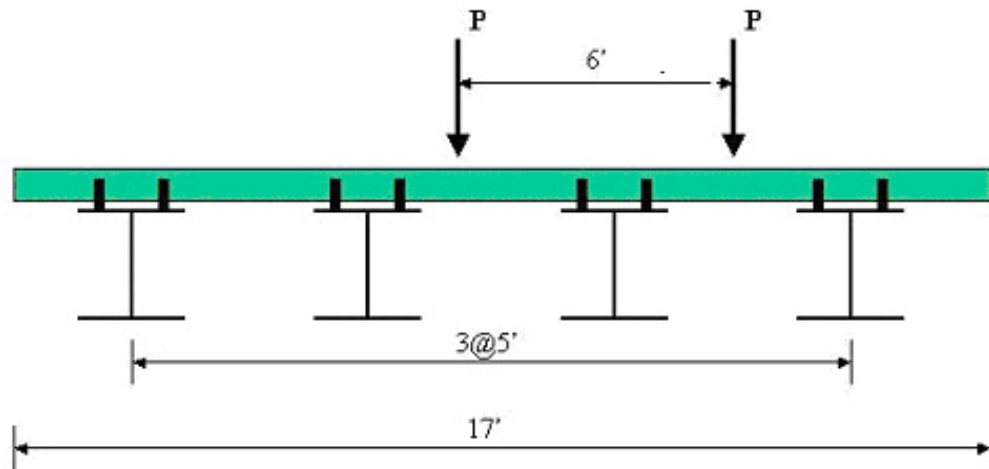


Figure 4-3 Elevation of Composite Deck (un-scaled)

To record deflection of the composite FRP deck, seven DCDTs (Direct Current Displacement Transducers) were placed on the continuous composite deck as can be shown in Figure 4-4.

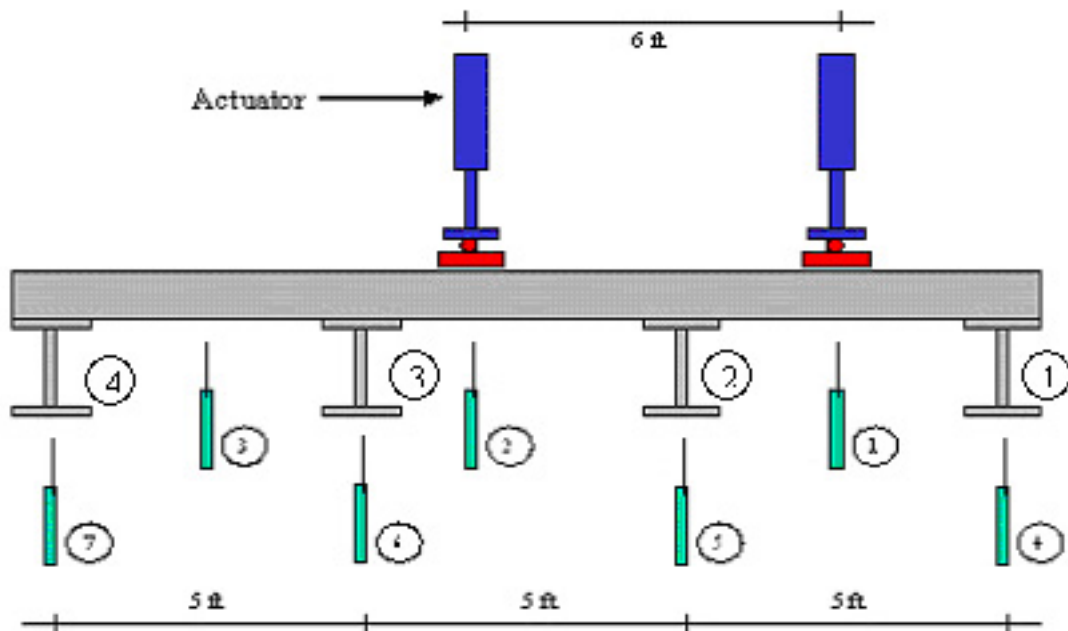


Figure 4-4 Instrumentation Set Up (not to scale)

DCDT #1 was placed under the FRP deck at the location of mid-span between supporting beam 1 and 2. The location of DCDT #1 was in the exact same location where the point load from one of the actuators applied to the tire contact area on the deck. DCDT #2 was placed at a distance of 6 ft from DCDT #1. This was a simulation of the distance between HS25-44 truck design wheels across the traffic direction. DCDT #3 was placed at mid section of the unloaded deck. DCDT #4, #5, #6 and #7 were placed under the supporting beam #1, #2, #3, and #4 respectively. Figure 4-5 below shows how the continuous deck was placed on the load frame. Tire patch was shown on Figure 4-6. It is pointed out that Figure 4-5 also depicts an important bracing system used in the testing of the deck system. A W8x10 was placed on the ends of the W21x62 girders, in a direction that was perpendicular to the stringer longitudinal axis, and then welded done both sided of the web. The end of this bracing member was then welded to the loading frame in such a way that the net effect was to brace the W21x62 stringers against any tendency to roll-over. This bracing system would be characterized as being a “nodal” in nature (AISC 1999).



Figure 4-5 Continuous Decks on the Load Frame



Figure 4-6 Tire Contact Areas

4.3 RESULTS and DISCUSSION

Load versus deflection data were recorded for each section of continuous decks between supporting beams. Deck deflections were subsequently obtained by correcting the raw data for the deformations of supporting beam. For example: deck deflection #1 was obtained from the data of DCDT #1 and corrected from the data of DCDT #4 and DCDT #5. The same method was applied to get the true deflection of other sections of the deck. Deformation of each sections of the deck is plotted in Figure 4-7, Figure 4-8, and Figure 4-9 respectively.

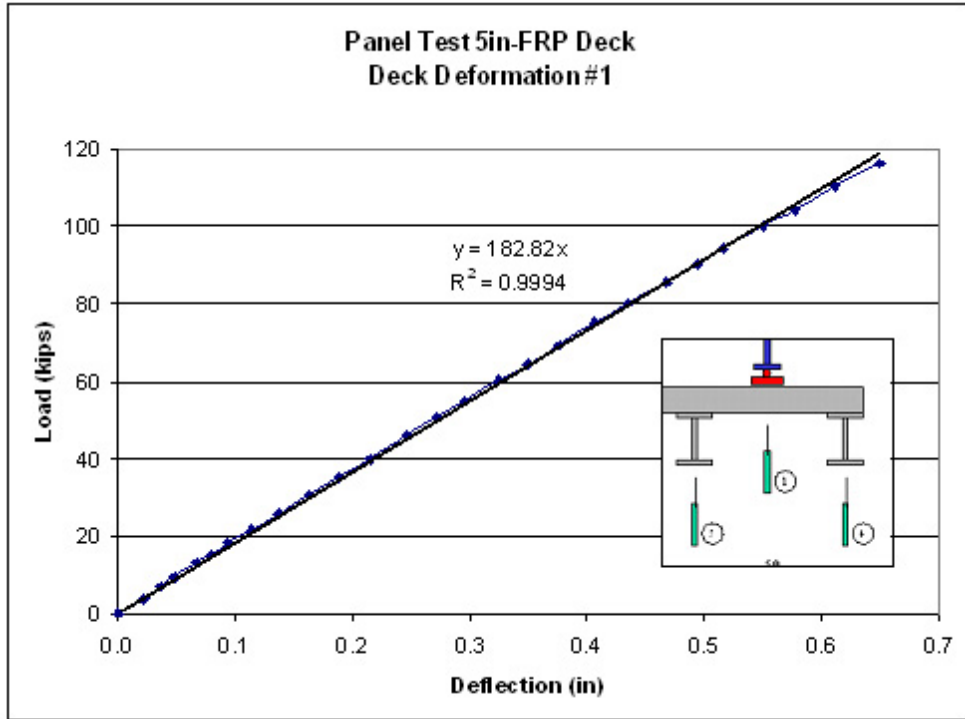


Figure 4-7 Deformation of Deck Section #1

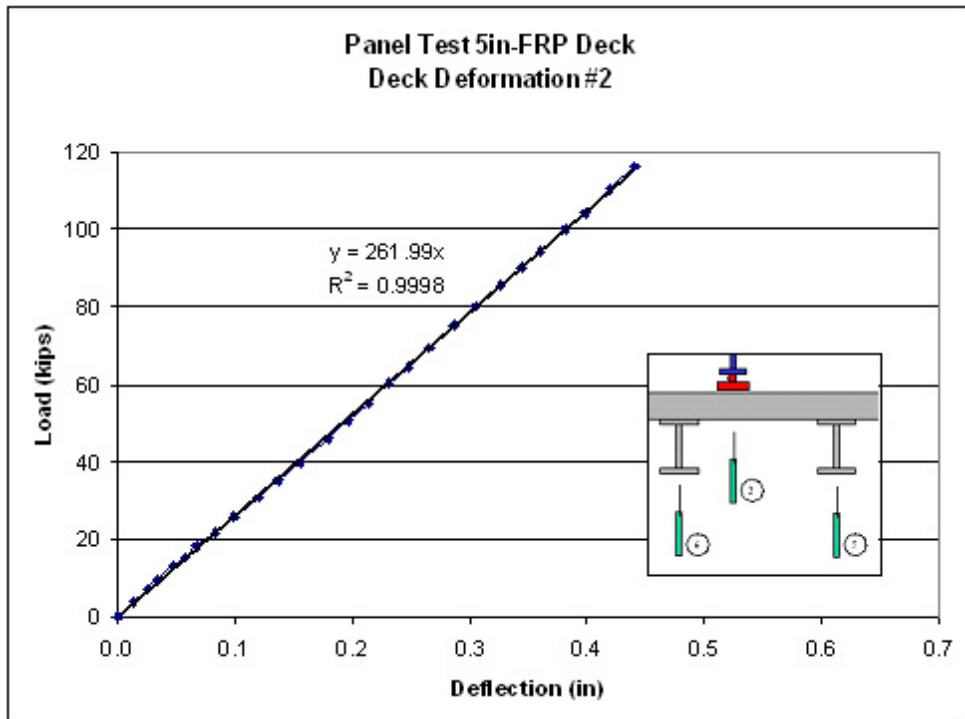


Figure 4-8 Deformation of Deck Section #2

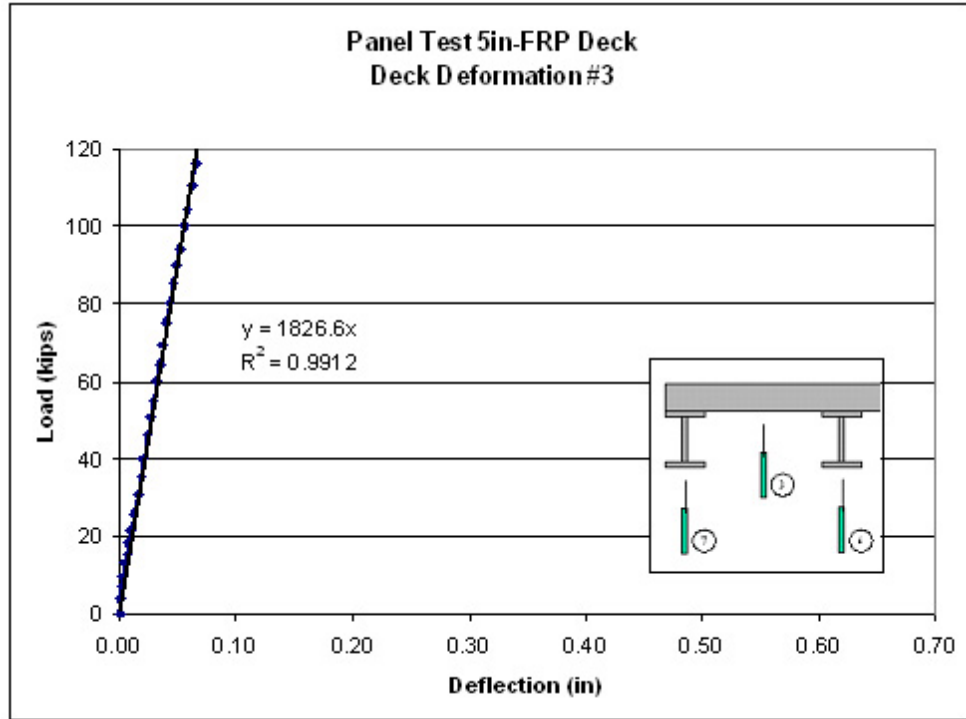


Figure 4-9 Deformation of Deck Section #3

The deformation-load plots are shown in Figure 4-7 to Figure 4-9. Also for all data, a linear equation is presented with displayed R-square value for each recorded deformations as means for judging the quality of response. All results showed linear deformation-load relationship, which indicates that, the FRP deck can be modeled as a linear material for this design context.

From the plotted deformation versus load results, it can be concluded that the maximum deformation developed in section #1 of the continuous deck for the tire contact areas of an HS25-44 design truck. HS25-44 design truck has a 40 kips loading on the back of two axles with 20 kips on each wheels. From Figure 4-7, at service load 20 kips, deck deflected to 0.109 in.

By substituting the maximum deformation at service load, the deflection index for this particular FRP deck is $L/550$ (AASHTO's deformation limit used for reinforced concrete deck is $L/800$). Thus in a parochial sense, the MMC DuraSpan 500 deck tested as described herein, fails

to satisfy the current AASHTO deck deflection limits. It is not clear that this should be a concern, or even if this increased deflection results in haunch rotations that might lead to reduced durability. More study, on much larger numbers of specimens, spanning a more reasonable design space are required in order to be more definitive.

5.0 ULTIMATE STRENGTH COMPOSITE BEAM

5.1 INTRODUCTION

In recent years, FRP composite deck systems have appeared as a practical alternative to conventional reinforced concrete slabs. The use of FRP composite deck systems to replace existing, deteriorated bridge deck systems offers several potential advantages, including the following:

- **Reduced Weight:** the reduced deck dead load allows the bridge to carry increased live loads. In addition, there is a concomitant reduction in erection costs resulting from the requirement for lower capacity cranes needed to install the decks.
- **Environmental Durability:** FRP decks are somewhat corrosion resistant and therefore the long term performance is expected to be improved; thus leading to lower maintenance and longer service life.
- **Speed of Installation:** FRP decks are light weight and deck sections can be pre-assembled in the factory, as a result they can be installed in less time than it would take to build a conventional reinforced concrete bridge deck.

DuraSpan 500 composite FRP deck systems are deployed to the field as one part of two main components: steel stringers and FRP DuraSpan 500 decking. One outstanding question to be answered involved the level of composite action that may be relied on during the design of these FRP-Steel systems. The development of the composite slab concept began in the early 1900s and current practice utilizes composite action between concrete deck and underlying stringers in nearly all situations (e.g. the case where the reinforced concrete deck is made to

develop sufficient horizontal shear capacity such that a single neutral axis develops within the depth of the composite action). However, this relatively mature theory of composite response has not been extended to the application of FRP composite system deck yet. Codes and design guidelines for the application of FRP composites in civil engineering are currently under development. However, this code writing effort is being hampered by lack of availability of good quality experimental testing of such systems and as a result there are no universally accepted codes or design guidelines for FRP bridge deck systems at this time. The present research effort seeks to add to the research base in such a way as to facilitate the specification development process.

While it is that any such specification, or codification of accepted design practice, must treat the composite system as a whole, several different phenomenological features and limit states must be considered individually. For instance, many FRP bridge decks are currently designed using deflection limit design criteria in conjunction with a requirement for low working stress under service conditions. However, there are many other issues related to the strength of FRP decks that need to be considered when designing FRP bridge decks in more efficient and economical ways. Deflection limits may provide designs that are not as economical as possible if the design had been governed with other performance criteria instead.

One very interesting complicating feature of FRP deck bridge systems is that the FRP deck itself is composed of a material type that is somewhat different from more traditional civil engineering materials in a fundamental way. FRP deck is anisotropic as a result of its architecture and manufacturing methodologies. The strength properties of FRP deck are affected by heat input into the system due to the nature of commonly used resin based matrices that have low glass-transition temperatures. Issues such as the delamination of the material components

also figure prominently into gross, or bulk, mechanical properties of thick composite elements (as are common in bridge deck applications).

Since FRP composite structures are generally anisotropic and non-homogeneous, their inner stress state is complicated; even when a simple stress is applied at the global level. The strength of FRP composite materials cannot be simply identified as a single stress level that causes the failure. It is known that the axial, transverse, vertical and shear failure do not independently occur in general FRP composite structures. In fact, a simple stress applied in only one direction at the global level will result in a complex stress state at the local level due to the interaction of the axial, transverse, vertical, and shear stresses as a result of complicated composite architectures. Failure criteria considering the combination and interaction of local stresses have been developed for FRP composites [Reifsnider, 2002]. These failure criteria are cast as functions of independent mechanical response measures that are usually applied individually to each ply of the FRP composite and then superimposed to predict the system response. Ply failure analysis is a more typical method used to investigate the strength of laminated FRP composite structures. The global failure can be defined then by the failure of the critical element in a structure [Reifsnider, 2002], an individual ply in this case. The scale of the critical element can be determined from the region of influence of the local process that determines final failure at the global level, such as the fiber-matrix level, the ply level, the sub-laminate level, and structural level.

All of these complicating factors related to the analytical prediction of strength properties in thick FRP composites, are interesting and important, but they pale when compared with the complexity of strength prediction on larger scale; a scale whose contextual basis is one of more tradition composite construction techniques involving the use of steel and concrete construction

elements. It is in this context that analytical estimates of strength properties are quiet difficult since almost no full-scale experimental data exists on these types of systems; as would be needed to asses the validity and robustness of any theoretical or analytically based strength prediction strategy. The following work endeavors to assist with this current absence of full-scale experimental testing response.

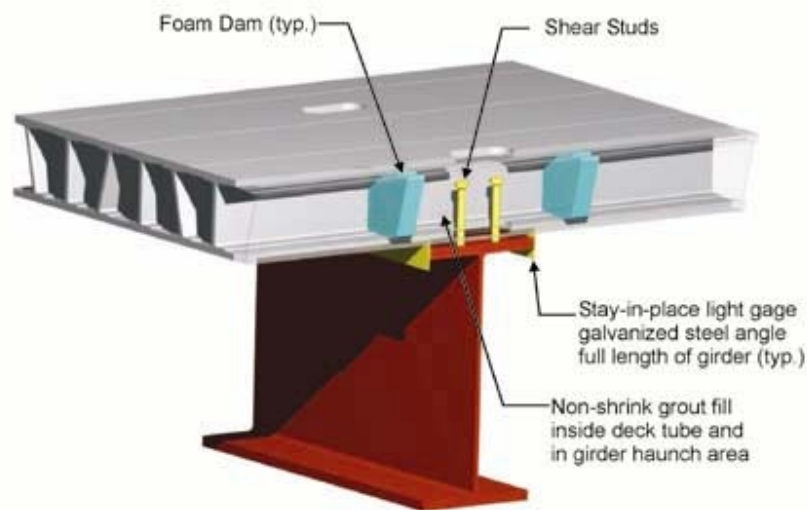


Figure 5-1 FRP Beam Composite Specimen

In this research, a series of two full-scale DuraSpan 500 FRP deck composite specimens were fabricated and tested on site in the Watkins-Haggart Structural Engineering Laboratory at the University of Pittsburgh. Both specimens were identical: consisting of a 12 ft. length of W21x62 Grade50 steel beam with a 12' long by 5'-6" wide FRP deck units attached to the underlying steel beam by way of 7/8 in. shear studs and a 1 in. grout haunch. Two (2) 7/8 in. headed shear studs were installed at locations along the longitudinal axis at 2 ft. intervals (measured on center between locations). The single 12' long, simply supported, specimens were

tested in flexure under the action of single concentrated load imposed monotonically at mid-span; increasing in intensity as a ramp function until failure.

5.2 EXPERIMENTAL PROCEDURE

5.2.1 Test Set-up

Each specimen was prepared, constructed and installed in the load frame according to the specification described in the previous section (i.e. the dimensions are consistent with those mentioned earlier). The specimens were then tested within the self-reacting loading frame depicted in Figure 5-2.



Figure 5-2 Typical Specimen FRP Composite Beam in the Load Frame

The load frame was configured to provide simple support conditions spaced at 11'-0" c/c at the beam ends. This positioning yielded a 6" beam overhang projecting on either side of the supports (i.e. a 6" overhang was used at the supports). A reusable portable formwork system was employed to create the 1" haunch; as specified for both composite beam specimens tested in this work. The FRP deck was placed onto the formwork which was supported by the underlying steel stringer in a way that permitted the shear studs to protrude into the grout pockets of the FRP deck. These pockets were then filled with grout to give the beam its composite nature. Each of the six pockets occupied a 15" wide section of the trapezoidal deck voids.

Prior to placement of the grout, a bead of caulking was employed to seal up the gaps between the deck, the steel beam, and the forms. The non-shrink grout (SikaGrout212) was mixed in a small mechanical mixer and poured into the funnel of a hand grout pump. The grout was then pumped through a hose and into the grout pocket openings on the top surface of the FRP deck. The grout then flowed into the haunch and other stud pockets and was then allowed to cure for 7 days. The results from the grout cube test can be seen in following table where the results from five grout cubes per beam specimen are reported on.

Table 5-1 Grout Cube Test Results

Specimen	Dimension (in)	Average Stress (psi)	Std. Deviation (psi)
1	2 x 2 x 2	3860	378
2	2 x 2 x 2	3540	310

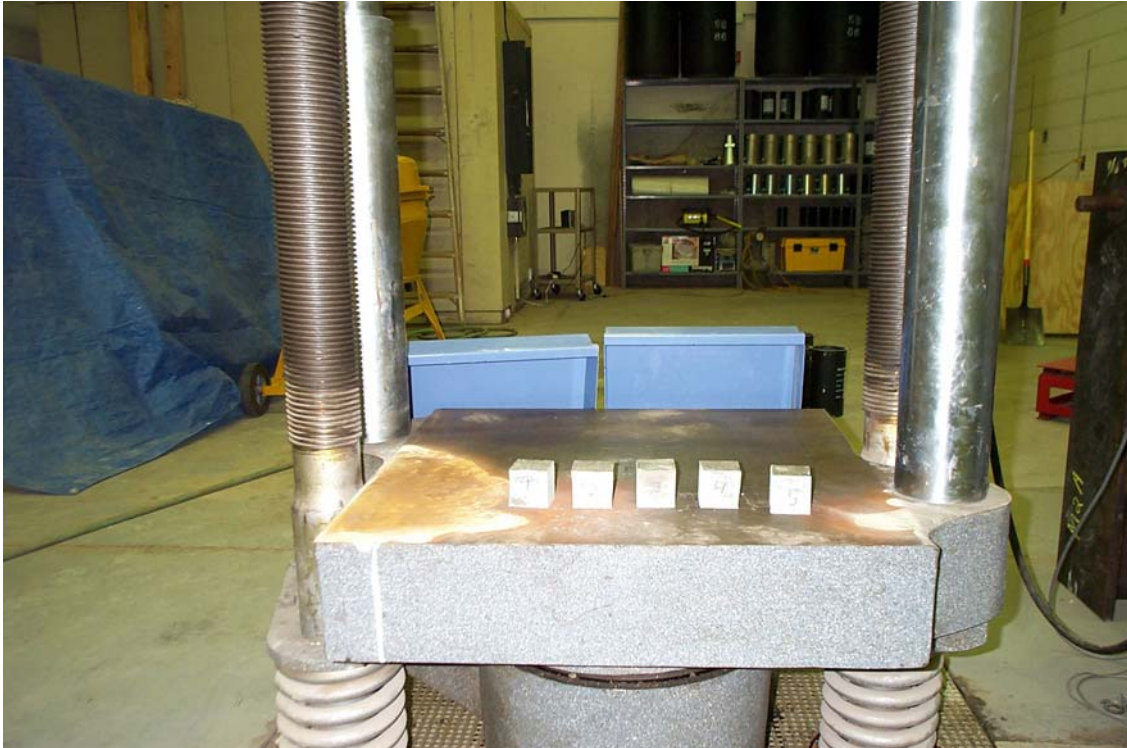


Figure 5-3 Grout Cube Samples

Two 200 kip capacity hydraulic actuators were used in the experiment. Each actuator was attached to a rigid steel frame that consisted of two columns and a cross beam; thus forming a rigid framed bent. The columns were bolted to the load frame through base plate assemblies, the cross beam connected the two columns, and the actuator was in turn attached to the cross beam. The two rigid steel bents were then positioned so as to be 2'-0" center to center; as measured from the centerline of the actuator cylinders. A tire patch, which consisted of a 3"x10"x 15" steel plate with a 3/4" diameter rod welded across the center, widthwise, was placed on the deck straddling the centerline of the specimen. A spreader beam was used so as to apply force from both actuators and have that force transferred to the tire patch right on center.



Figure 5-4 Spreader Beam

Small beams were welded to the frame to provide lateral bracing at the supports. Figure 5-18 and 5-19 are photos displaying the loading configuration described above.

5.2.2 Instrumentation

Each test specimen was instrumented with both strain gages and displacement transducers. The gage instrumentation consisted of a combination of bonded foil gages for steel applications as well as FRP deck applications. The WFLA-6-11-5LT gages (gage length 6 mm) were applied directly to the steel stringer while the FLA-6-11 gages (gage length 6 mm) were applied directly to the face sheet of the FRP deck. Displacement transducers (DCDTs) were used to monitor deflections at mid-span and at the quarter points of the beam. Two transducers were also placed at the ends of rigid bars welded to the beam over the supports for monitoring the end rotations of the specimen. All DCDTs are from RDP-Group LDC3000C model with linear range ± 2.9527 in. Two additional (highly sensitive) displacement transducers (RDP-Group LDC500C with linear

range ± 0.492 in.) were positioned along the interface between the FRP deck and the steel stringer (F-F and G-G cross sections) to monitor interfacial slip during the test (Figure 5-5).

The strain gage is a very sensitive piece of instrumentation capable of recording the smallest imperfections in the bond associated with installation. Therefore, much care must be given to the installation of the strain gage. The rationale behind surface preparation is to acquire a chemically unsoiled surface having an appropriate roughness to that of the gage installation requirements, a surface alkalinity of the proper pH, and discernible gage layout lines for positioning and orienting the strain gage. This surface preparation activity, for the gage installation, was accomplished in three steps. These steps include: solvent degreasing, surface abrasion, and surface neutralizing.

The first step in the preparation of the surface was solvent degreasing in order to remove any grease or oils from the surface. This was done by spraying the surface with the degreaser and immediately wiping it clean. The next step was the abrasion of the surface to remove any paint, scale, or rust buildup on the surface. A grinder was first used remove the heavy rust and scaling at the points of the gage application to the beam. The application points were spaced longitudinally at two feet apart, starting at one foot from the ends of the beam. This coincides with the vertical position of the stud connectors. Vertically along the face of the beam the application points were on the top side of the bottom flange, at points on the web 7 and 14 inches from the bottom of the beam, and on the underside of the top flange. This yielded a total of 36 steel strain gages (Figure 5-5).

Once the base metal was clearly visible via the grinding process, the M-Prep Conditioner A (Vishay Micro-Measurements, Inc) was applied to the surface and the surface was then sanded with coarse sandpaper. The surface was then wiped dry with a clean gauze pad and the process

repeated with the coarse sandpaper and then with finer sandpaper until the surface reached the desired texture.

Once the surface had been conditioned, it was then neutralized with M-Prep Neutralizer 5A (Vishay Micro-Measurements, Inc). The neutralizer was applied liberally to the surface and then dried by wiping through the cleaned area with a single stroke of a clean gauze pad, first in one direction, then with a new pad in the other direction. The strain gages were then applied to the surface. A catalyst was applied to the strain gage in order to accelerate the drying of the M-Bond 200 Adhesive System (Vishay Micro-Measurements, Inc). The adhesive was then applied to the interface between the underside of the gage and the specimen bonding surface; the strain gage was consequently bonded to the surface. This same process, with the exception of the grinding, was done on the FRP deck on the top and bottom faces at a 1' spacing along the width of the deck with respect to the centerline and at a 2' spacing along the length of the beam starting at 1' in from the edge of the deck (i.e. the same longitudinal spacing as used in the steel beam). There were a total of 44 FRP strain gages (Figure 5-6). The gages on the steel were used to locate the neutral axis in the composite cross-section. Additionally, the gages installed on the FRP were used to study the shear lag effects across the FRP deck width and along the beam length during testing.

The strain gages were individually checked after installation to make sure they were functioning properly by using a digital strain indicator P-3500, from Vishay Measurements Group. A steady strain reading from the P-3500 strain indicator signals a successful installation. All strain gages were numbered and connected to Vishay-Micro Measurements System 5000 and attached to a data acquisition system running the software StrainSmart.

The actuators were each controlled on independent channels of an MTS 458 Controller, running in load control, through a single command signal generated by a micro-profiler whose signal was split in two at the micro-console back-plane; thus sending the same command signal to both channels. The total load was monotonically increased in increments of 10 kips, using a ramp function; until failure occurred.

Ultimate Strength Test for 5" FRP Deck

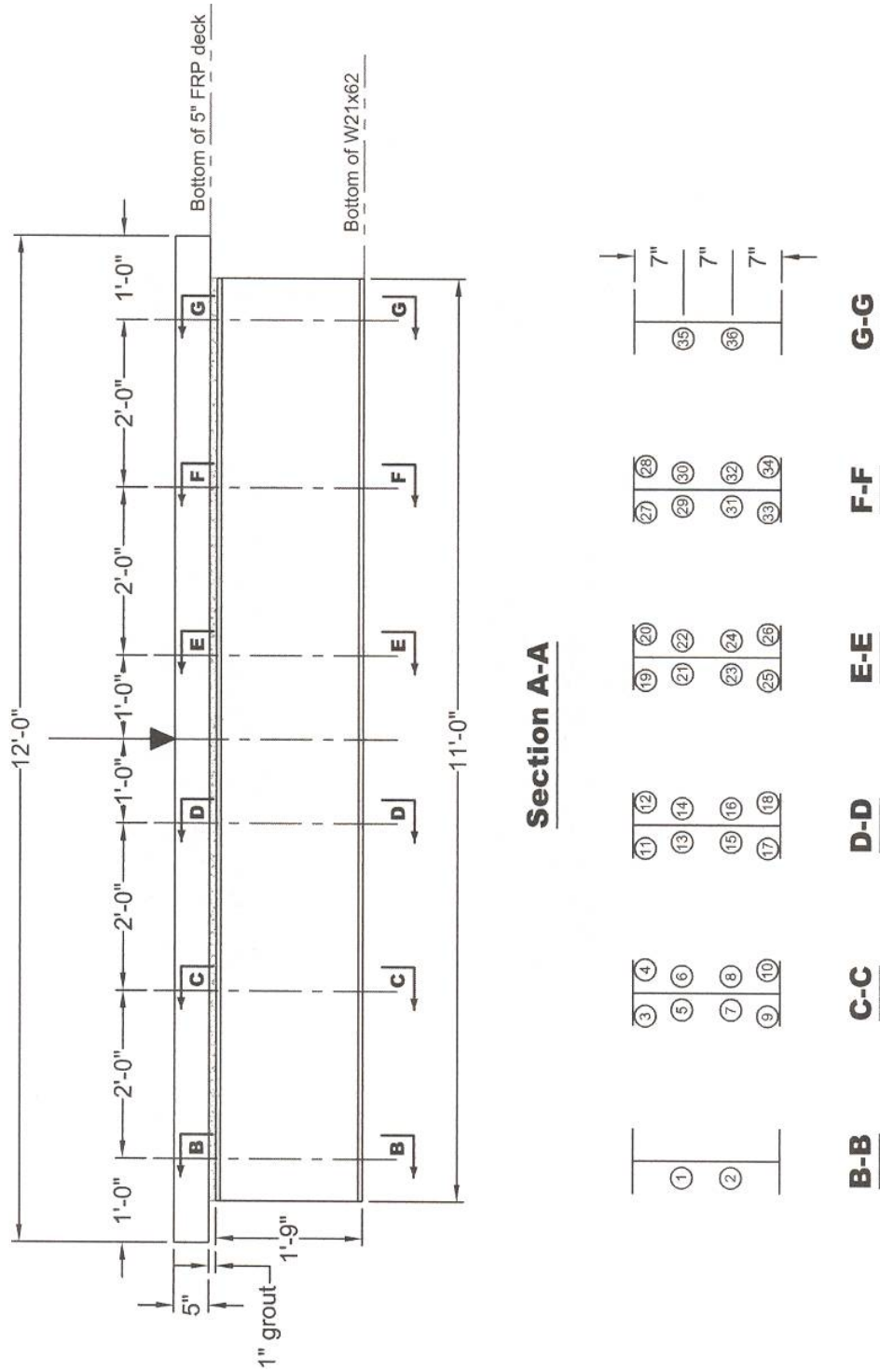
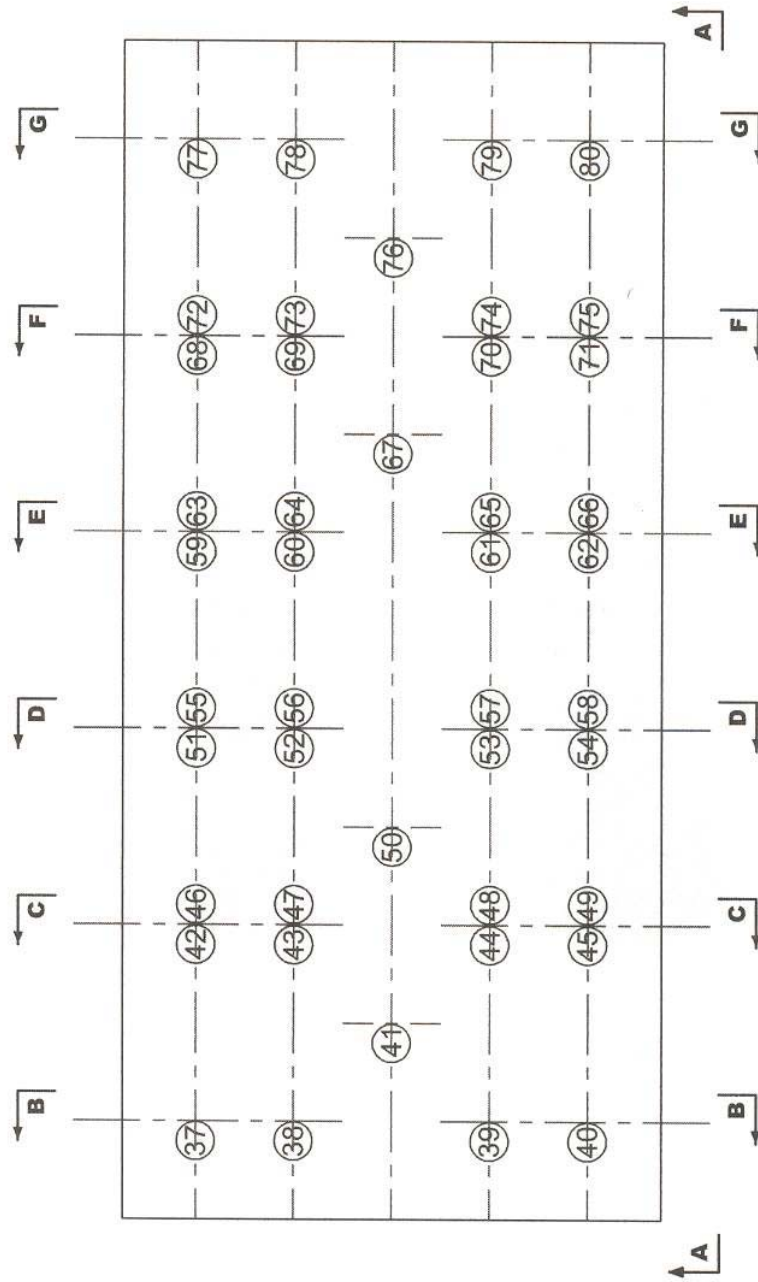


Figure 5-5 Elevation & Cross Section of Composite Beam

Ultimate Strength Test for 5" FRP Deck



Note: All gauges are aligned with the center line. Numbers on the **left** of the centerline indicate **top** placement, numbers on the **right** of the centerline indicate **bottom** placement.

Plan View of FRP Deck

Figure 5-6 Plan View of Composite Deck

5.3 RESULTS and DISCUSSION

Composite bending action between FRP deck and the underlying steel stringer is similar to the behavior of conventional composite construction involving reinforced concrete – steel beam behavior.

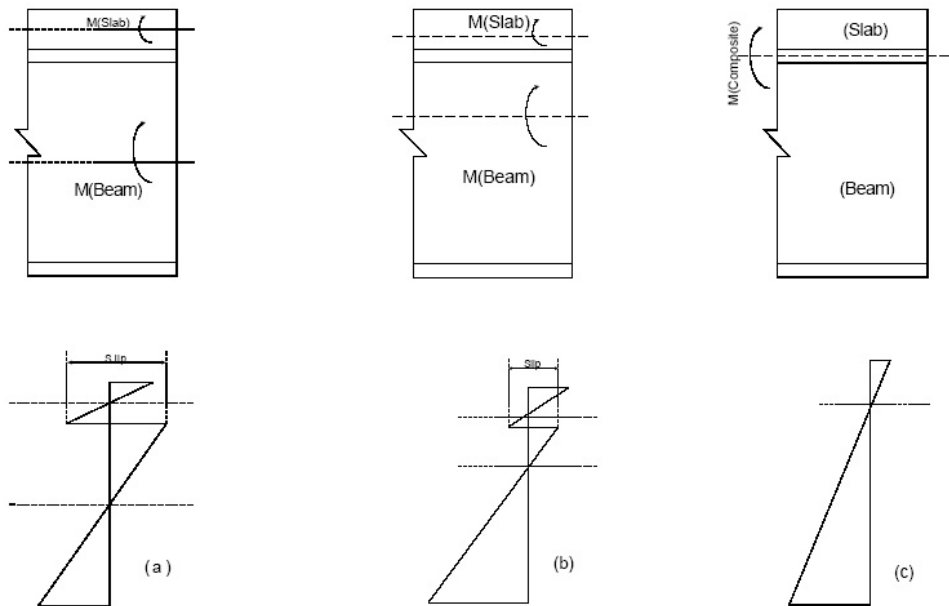


Figure 5-7 Strain Variation in Composite Beam

When a system acts compositely (Figure 5-7b and 5-7c) the deck and stringer are interacting, and the neutral axes begin to migrate toward one another; becoming a single neutral axis when deck and stringer act as a fully composite system.

All the obtained data using the StrainSmart Data Acquisition System from the tests reported on herein were used to calculate the location of the neutral axis for each of the four instrumented cross sections in each of the two beam specimens. The experimental results reveal the canonical linear relationship between longitudinal strain distributions through the cross-

sectional depth of the beam as predicted from Navier's hypothesis. The strain variation plots can be seen in Figures 5-8 to Figure 5-11 respectively.

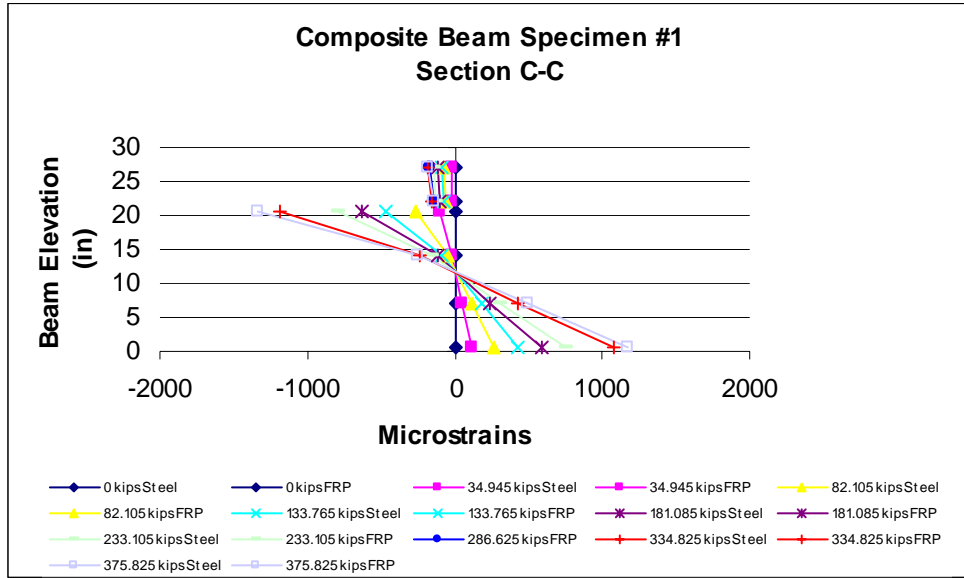


Figure 5-8 Strain Variation Section C-C Specimen #1

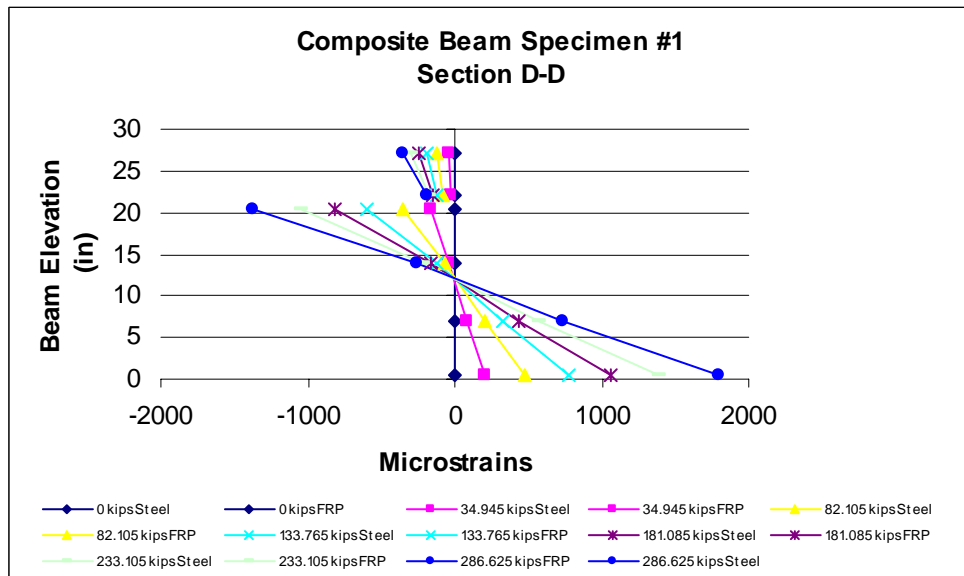


Figure 5-9 Strain Variation Section D-D Specimen #1

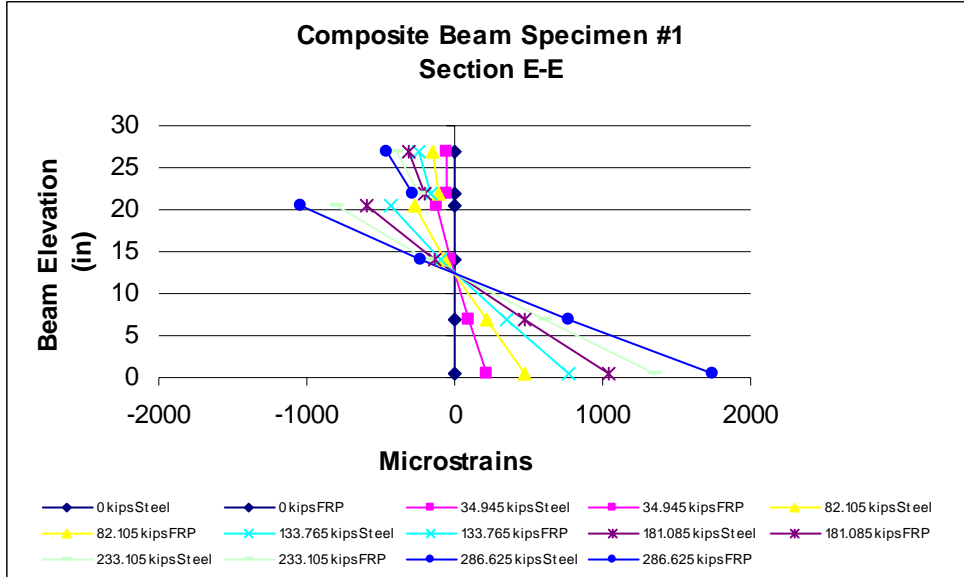


Figure 5-10 Strain Variation Section E-E Specimen #1

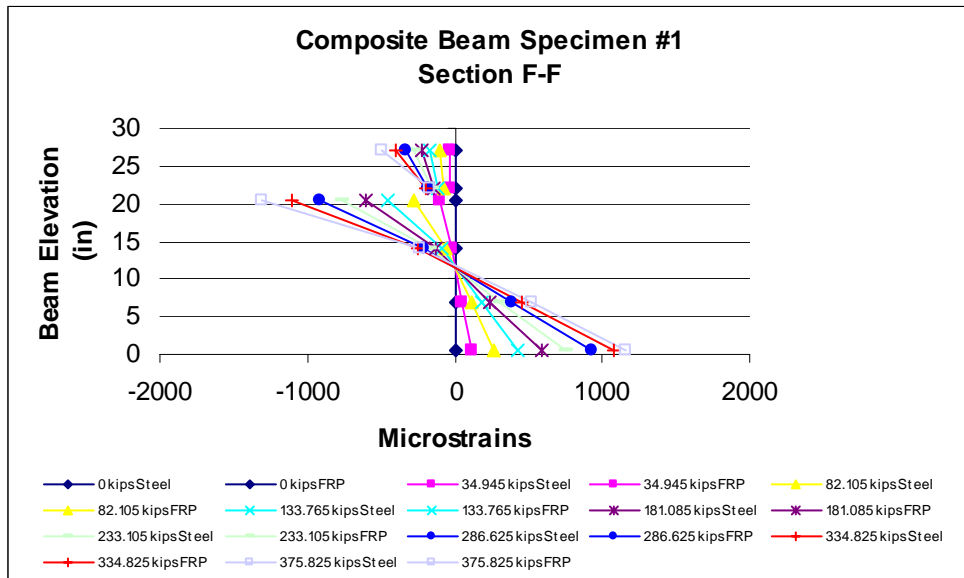


Figure 5-11 Strain Variation Section F-F Specimen #1

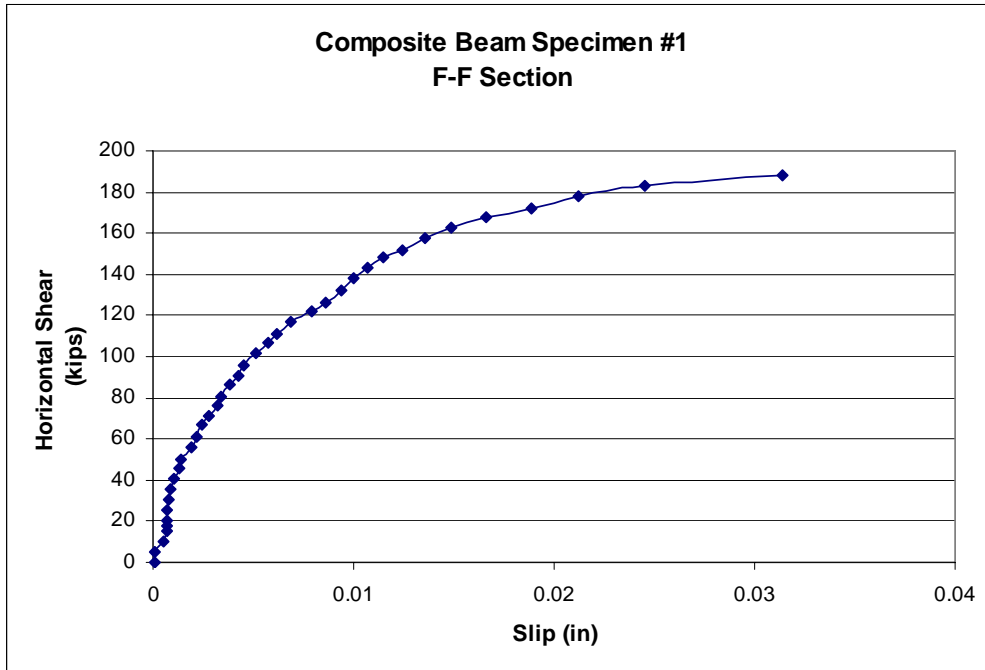


Figure 5-12 Slip between Deck and Beam Test #1

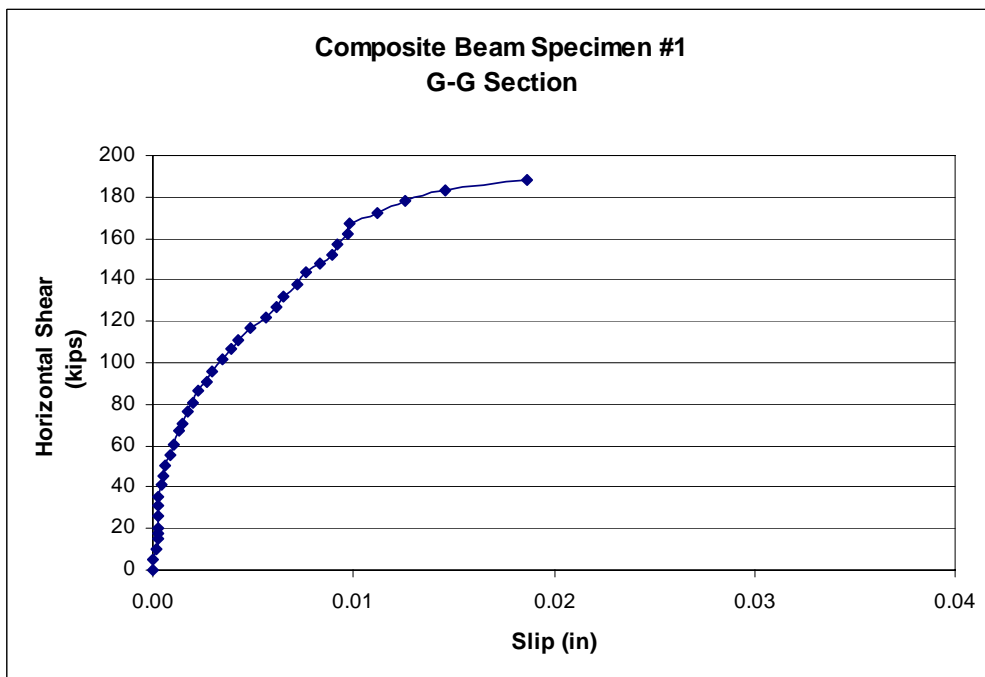


Figure 5-13 Slip between Deck and Beam Test #1

From strain variation in composite beam plots (Figure 5-8 to Figure 5-11 respectively), it can be said that FRP deck and the beam specimen #1 are interacting in a partially composite way at large loads as evidence by the discontinuity in strain at the FRP-to-steel interface. This result means that there was slip between FRP deck and steel beam. It is also noted, from the Figure below, the strain variations are relatively small; thus it can be said that at service load (e.g. 0-30 kips) the FRP deck and steel beam are acting partially composite (Figure 5-14 to Figure 5-17 respectively).

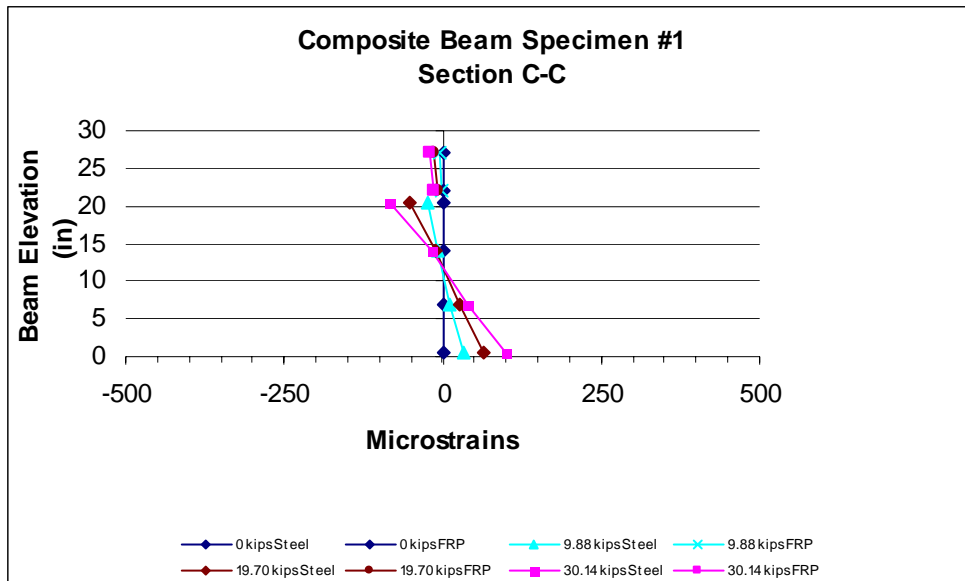


Figure 5-14 Strain Variation at Service Load

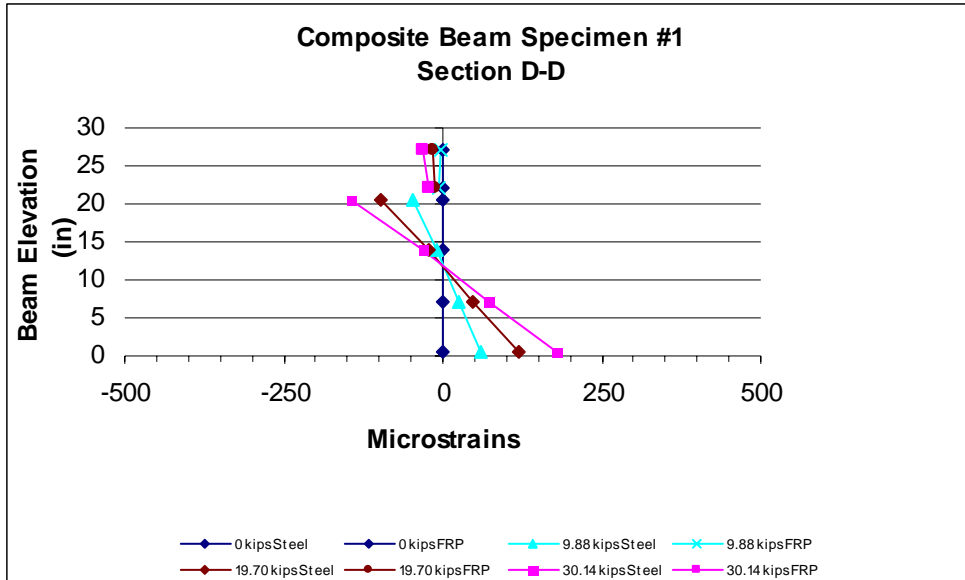


Figure 5-15 Strain Variation at Service Load

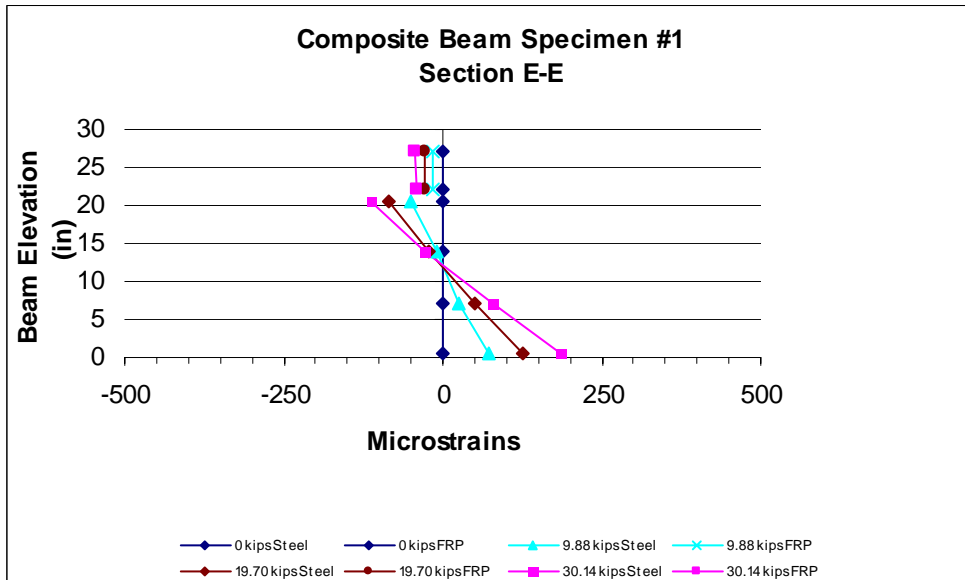


Figure 5-16 Strain Variation at Service Load

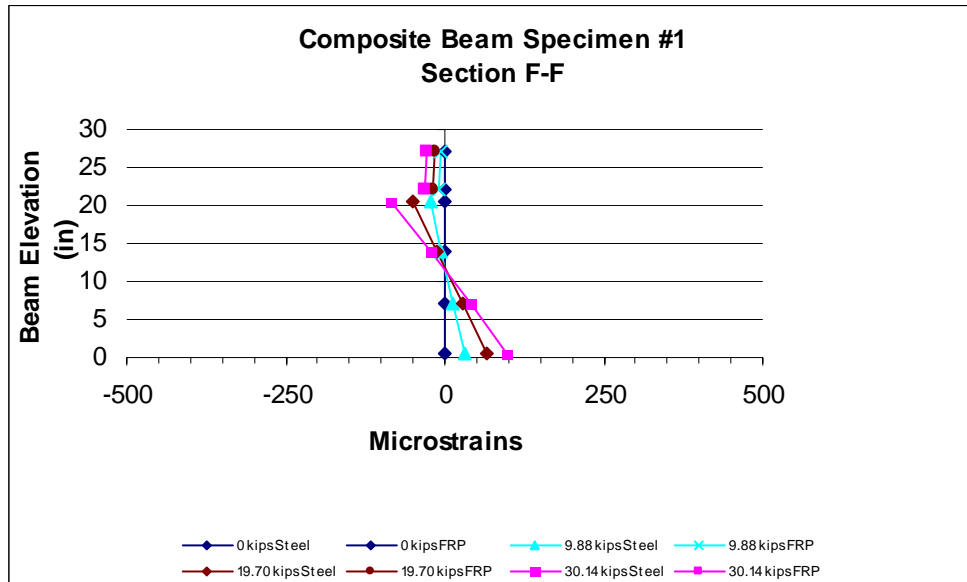


Figure 5-17 Strain Variation at Service Load

The calculation of location of neutral axis for each load and each cross section area of the beam can be seen in the table following:

Table 5-2 Calculated Neutral Axis Beam Specimen #1

No.	Load (kips)	Bare Steel	C-C (in.)	D-D (in.)	E-E (in.)	F-F (in.)
1	0					
2	34.945	10.500	11.524	11.730	12.627	11.332
3	82.105	10.500	11.075	12.037	12.946	10.876
4	133.765	10.500	10.789	11.951	12.893	10.877
5	181.085	10.500	10.869	11.934	12.848	10.894
6	233.105	10.500	10.871	11.962	12.730	10.907
7	286.625	10.500	10.761	11.920	12.725	11.021
8	334.825	10.500	10.687			10.892
9	375.825	10.500	10.653			10.789

The FRP composite beam test #1 failed at 375.825 kips with the failure mode being a breach of the face sheet of the FRP deck by the loading pad (i.e. the composite beam system did not fail – the tire patch locally damaged the deck and interrupted the testing). It is pointed out that this local failure occurred despite the fact the pultruded FRP tube directly under the load was purposely filled with grout to provide extra support for the loading pad. The precipitating cause of this failure was the spreader beam changing angle from the horizontal to such a degree that the edge of the bottom flange began cutting into the top face sheet of the FRP deck.

However, useful information can still be obtained from this test. By employing transformed section method from elementary mechanics of materials, in conjunction with some approximating assumptions, the effective width of the FRP composite beam test #1 can be calculated. The assumptions are as follows:

- The analysis for effective width involved theory of elasticity applied to plates, using an infinitely long continuous beam on equidistant supports, with infinitely wide flange with small thickness compared to the beam depth.
- Only a portion of the FRP cross section is effective in resisting the compressive stresses that develop during the formation of the internal equilibrating moment of the composite cross section.
- The neutral axis located at the steel section is considered as basis for calculating effective width. It is shown that FRP deck and steel beam are not interacting in a fully composite fashion.



Figure 5-18 Typical FRP Composite Beam Specimen



Figure 5-19 Typical Specimen FRP Composite Beam in the Load Frame

The second, identical, FRP Composite Beam Test Specimen #2 gave the results presented below. The FRP Composite Beam Test Specimen #2 failed at 351.145 kips with failure mode involving a catastrophic break-down of the composite interfacial bond between the FRP and the steel beam. It is encouraging to note that based on this failure load, the local failure load associated with Specimen #1 was clearly close to that of the more pertinent global mode exhibited by Specimen #2.



Figure 5-20 Failed Specimen #2 (note: web side-sway buckling followed after interfacial bond failure)

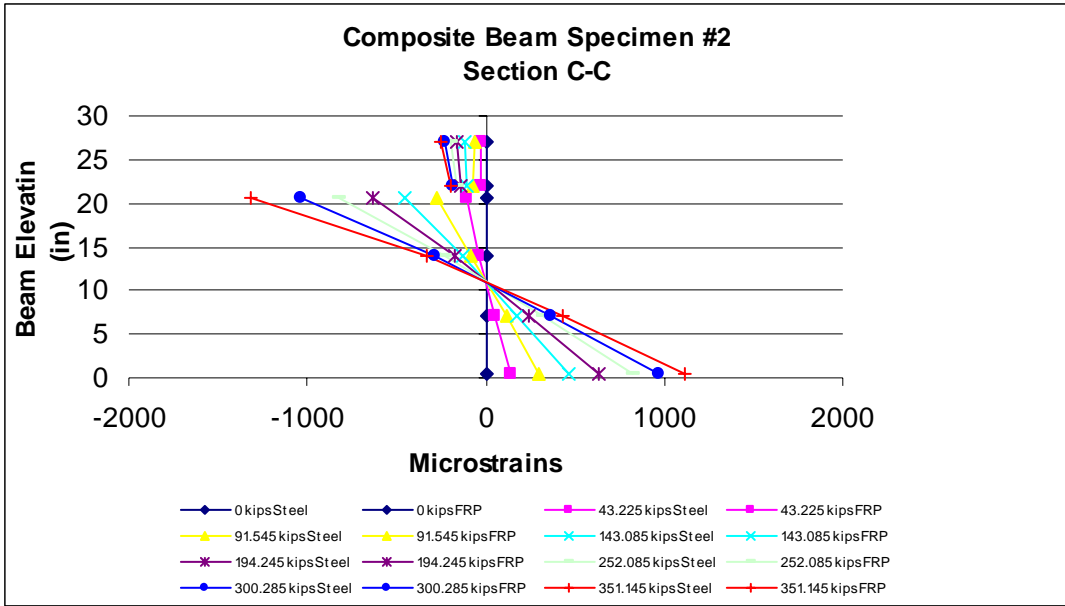


Figure 5-21 Strain Variation Section C-C Specimen #2

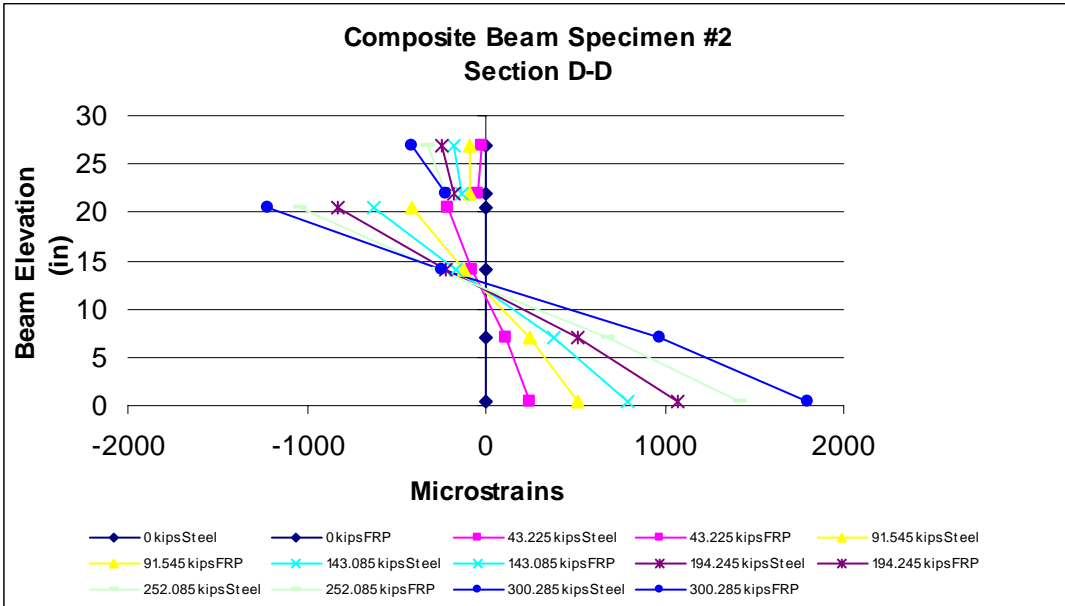


Figure 5-22 Strain Variation Section D-D Specimen #2

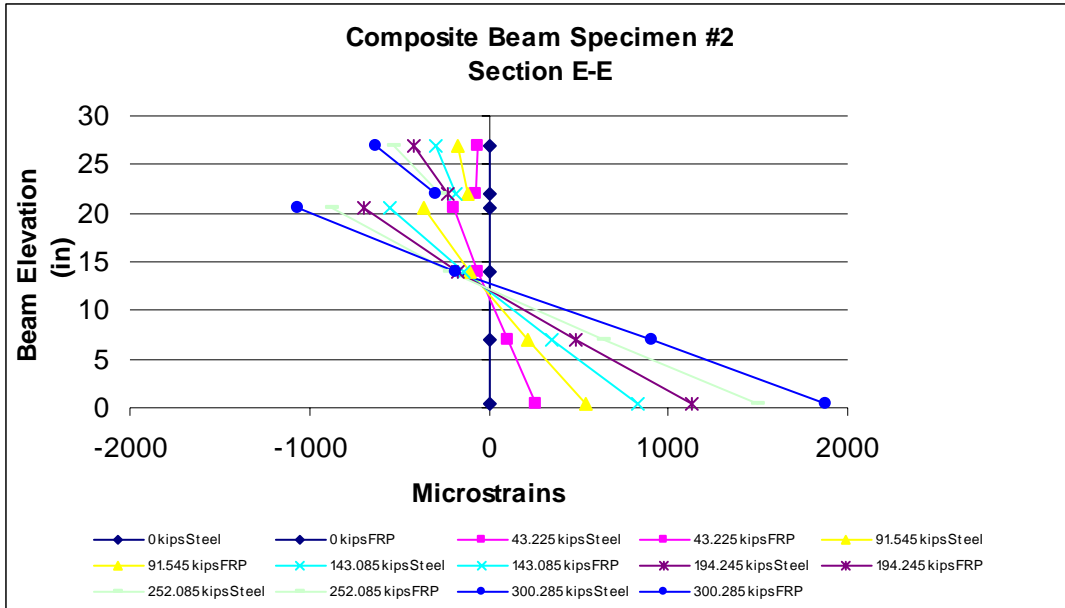


Figure 5-23 Strain Variation Section E-E Specimen #2

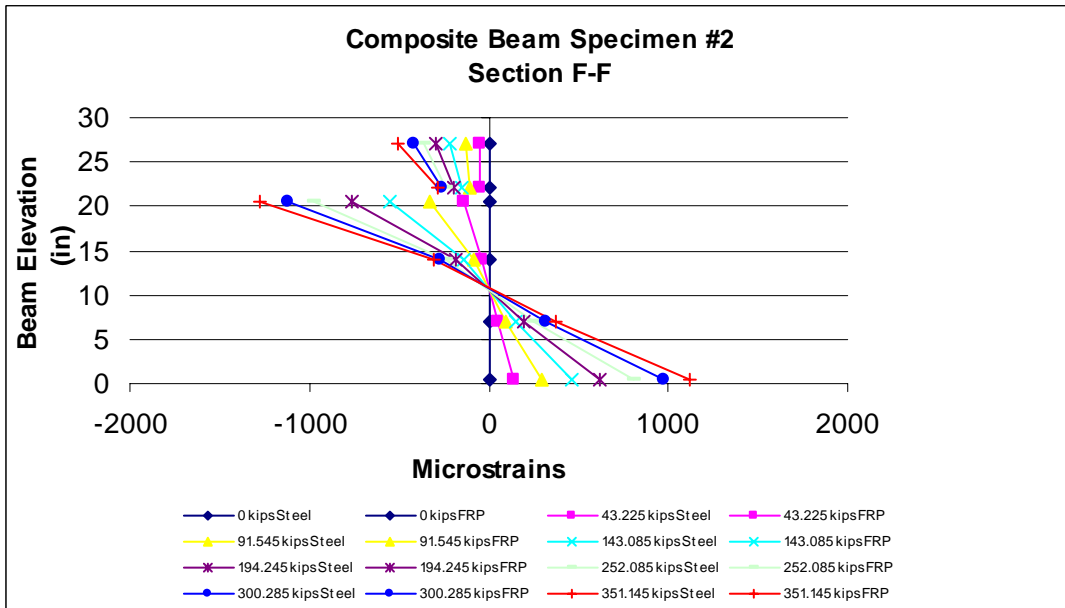


Figure 5-24 Strain Variation Section F-F Specimen #2

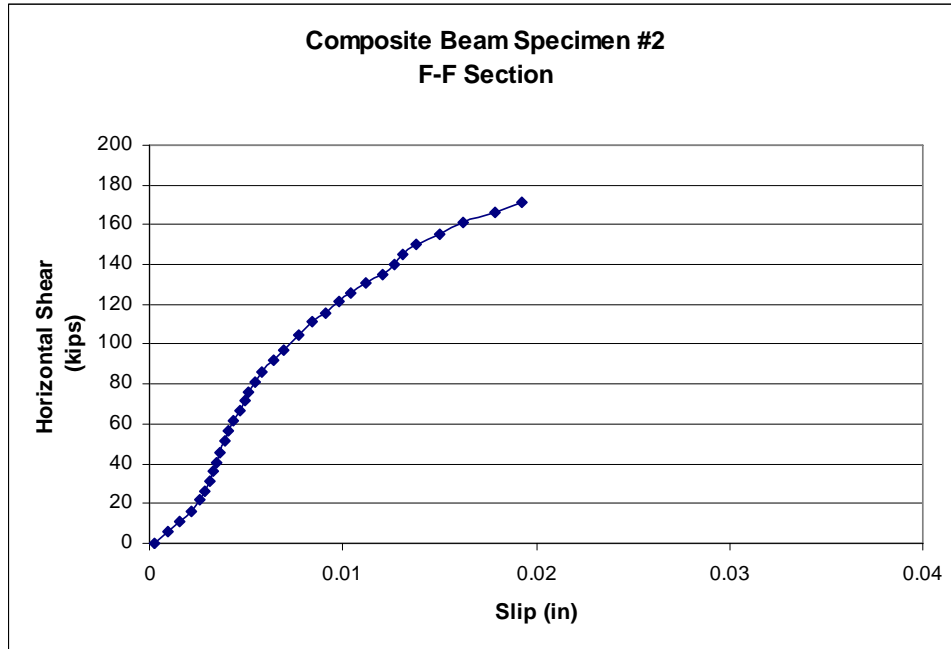


Figure 5-25 Slip between Deck and Beam Specimen #2

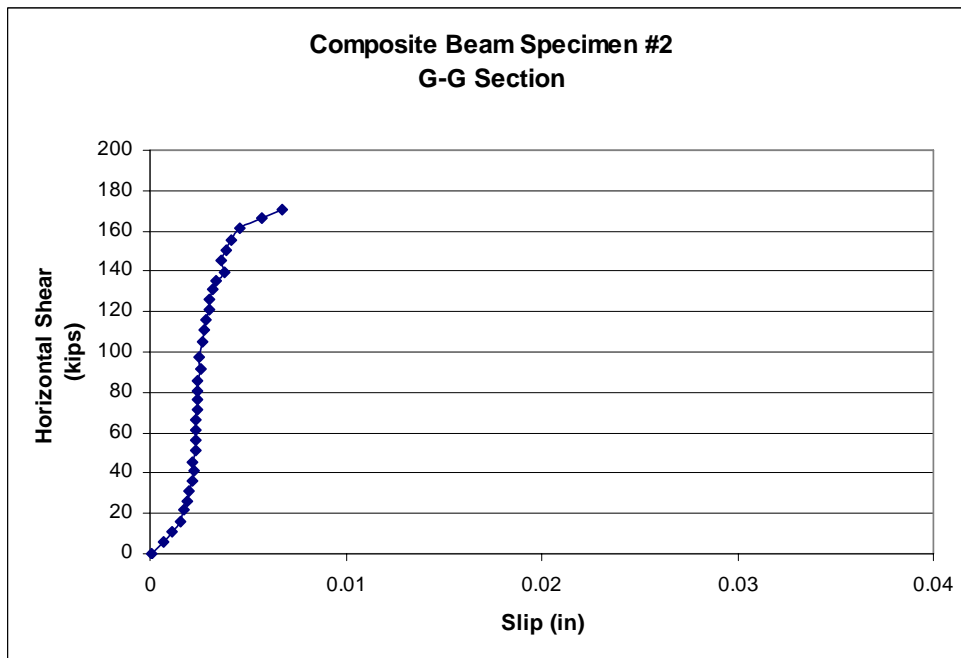


Figure 5-26 Slip between Deck and Beam Specimen #2

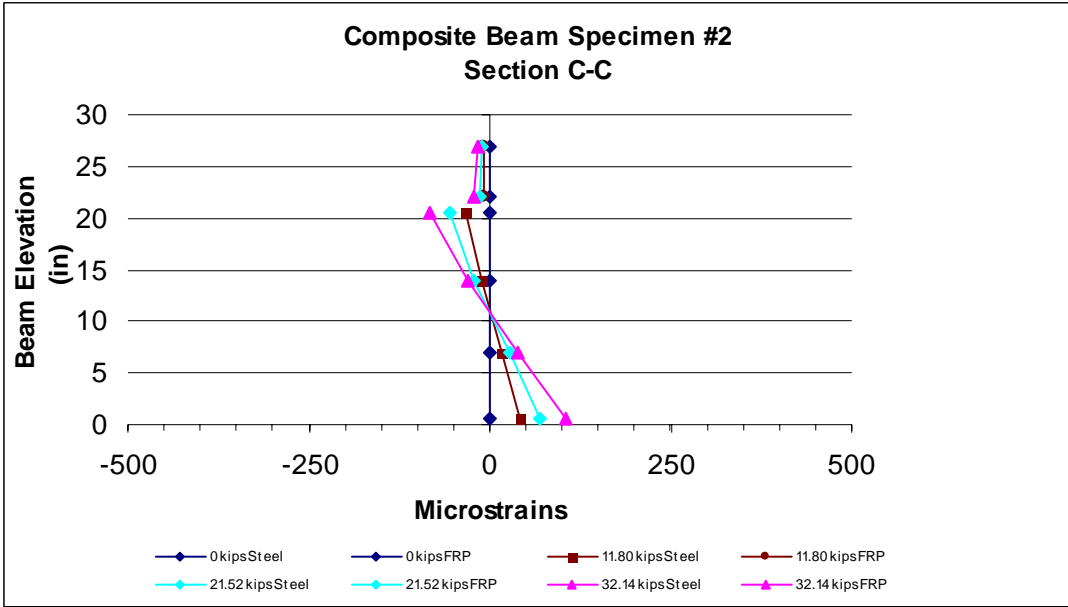


Figure 5-27 Strain Variation at Service Load

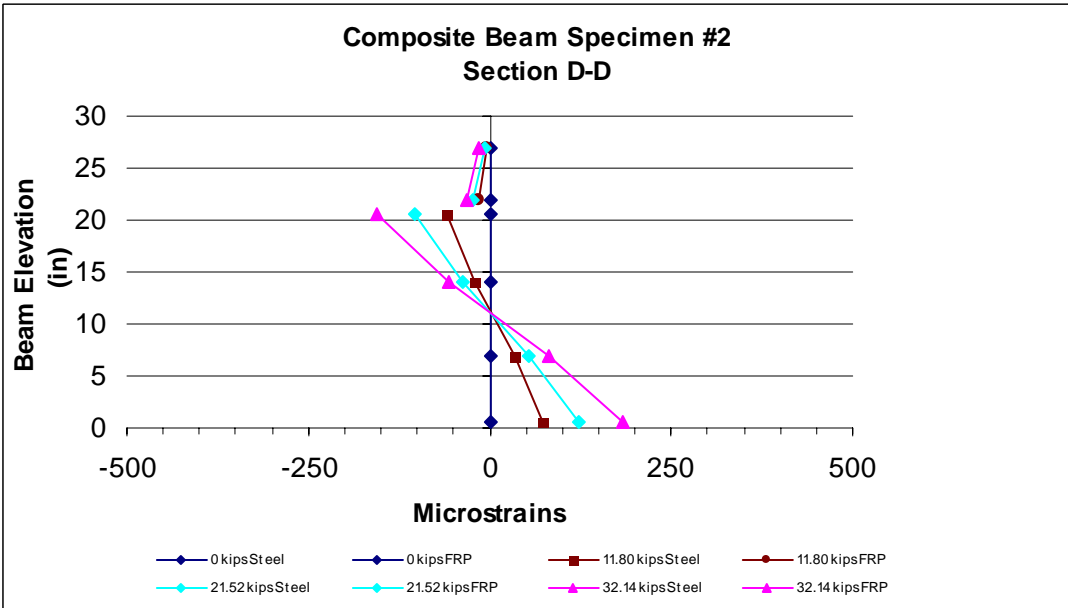


Figure 5-28 Strain Variation at Service Load

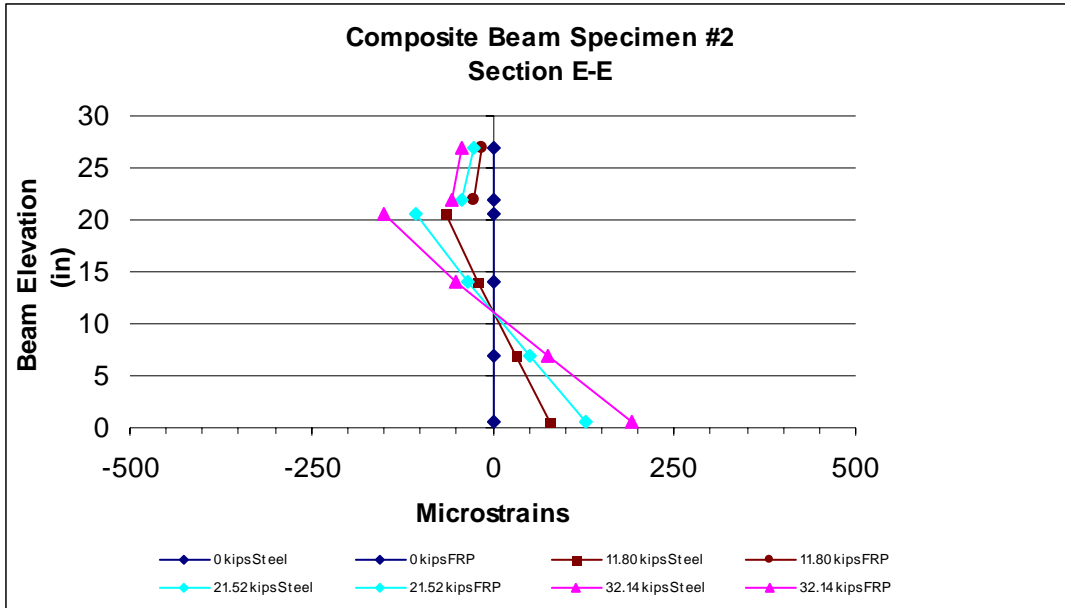


Figure 5-29 Strain Variation at Service Load

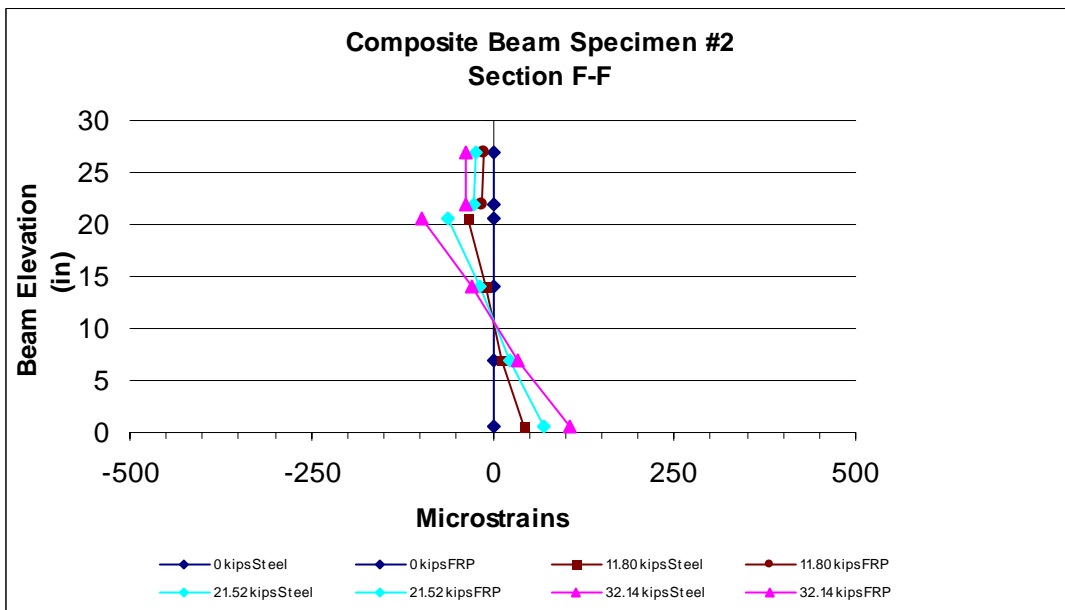


Figure 5-30 Strain Variation at Service Load

Figure 5-25 and 5-26 show that there was slip between FRP deck and steel beam similar to that occurred in composite beam testing specimen #1. Those interfacial slip characteristics behaved fairly consistently within each shear span of the composite beam.

From the strain variation in composite beam plots (Figure 5-21 to Figure 5-24 respectively), it can be said that FRP deck and the beam specimen #2 are interacting and were not acting as a full composite system. There was slip between the FRP deck and steel beam. However, Figure 5-27, 5-28, 5-29, and 5-30 show that the strain variations are relatively small; it can be said that at service load (e.g. 0-30 kips) FRP deck and steel beam are not acting in a fully composite fashion.

The calculation of location of neutral axis for each load and each cross section area of the beam can be seen in the table following:

Table 5-3 Calculated Neutral Axis Beam Specimen #2

Number	Load (kips)	Bare Steel	C-C (in.)	D-D (in.)	E-E (in.)	F-F (in.)
1	0					
2	43.225	10.500	11.368	11.272	11.666	10.690
3	91.545	10.500	11.044	11.664	12.100	10.291
4	143.085	10.500	10.857	11.818	12.284	10.112
5	194.245	10.500	10.800	11.923	12.498	10.046
6	252.085	10.500	10.784	12.084	12.703	10.062
7	300.285	10.500	10.531	12.625	13.091	10.254
8	351.145	10.500	10.312			10.312

Cross section of a typical FRP composite beam can be shown as follows:

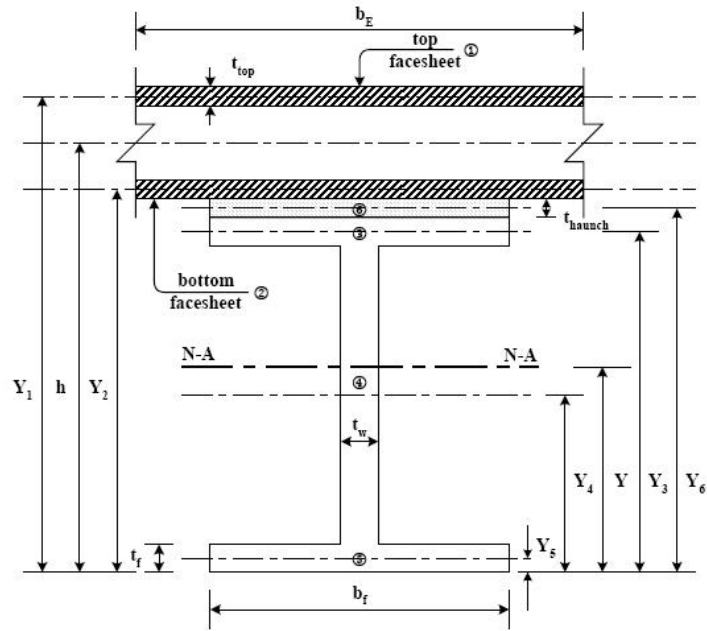


Figure 5-31 Typical Cross Section Composite Beam

Table 5-4 Transformed Area Method

Element	Area	y	yA
1	.033*B _E	26.745	0.88*B _E
2	.033*B _E	22.255	0.73*B _E
3	1.31	21.50	28.17
4	5.07	20.69	104.90
5	7.91	10.50	83.06
6	5.07	0.31	1.57
Total	19.36+.066*B_E		217.69+1.62*B_E
Equilibrium Equation	(19.36+.066*B_E)*Y = 217.69+1.62*B_E		

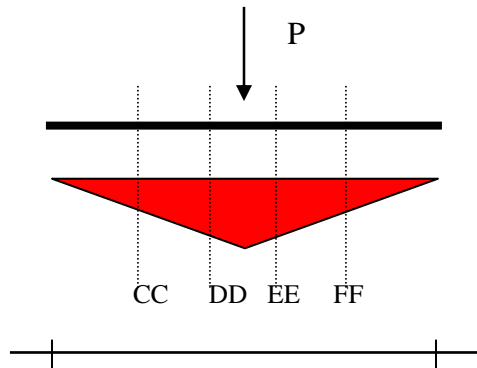
By substituting the measured neutral axes for Specimen #1 and Specimen #2 into the Equilibrium Equation, the effective width of the composite beam Specimen #1 and Specimen #2 can be shown in next table.

Table 5-5 Effective Width

Specimen	Neutral Axes (in)	Deck Width (in)	Effective Width (in)
1	12.946	66.000	43.03
2	13.091	66.000	47.29

Based on the results from the testing of both specimens, several interesting feature of response are discerned. Firstly, based on the consideration of the load versus interfacial slip response presented in Figure 5-12, 5-13, 5-25, and 5-26, there appears to be only small interfacial slip occurring at service loads in the composite beam testing.

Determining the neutral axis can be approached by using different methods. Since that the dimension and properties of the composite beam are known, the elastic section properties of the composite beam can be calculated based on the assumption that FRP deck and steel beam are acting in a fully composite fashion.



Steel Beam : W21x62

$$M_{int} = \frac{\epsilon_t EI_{composite}}{(y)}$$

Equation 5-1

Table 5-6 Elastic Section Properties

Element	A	n	A/n	y	Ay	d ²	Ad ²	I
Top Sheet	33.66	15.68	2.15	26.75	57.41	174.79	375.23	0.05
Btm Sheet	33.66	15.68	2.15	22.26	47.77	76.23	163.64	0.05
Haunch	8.24	8	1.03	21.50	22.15	63.62	65.53	0.09
Beam	18.30	1	18.30	10.50	192.15	9.14	167.35	1330.00
			23.82		319.48		771.74	1330.18

$$y = 13.52 \text{ in.}$$

$$I_{composite} = 2102 \text{ in}^4$$

$$M_{CC} = M_{FF} = \frac{1}{2} * P * (2.5*12) = 15 P \text{ kips-in}$$

$$M_{DD} = M_{EE} = \frac{1}{2} * P * (4.5*12) = 27 P \text{ kips-in}$$

Using the data from strain variation for both specimens, and the results can be shown in the table below.

Section C-C (Specimen #1)

Load	ϵ	σ	P _{actual}	M	y
load 5	112.50	3.26	34.32	514.80	13.32
load 10	262.50	7.61	81.48	1222.20	13.09
load 15	432.50	12.54	133.14	1997.10	13.20
load 20	588.50	17.07	180.46	2706.90	13.25
load 25	755.50	21.91	232.48	3487.20	13.21
load 30	927.50	26.90	286.00	4290.00	13.18
load 35	1072.50	31.10	334.20	5013.00	13.04
Average					13.18
Effective Width					48.46

Section D-D (Specimen #1)

Load	ϵ	σ	P_{actual}	M	y
load 5	203.50	5.90	34.32	926.64	13.39
load 10	477.50	13.85	81.48	2199.96	13.23
load 15	782.00	22.68	133.14	3594.78	13.26
load 20	1066.50	30.93	180.46	4872.42	13.34
load 25	1394.00	40.43	232.48	6276.96	13.54
load 30	1791.00	51.94	286.00	7722.00	14.14
Average					13.48
Effective Width					59.27

Section E-E (Specimen #1)

Load	e	s	P_{actual}	M	y
load 5	210.00	6.09	34.32	926.64	13.81
load 10	478.00	13.86	81.48	2199.96	13.24
load 15	770.00	22.33	133.14	3594.78	13.06
load 20	1038.00	30.10	180.46	4872.42	12.99
load 25	1350.00	39.15	232.48	6276.96	13.11
load 30	1740.00	50.46	286.00	7722.00	13.74
Average					13.32
Effective Width					54.24

Section F-F (Specimen #1)

Load	ϵ	σ	P_{actual}	M	y
load 5	112.50	3.26	34.32	514.80	13.32
load 10	264.00	7.66	81.48	1222.20	13.17
load 15	430.50	12.48	133.14	1997.10	13.14
load 20	584.00	16.94	180.46	2706.90	13.15
load 25	752.50	21.82	232.48	3487.20	13.15
load 30	933.50	27.07	286.00	4290.00	13.26
load 35	1078.50	31.28	334.20	5013.00	13.11
Average					13.19
Effective Width					48.75

Using the same method and approach, the result for composite beam test specimen #2 can be seen in tables below.

Section C-C (Specimen #2)

Load	ϵ	σ	P_{actual}	M	y
load 5	142.50	4.13	43.20	648.00	13.41
load 10	300.50	8.71	91.52	1372.80	13.34
load 15	468.50	13.59	143.06	2145.90	13.31
load 20	635.00	18.42	194.22	2913.30	13.29
load 25	827.00	23.98	252.06	3780.90	13.33
load 30	972.00	28.19	300.26	4503.90	13.16
Average					13.31
Effective Width					55.48

Section D-D (Specimen #2)

Load	ϵ	σ	P_{actual}	M	y
load 5	246.00	7.13	43.20	1166.40	12.86
load 10	515.00	14.94	91.52	2471.04	12.70
load 15	793.50	23.01	143.06	3862.62	12.52
load 20	1071.00	31.06	194.22	5243.94	12.45
load 25	1418.50	41.14	252.06	6805.62	12.71
load 30	1800.50	52.21	300.26	8107.02	13.54
Average					12.80
Effective Width					44.31

Section E-E (Specimen #2)

Load	ϵ	σ	P_{actual}	M	y
load 5	257.00	7.45	43.20	1166.40	13.43
load 10	539.00	15.63	91.52	2471.04	13.30
load 15	833.50	24.17	143.06	3862.62	13.15
load 20	1127.00	32.68	194.22	5243.94	13.10
load 25	1497.50	43.43	252.06	6805.62	13.41
load 30	1877.50	54.45	300.26	8107.02	14.12
Average					13.42
Effective Width					64.11

Section F-F (Specimen #2)

Load	ϵ	σ	P_{actual}	M	y
load 5	142.00	4.12	43.20	648.00	13.36
load 10	297.50	8.63	91.52	1372.80	13.21
load 15	461.50	13.38	143.06	2145.90	13.11
load 20	622.00	18.04	194.22	2913.30	13.01
load 25	807.00	23.40	252.06	3780.90	13.01
load 30	976.00	28.30	300.26	4503.90	13.21
Average					13.15
Effective Width					54.86

Final results calculated effective width for both tests can be shown in next table:

Table 5-7 Effective Width (Bernoulli-Navier Theorem)

Section	Specimen #1 (in)	Specimen #2 (in)
C-C	48.46	55.48
D-D	59.27	44.21
E-E	54.24	64.11
F-F	48.75	54.86
Average	52.68	54.67
Std. Deviation	5.14	8.15

Next table shows the determined effective width of the FRP deck using both methods:

Table 5-8 Effective Width FRP Deck (Both Method)

Effective Width (in.)	Considered Slip Occurring	Bernoulli-Navier Theorem
Specimen #1	43.03	52.68
Specimen #2	47.29	54.67

6.0 CR 46 BRIDGE: A COMPARATIVE STUDY

6.1 INTRODUCTION

A recently rehabilitated bridge on Country Road 46 over the East Branch of the Salmon River, Lewis County, NY has a new Fiber Reinforced Polymer (FRP) deck. This bridge has undergone a major rehabilitation and reconfiguration. Field tests done by Bridge Diagnostic, Inc. were used to verify that the FRP deck was acting compositely with the beams. This bridge has deck geometry and properties that are the same as the deck used in this current research (DuraSpan 500), and used seven W21x62 steel beams spaced 4.10 ft. apart. In other words, this current research and the CR 46 Bridge have a similar composite deck system. Thus, the field tests result of the CR 46 Bridge can be compared to the results of this current research.

6.2 STRUCTURE DESCRIPTION

The CR 46 Bridge has a beam spacing that was narrowed slightly to 4.10 ft.; as compared with the composite beam specimens tested in the lab (as detailed in Chapter 5). In addition, according to Martin Marietta Composite DuraSpan 500 specification, a typical allowable beam spacing is 5.0 ft. for this particular deck system. The structural type of this bridge is a steel beam bridge with composite FRP deck system with single span of 32.81 ft. center-to-center of the bearings. The bridge superstructure consists of seven W21x62 steel beams spaced at 4.10 ft. Table 6-1 contains a detailed description of the structure.

Table 6-1 Description of CR 46 Bridge Structure

Structure Identification	County Road 46 over East Fork Salmon River Bin 3340500
Location	Lewis, New York
Structure Type	Steel beam bridge with composite FRP floor system
Span Length	32.81' c.c. bearings
Skew	0 (Perpendicular)
Structure/Roadway Widths	27.69' / 25.98' roadway
Beams	7 – W21x62 beams @ 4.10'
Deck	DuraSpan 500. Trapezoidal tubes run transverse to the direction of traffic 3.5" asphalt wearing surface (thickness varies)
Visual condition	Structure appears to be in good condition, with no apparent damage. Several girders have lost some cross-sectional area.

6.3 INSTRUMENTATION & TESTING PROCEDURE

The load test consisted of measuring strains at numerous locations on the bridge beams during controlled load applications. Instrumentation consisted of portable strain gage units placed so as to measure strains at the top and bottom flanges at the mid-span and near both ends on all seven steel beams. In addition to the steel beam instrumentation, two gages were also placed on the underside of the FRP deck near mid-span of beam G4. A total of 44 removable strain transducers were attached to the bridge. The locations of each gage and the two truck paths are shown in Figure 6-1.

The load tests were performed by driving a 56.7 kip dump truck across the bridge along prescribed paths. Data were recorded continuously at a sampling rate of 33Hz during each pass and the truck position was monitored in order to record strain as a function of vehicle position. Axle weights and spacing of the test truck are shown in Figure 6-2.

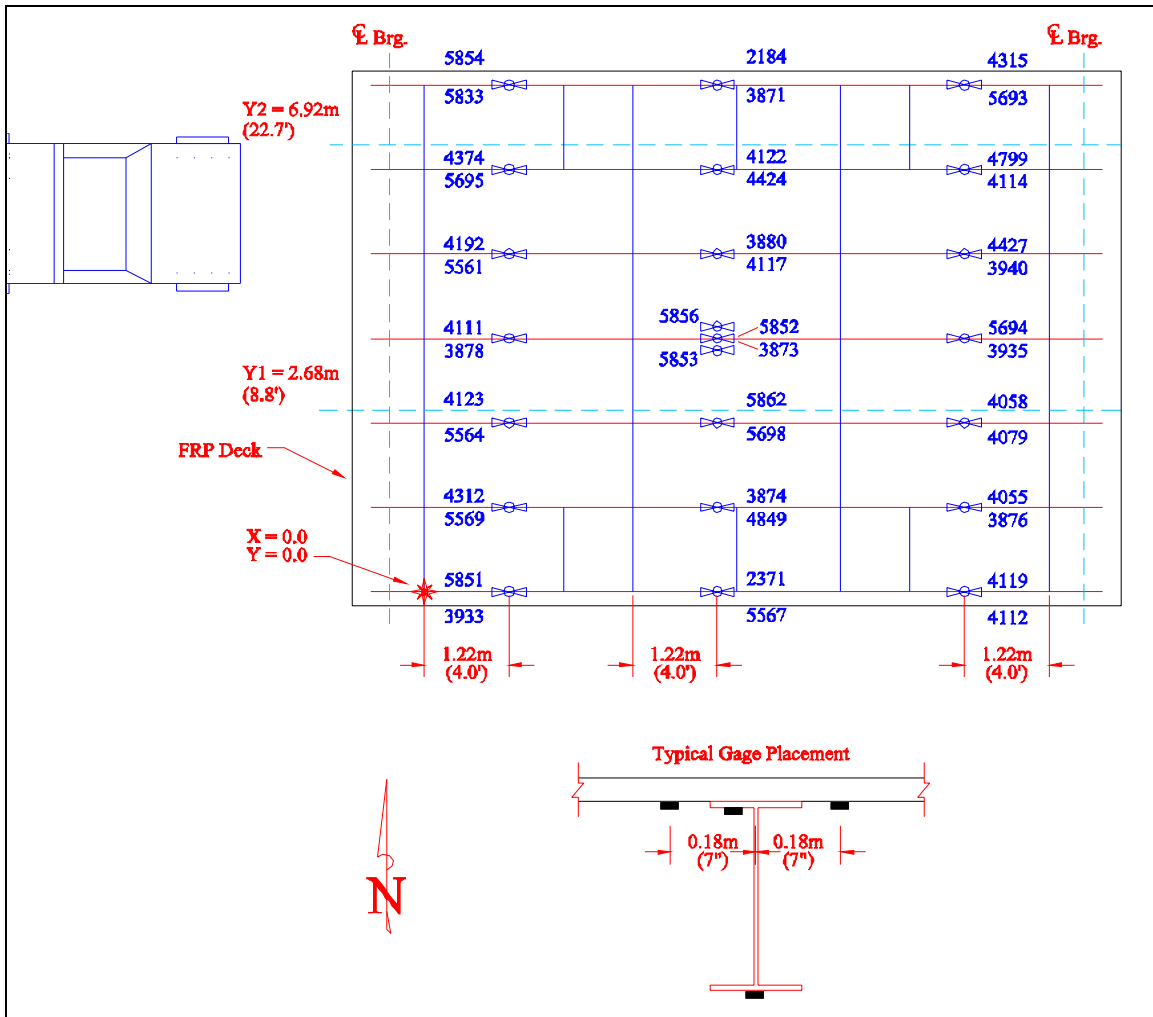


Figure 6-1 Instrumentation & Test Plan

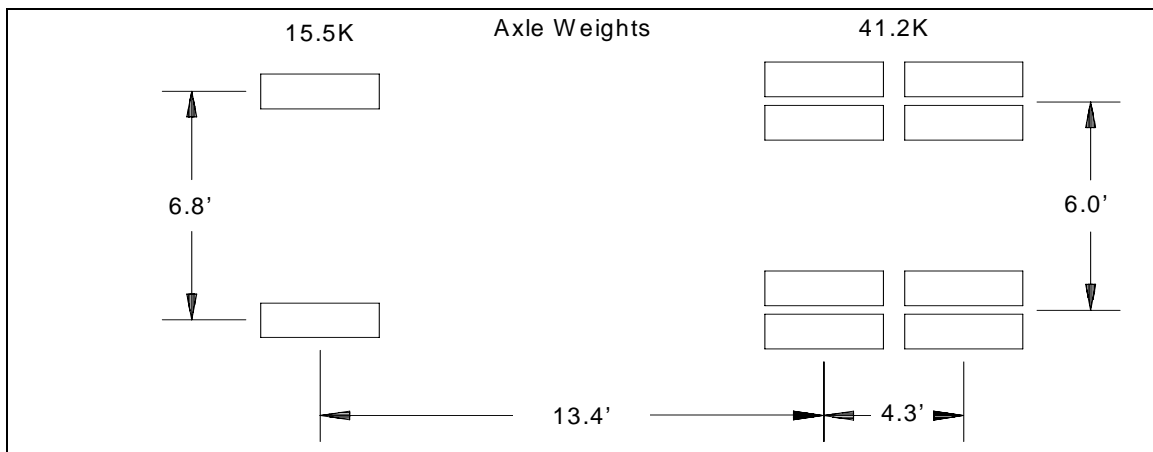


Figure 6-2 Load Configuration of Test Truck



Figure 6-3 CR 46 Bridge, Salmon River, Lewis County, NY

6.4 MEASURED STRAIN

To measure the strain, a test truck was driven across the bridge along prescribed paths. Two truck paths were defined for the load test. The Y position refers to the distance between the driver side front wheel and centerline of the beam G7 ($Y=0$); G7 was an exterior beam. All tests were performed in east bound direction; that was considered to be the positive X direction sense (Figure 6-1). Data acquisition began with the front axle at $X = -12.9$ ft. which was used to zero out an auto clicker position measuring device used to record the position data using the driver side front wheel. The auto clicker recorded truck position at each wheel revolution (where the wheel circumference was 10.7 in.) Data was recorded while the test truck crossed the bridge at speeds of less than 5 mph. Each truck path was run twice to check reproducibility.

6.5 RESULTS and DISCUSSION

Strains gage data recorded from the field tests were reduced in the same manner that was employed in the discussion associated with Chapter 5 herein. Strain variations at mid-span were plotted for all beams (interior beams and exterior beams) for Y1 and Y2 truck path. G1 and G7 are exterior beams whereas G2, G3, G4, G5 and G6 are interior beams (see Figure 6-1).

The neutral axis location for each beam was calculated based on the strain profile for each beam (assuming that the deck was designed to be fully composite at service loads). This measured neutral axis was then used as a basis for determining the effective compression flange width in the FRP deck system at service load.

Strain variations for each beam are plotted in Figures below:

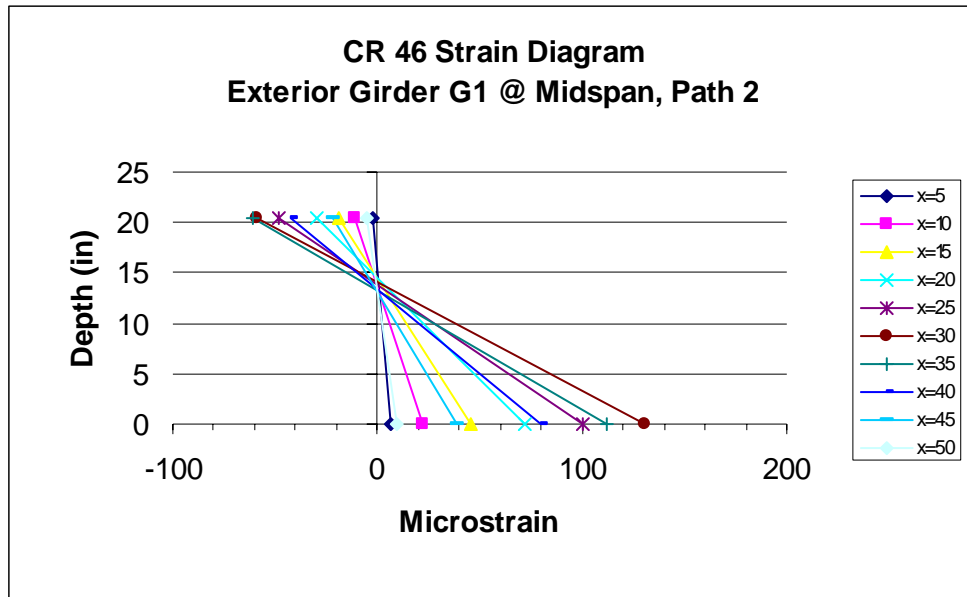


Figure 6-4 Strain Variation G1, Path Y2

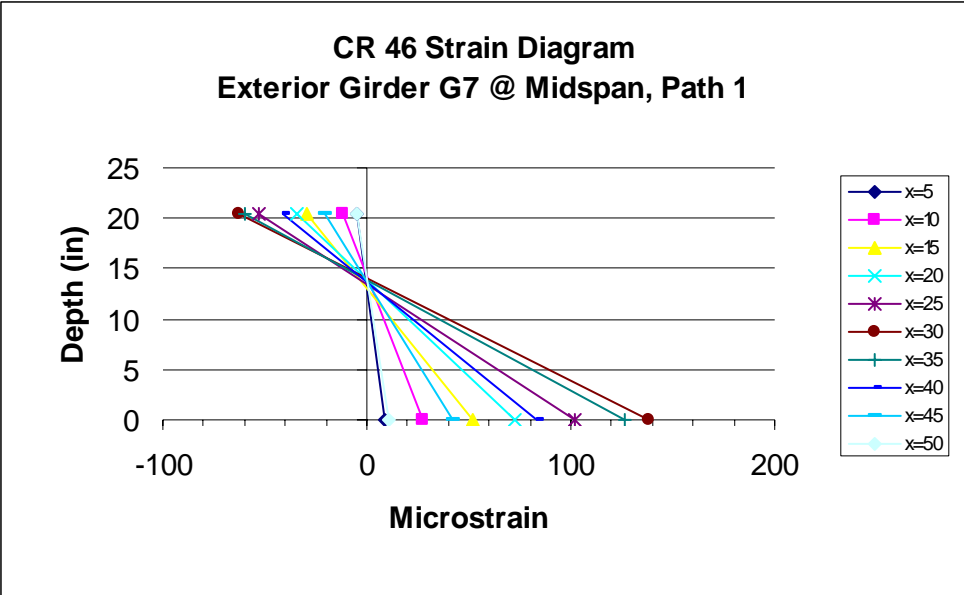


Figure 6-5 Strain Variation G7, Path Y1

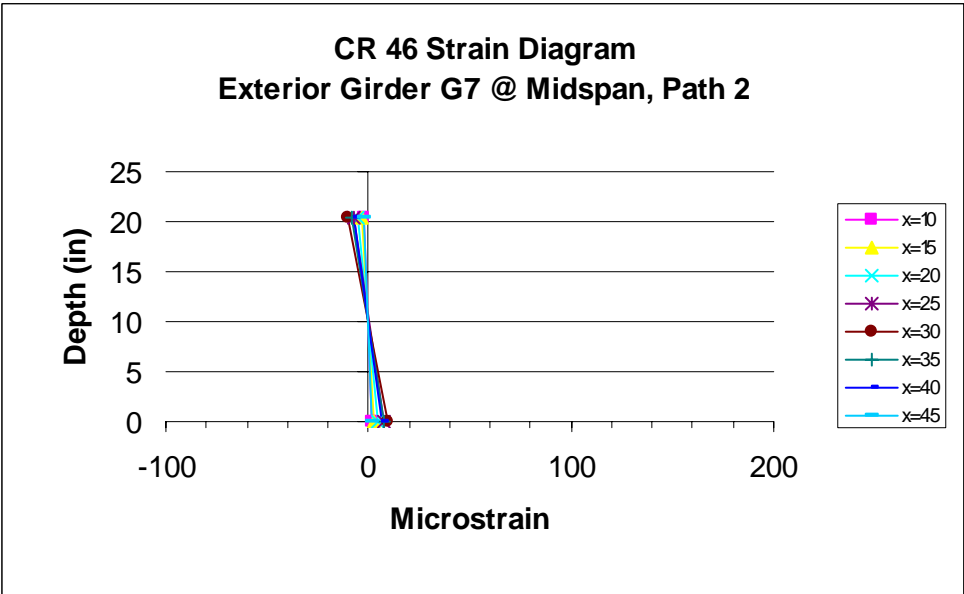


Figure 6-6 Strain Variation G7, Path Y2

Exterior beam G7 path Y2 and G1 path Y1 were un-load beams, and both beams did not response well to the loading truck along that path. The data of strain variation beam G1 path Y1 could not be plotted due to bad response of strain gage at that location. The bad data was caused by the insufficient loading by the truck, i.e. the strains were in the ‘noise range’ and unreliable. Strain variation beam G7 path Y2 will not be included to calculate position of neutral axis of beam G7. Calculated neutral axes for exterior beams G1 and G7 can be seen in Table 6-2. Average Neutral Axis of exterior beam is 13.06 in. (0.27% Std. Deviation).

Table 6-2 Average Exterior Beam N.A

Beam G1 Path 2 (in)	13.03
Beam G7 Path 1 (in)	13.08
Average	13.06

Strain variations for interior beams were plotted in the next figures.

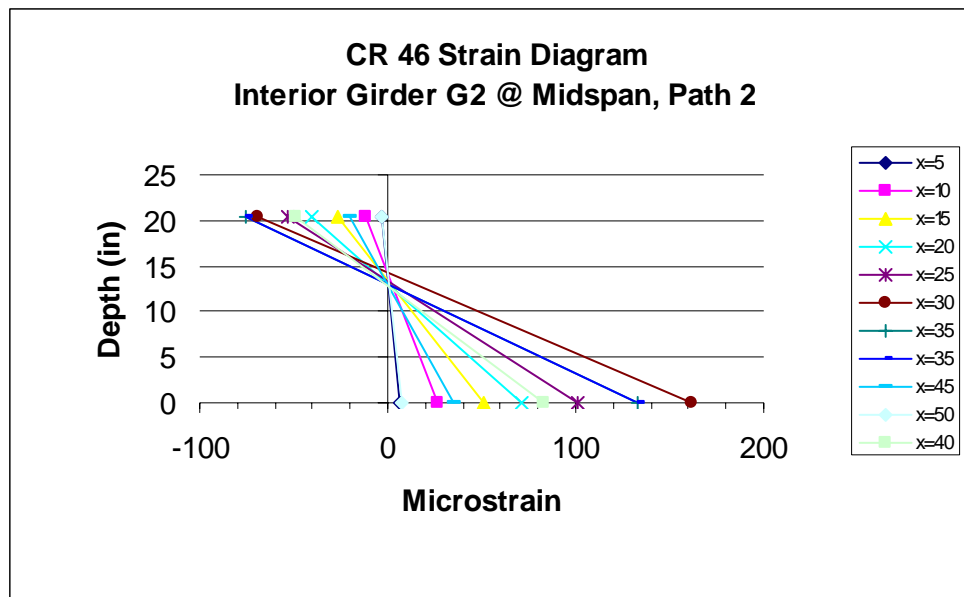


Figure 6-7 Strain Variation G2, Path Y2

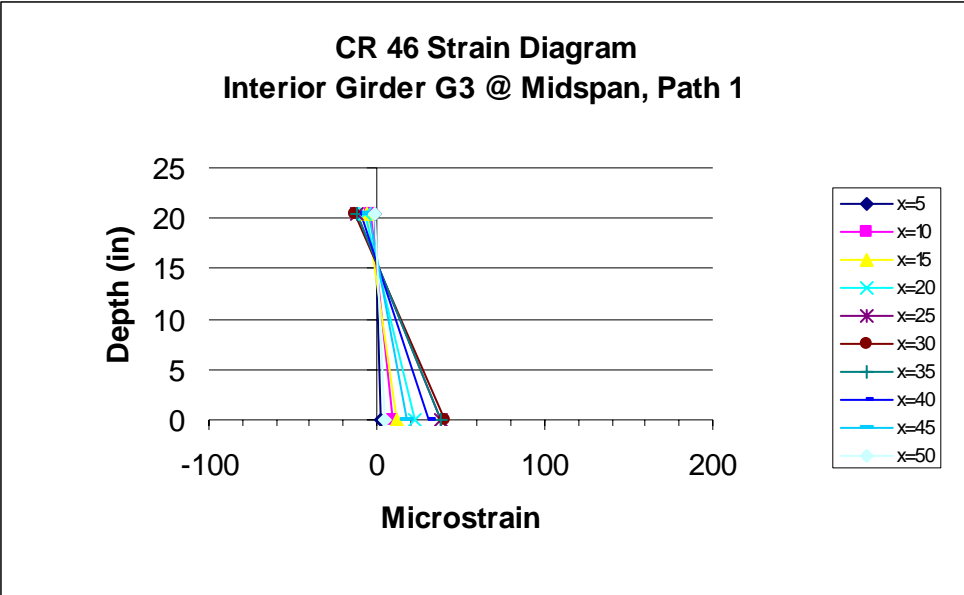


Figure 6-8 Strain Variation G3, Path Y1

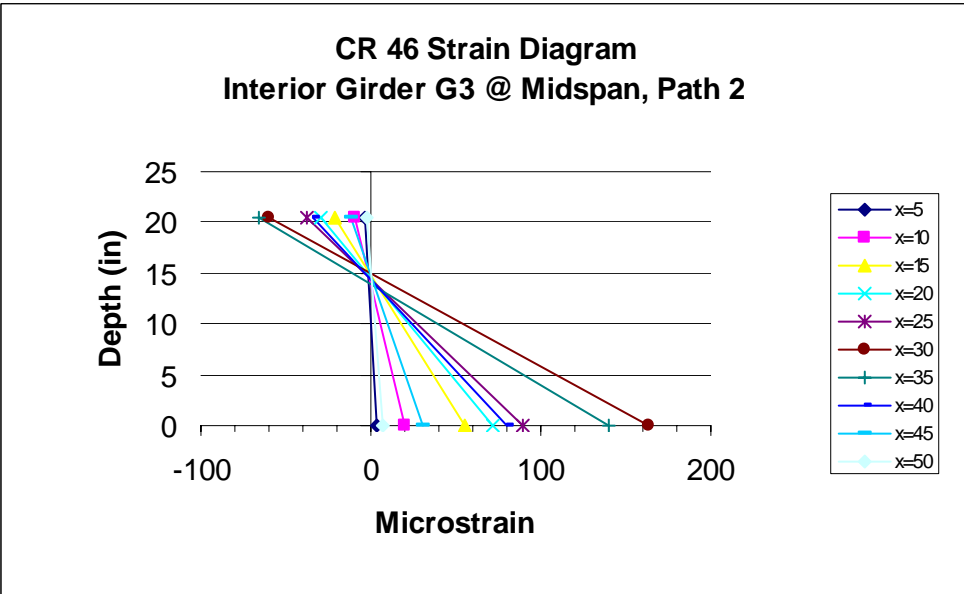


Figure 6-9 Strain Variation G3, Path Y2

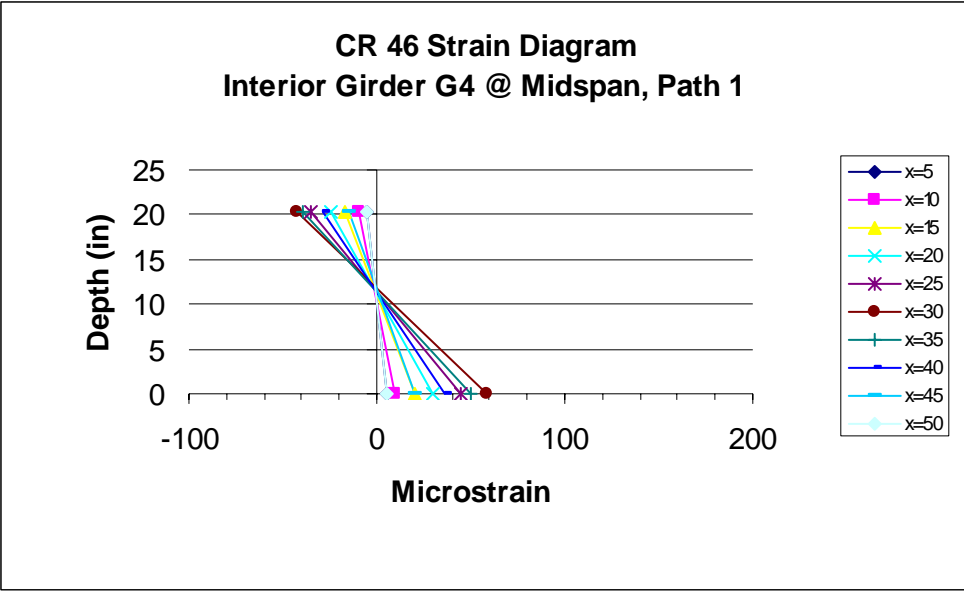


Figure 6-10 Strain Variation G4, Path Y1

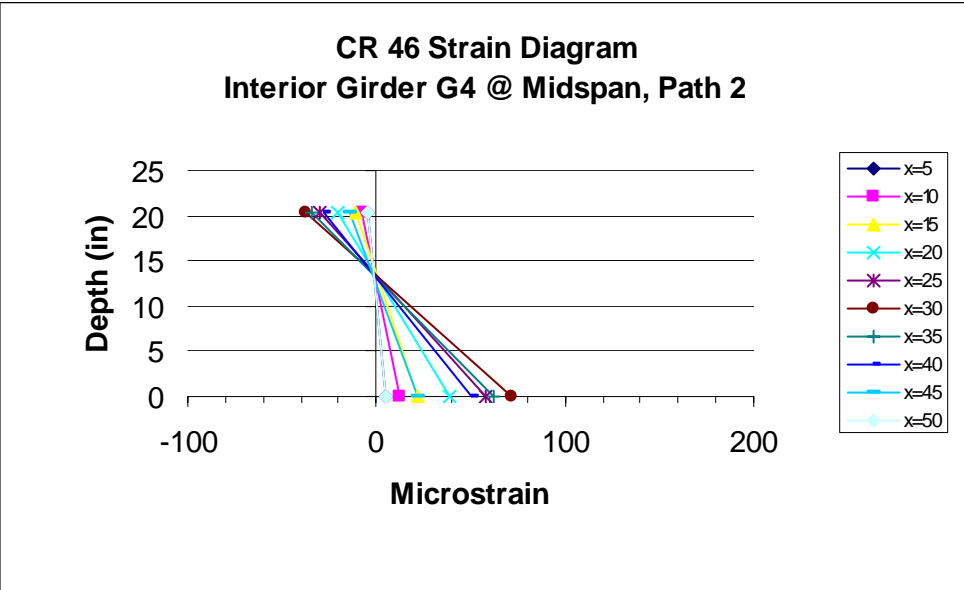


Figure 6-11 Strain Variation G4, Path Y2

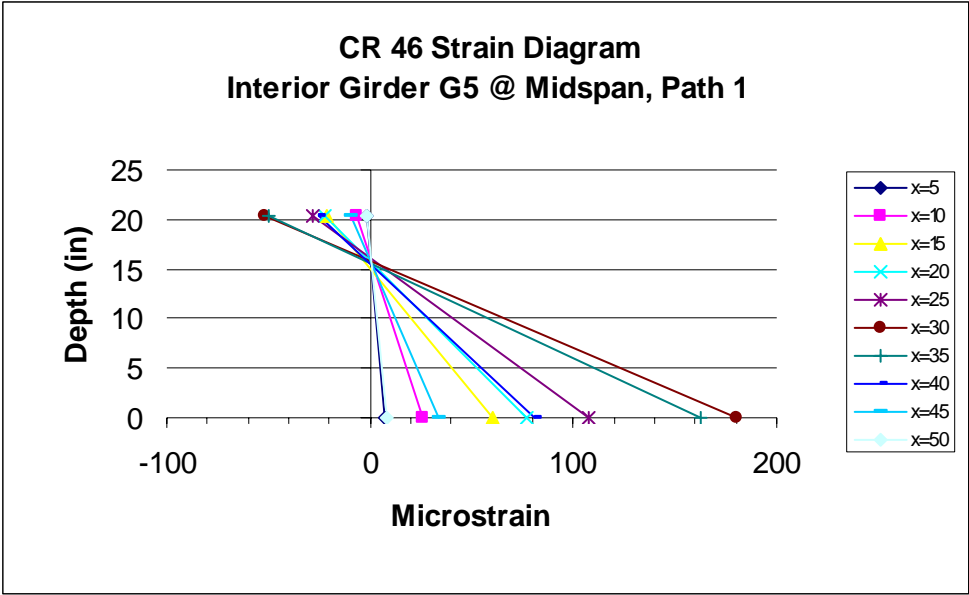


Figure 6-12 Strain Variation G5, Path Y1

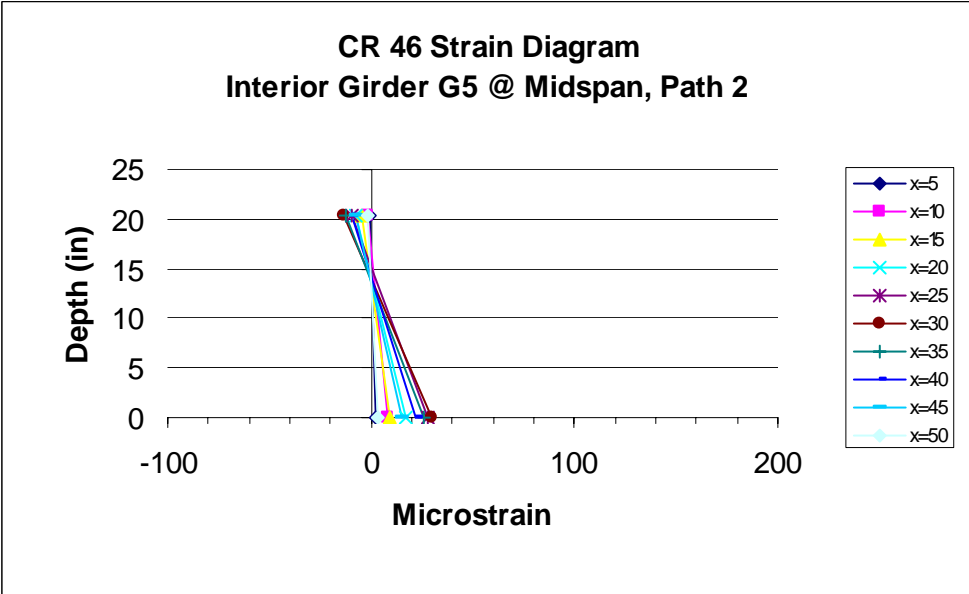


Figure 6-13 Strain Variation G5, Path Y2

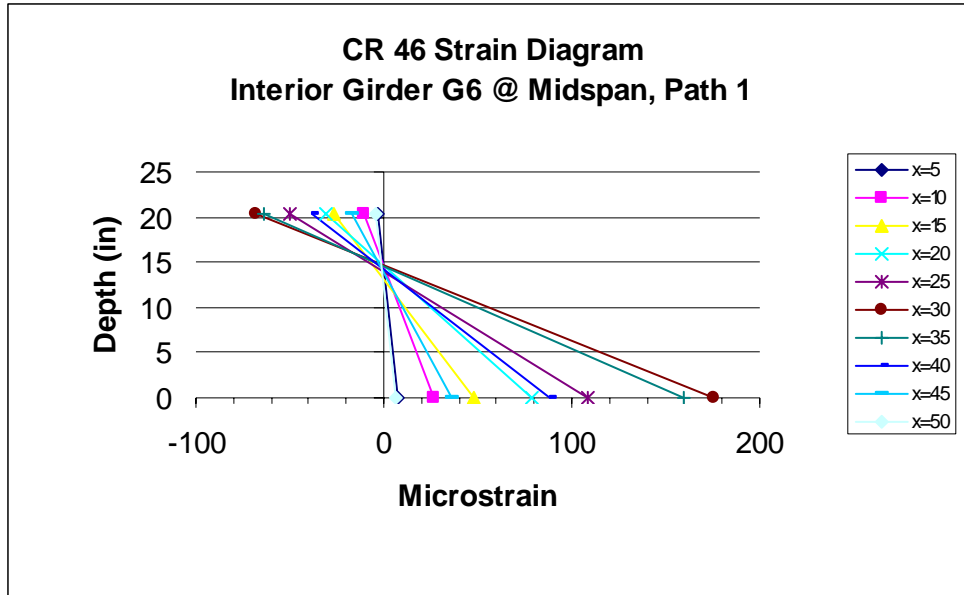


Figure 6-14 Strain Variation G6, Path Y1

The neutral axis for the interior beams was calculated based on strain variations for the interior beams (Figure 6-6 to Figure 6-13 respectively) and they can be seen in Table 6-3.

Table 6-3 Average Interior Beam N.A

Beam G2 Path 2 (in)	12.81
Beam G3 Path 1 (in)	13.58
Beam G4 Path 1 (in)	10.19
Beam G5 Path 1 (in)	15.09
Beam G6 Path 1 (in)	12.23
Average	12.78

Average Neutral Axis of exterior beam is 12.78 in. (14.121% Std. Deviation).

By using observed data obtained from Chapter 5 and comparing them to the recorded data for this bridge (as reported by Bridge Diagnostic, Inc., Load Test and Rating Report CR-46 Bridge, January 2004), it can be seen that some composite action exists between the deck and the beams. The beams' neutral axes were measured by comparing the relative magnitudes of strains between the upper and lower flanges. Neutral axis values for the beams at mid-span ranged between 10" and 15" from the bottom flange (obtained from Figure 6-4 to Figure 6-14 respectively), indicating slight variations in the level of composite action for each beam.

There were variations in measured neutral axis. The reasons for variation may be caused by the deck attachment to the steel beam in the construction process.

By employing the transformed section method, the effective width for exterior and interior beam was calculated.

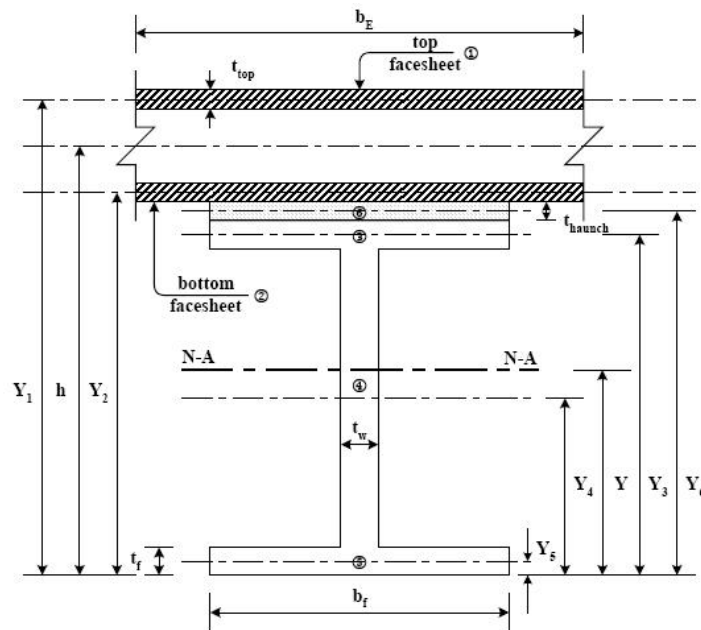


Figure 6-15 Transformed Area Section

Using the same properties employed in this current research, in conjunction with the modular ratio, the transformed area calculation proceeds as follows:

$$n_1 = E_s/E_{FRP} = 15.68$$

$$n_2 = E_s/E_{Gr} = 6.28$$

Calculation of the neutral axis for exterior and interior beams can be seen in Table 6-4.

Table 6-4 Transformed Area Method

Element	Area	y	yA
1	.033*B _E	26.745	0.88*B _E
2	.033*B _E	22.255	0.73*B _E
3	1.31	21.50	28.17
4	5.07	20.69	104.90
5	7.91	10.50	83.06
6	5.07	0.31	1.57
Total	19.36+.066*B_E		217.69+1.62*B_E
Equilibrium Equation	(19.36+.066*B_E)*Y = 217.69+1.62*B_E		

By substituting the measured neutral axes for exterior and interior beams into the Equilibrium Equation, the effective width of the exterior and interior beams can be shown in next table.

Table 6-5 Exterior and Interior Beam Effective Width

Beam	Neutral Axes (in)	Effective Width (in)	B_{eff} / Beam Spacing
Exterior	13.06	46.99	0.953
Interior	12.78	38.79	0.788

Both effective widths for exterior and interior beam are smaller than beam spacing. Using specification both LRFD (Load Resistance Factor Design) 1998 and AASHTO (The American Association of State Highway and Transportation Officials) 1998, the effective width for exterior and interior beams as follows:

LRFD 1998 section I3.1, the effective width of each side of the beam:

- One-eighth of the beam span, center-to-center, of supports (49.22 in.)
- One-half the distance to the centerline of the adjacent beams (24.6 in.)
- The distance to the edge of the slab (0.0 in.)

AASHTO 1998:

-. Exterior Beams, one-half of the adjacent interior beams, plus the least of:

- One-eighth of the effective span length (49.22 in.)
- 6.0 times the average thickness of the slab, plus the greater of half the web thickness or one-quarter of the width of the flange of the beam (34.12 in.)
- The width of over-hang (0.0 in)

-. Interior Beams

- One-quarter of the effective span length (98.43 in.)
- 12.0 times the average thickness of the slab, plus the greater of web thickness of one-half the width of the top flange of the beam (64.12 in.)
- The average beam spacing (49.2 in.)

Table 6-6 Effective Width (LRFD/AASHTO)

Beam	LRFD (in)	AASHTO (in)
Exterior	24.6	24.6
Interior	49.2	49.2

Effective width that was calculated in this current research can be compared to effective measured for CR 46 Bridge. Table 6-7 compares those results.

Table 6-7 Measured Effective Width

Beam	U. of Pittsburgh (in.)	Neutral Axis (in.)	CR 46 Bridge (in.)	Neutral Axis (in.)
Test #1	43.033	12.95	-	-
Test #2	47.291	13.09	-	-
Exterior	-	-	46.992	13.06
Interior	-	-	38.787	12.78

Note: B_{eff} = Effective Width

W_d = Width of FRP Deck

S_b = Beam Spacing

7.0 CONCLUSIONS, RECOMMENDATION for FUTURE WORK

7.1 CONCLUSIONS

To be efficiently used in modern bridge decking application, FRP decks must be made to act compositely with underlying stringers (this work focuses on the use of steel stringers). To behave compositely, a sufficiently robust shear transfer interface at the FRP to steel transition zone is required. While some efforts to achieve such interfacial shear transfer have been undertaken current understanding is weak and existing theories inadequate. The current research has contributed to our evolving understanding of this complex and important interface.

Through the performance of a series of laboratory based experimental tests, the performance of the interfacial shear performance of the Fiber Reinforced Polymer (FRP) deck when mechanically attached to steel stringer(s), as required in the bridge deck system, was quantified. As a result of this testing, guidelines for computation of effective flange widths, for use in engineering design calculations carried out within a design context involving FRP deck systems were obtained

The types of supporting experimental testing conducted as part of the present research include: compressive and tensile material testing, push-off testing to quantify shear stud capacity, continuous panel testing to assess serviceability requirements, and ultimate strength composite beam testing as noted in the previous paragraph. A number of conclusions are drawn from this work:

- Composite materials have many mechanical behavioral characteristics that are different from those of more conventional engineering materials. The structural behavior of an FRP section can be quite different from its conventional counterpart; mainly because an FRP section usually consists of thin-walled panels with distinct fiber architectures leading to material anisotropy. Due to the complexity of composite materials, the analytical and design tools developed for members made from conventional materials cannot be readily applied to FRP shapes and profiles.
- Mechanical properties of FRP deck in this research were obtained by compressive and tensile material testing. These tests had 5 specimens for each direction: 0° (parallel to the direction of pultrusion) and 90° (perpendicular to the direction of pultrusion).
- Average ultimate strength of coupon specimens for compressive testing in the 0° direction was $3.41\text{E}+04$ psi with $3.79\text{E}+03$ psi standard deviation. Average modulus elasticity of these coupon specimens was $5.09\text{E}+06$ psi with $2.65\text{E}+06$ psi standard deviation. However, it is noted that, if only sample #3 and #4 (see Chapter 2) were considered to determine modulus of elasticity, gave a result of $2.80\text{E}+06$ with $1.76\text{E}+05$ psi standard deviation.
- Average ultimate strength of coupon specimens for compressive test 90° direction was $2.27\text{E}+04$ psi with $8.58\text{E}+02$ psi standard deviation. Average modulus of elasticity of these coupon specimens was $1.85\text{E}+06$ psi with $4.34\text{E}+05$ psi standard deviation.
- Average ultimate strength of coupon specimens for tensile test 0° direction was $2.89\text{E}+04$ psi with $8.86\text{E}+03$ psi standard deviation. Average modulus of elasticity of these coupon specimens was $3.99\text{E}+06$ psi with $2.46\text{E}+05$ psi standard deviation.

- Average ultimate strength of coupon specimens for tensile test 90° direction was 1.19E+04 psi with 3.74E+02 standard deviation. Average modulus of elasticity of these coupon specimens was 2.51E+06 psi with 4.29E+05 standard deviation.
- An important consideration when utilizing an all composite deck for use in a bridge system is type and capacity of the deck-to-girder connection. From the result of push-off testing it can thus be said that the shear studs were unable to reach their nominal capacity, as predicted by the AASHTO equation for studs installed in concrete deck (52% - 58% of nominal stud capacity). In addition, the push-off test specimens associated with DuraSpan 500 deck failed at 85% to 95% of the value suggested by Moon et al (2002) for similar, but deeper FRP deck sections (DuraSpan 766).
- In continuous panel testing to assess serviceability requirements, the deformation-load plots (Chapter 4) considering the entire data set, display a linear relationship describable by an equation exhibiting a closer to a unity R-square value. All results showed linear deformation-load relationship, which indicates that, the FRP deck can be modeled as a linear material for the deck deformation serviceability design context.
- The first FRP deck research programs conducted in the U.S. [Henry, 1985; Ahmad and Plecnic, 1989] were limited to the development of conceptual design procedures. The results of this early works indicated that the design of FRP deck systems was always controlled by the deflection limit state (serviceability limit state) rather than the strength limit states. AASHTO (2004) limits the deflection of the deck bridge system as a function of the stringer spacing. The MMC DuraSpan 500 deck tested as described in Chapter 4 fails to satisfy the current AASHTO deck deflection limits. It is not clear that this should be a concern. In fact,

based on the current work, it is suggested that the existing AASHTO deflection requirements may not be appropriate for use in FRP installations.

- From the strain variation in the composite beam plots described in Chapter 5, it can be observed that FRP deck and the underlying steel beam on both specimens tested as part of this work are interacting in a partially composite way at large load; as evidence by the discontinuity in strain at the FRP-to-steel interface. This result means that there was observed to be significant slip between FRP deck and underlying steel beam. It is also noted that at service load, the strain variations are relatively small; thus it can be said that at service load (e.g. 0-30 kips) the FRP deck and steel beam are not acting fully composite.
- The calculated effective width (for each of the individual specimens) of FRP deck is 43.03 in. and 47.29 in, respectively based on the experiments with the interfacial slip occurring.
- Effective width can be calculated also by using elastic section properties method which is based on Bernoulli-Navier Theorem, assuming that FRP deck and underlying steel beam are interacting in a full composite. This effective width of FRP deck is 52.68 in. and 54.67 in. for specimen #1 and specimen #2 respectively.
- As a comparison, the data from field test on CR-46 Bridge as described in Chapter 6 was reduced in the same manner that was employed in the discussion associated with Chapter 5 herein. The CR 46 Bridge has a beam spacing that was slightly narrower (4.10 ft) as compared with the composite beam specimens tested in the lab (as detailed in Chapter 5). For this case, the effective width of this FRP bridge deck system is 38.79 in.
- Effective width calculations for FRP deck show that they are less than AASHTO prescribed effective width for concrete decks. This is expected since that FRP decks are not as axially stiff as concrete decks. In addition, complexities associated with the manifestation of shear

lag in the deck coupled with the poorly understood interfacial coupling makes the prescription of a single effect width that is useful for all load levels, problematic. It is suggested that one effective width efficiency maybe useful for service load calculations, while a completely different efficiency might be appropriate for the case of determining ultimate strength.

7.2 RECOMMENDATION for FUTURE WORKS

- Develop methods and procedures to determine shear stud capacity in order to provide more accurate capacity prediction for design use.
- Additional study of the serviceability limit state in FRP deck systems is needed. Additional studies should focus on much larger numbers of specimens spanning a more reasonable design space in order to be more definitive.
- Extended monitoring an FRP bridge deck installation from when it is constructed through multiple years of seasonal temperature and climate variations would yield very useful and important durability information.
- Fatigue behavior of FRP Deck. The damage and failure of the deck system indicates that research on the fatigue cracking and damaging for deck system may be warranted.

These conclusions and recommendations are based solely on the testing of a particular FRP bridge deck system as manufactured and provided by Martin-Marieta Composites: DuraSpan 500.

APPENDIX A

MATERIAL SAFETY DATA SHEET

Material Safety Data Sheet

(Revised April 29, 1999)	
Trade Name and Synonym:	DuraSpan Fiberglass Reinforced Polymer (FRP) Bridge Deck
Chemical Name and Family:	FRP Thermoset Polyester
CAS #:	None
Formula:	Not Applicable

Section I Manufacture			
Creative Pultrusions, Inc.	<i>Phone:</i> 814-839-4186 or Toll-free: 888-274-7855 (8:00am – 4:30pm EST)		
214 Industrial Lane	<i>Fax:</i> 814-839-4276		
Alum Bank, PA 15521	<i>E-mail:</i> crpul@pultrude.com		
	<i>Web site:</i> www.creativepultrusions.com		
Section II Hazardous Ingredients/Identity Information			
Ingredients	CAS #	Percent by Weight	Exposure Limits
Fiberglass	659997-17-3	35% - 70%	OSHA PEL: 5mg/m ₃ (Respirable Nuisance Dust) ACGIH TLV 10mg/m ₃
Styrene	100-42-5	Trace Amounts	OSHA PEL: 100 ppm (8 Hour TWA)

Section III Physical/Chemical Characteristics

Boiling Point:	N/A
Vapor Pressure (mm Hg.):	N/A
Vapor Density (AIR=1):	N/A
Solubility in Water:	None
Appearance and Odor:	1Phase Solid With Various Colors & Possible Slight Odor
Specific Gravity:	1.61 – 2.0 %
Volatiles By Volume:	None (75° F)
Evaporation Rate 0 pH (Neutral = 7):	6 – 8

Section IV Fire and Explosion Hazard Data

Flash Point:	N/A
Extinguishing Media:	Water, Foam: Type A, B or C Extinguishers
Special Fire Fighting Procedures:	Use Self-contained Apparatus
Unusual Fire & Explosion Hazards:	Heavy Smoke, Products of Combustion (CO, CO ₂)

Section V Reactivity Data

Stability: Stable
Condition to Avoid: N/A
Incompatibility (Materials to Avoid): N/A
Hazardous Decomposition Products: N/A
Hazardous Polymerization: Will Not Occur

Section VI Health Hazard Data

Threshold Limit Value: N/A
Effects of Overexposure: Dust from grinding or finishing can cause mild irritation to the eyes and skin. Nuisance dust.
Emergency and First Aid: Wash skin well without rubbing. For the eyes, use a sterile
Procedures: Solution and flood the eye area. Change clothing after exposure. Apply antiseptic to abraded skin areas.

Section VII Precautions for Safe Handling and Use

Precautions to be taken
in Handling and Storage: None
Other Precautions: None

Section VII Control Measures

Respiratory Protection	Dust mask when cutting.
Ventilation (Local Exhaust)	Vented area
Ventilation (Mechanical)	Dust collector
Protective Gloves	For handling comfort.
Eye Protection	Safety glasses when machining.
Other Protective Equipment	Cream and protective clothing while machining.

While The Information And Recommendations Set Forth In This MSDS Are Believed To Be Accurate As Of The Date MSDS Preparation, Creative Pultrusions, Inc. Makes No Representation Or Warranty, Direct Or Indirect, Regarding Their Accuracy Or Completeness Nor Do We Assume Any Obligations To Advise You Of Any Modifications Or Corrections To Or Of Such Information And Recommendations Of Which We May Become Aware From The Date Hereof.

Recipients Are Advised To Confirm As They May Deem Acceptable That The Information And Recommendations Are Current And Applicable To Meet Their Requirements. Since The Conditions Are Methods Of Use Of This Product Are Beyond Our Control, Creative Putlrusions, Inc. Disclaims Any And All Liability Arising Out Of The Use Of This Product Or The Information Provided Herewith.

BIBLIOGRAPHY

- AASHTO, *AASHTO LRFD Bridge Design Specification (2nd Edition)*, The American Association of State Highway and Transportation Officials, Washington, D.C. USA, 1998
- AASHTO, *Standard Specification for Highway Bridges (16th Edition)*, The American Association of State Highway and Transportation Officials, Washington, D.C, USA, 1996
- Adams, DF. and Finley, GA, *Experimental Study of Thickness-tapered Unidirection Composite Compression Specimens*, Experimental Mechanics, SAGE Social Science Collection, Volume 36, No.4, 1995, 345-52
- Ahmad SH and Plecnik JM, *Transfer of Composite Technology to Design and Construction of Bridges*, U.S. DOT Report, September, 1989.
- Ahmadi, A. (1996). "Full scale test of half depth grid on upper buckeye bridge to determine effective flange width, live load distribution, and grid deck stresses." *Bridge Grid Flooring Manufacturers Report*, Pittsburgh.
- American Society for Testing and Material (ASTM) D3039/D3039M-00, *Standard Test Method for Tensile Properties of Polymer Matrix Composite Materials*, 2000
- American Society for Testing and Material (ASTM) D3410/D3410M-95, *Standard Test Method for Compressive Properties of Polymer Matrix Composite Materials with Unsupported Gage Section by Shear Loading*, 1995
- American Society for Testing and Material (ASTM) D695-96, *Standard Test Method for Compressive Properties of Rigid Plastic*, 1996
- Aref AJ and Parsons ID, *Design and analysis procedures for a novel fiber reinforced plastic bridge deck*, Advanced Composite Materials in Bridges and Structures, CSCE, Montreal, Quebec, Canada, 1996.
- Bridge Diagnostics, Inc., *Load Test and Rating Report CR46 Bridge over E. Branch Salmon River Lewis County, New York, Boulder, Colorado 80303*, January 2004
- Cassenti BN. *Probability static failure of composite material*. AIAA Journal 1984;22:103-110
- Chaklos, J.M., Yulismana, W., Earls, C.J. (2004) *Concrete - Steel Interfacial Bond Strength in Composite Flooring: Shoring and Form Removal*, Practice Periodical on Structural

- Design and Construction, American Society of Civil Engineers, Vol. 9 No. 1, Reston, Virginia, pp. 9-15.
- Civil Engineering Research Foundation, “*High Performance Construction Materials and Systems: An Essential Program for America and Its Infrastructure*”, Executive Report 93-5011, 1993.
- Dally, JW. and Riley, WF. *Experimental Stress Analysis, 2nd Ed.*, McGraw-Hill Book Co., New York, NY, 1978
- Davalos JF, Salim HA, Qiao P, Lopez-Anido R, Barbero EJ. *Analysis and design of pultruded FRP shapes under bending*. Compos Part B: Engng J 1996;27:295-305
- Dunker KF and Rabbat BG, “*Why America’s Bridges are Crumbling*”, Scientific America, March 1993.
- Federal Highway Administration, *Deficient Bridges by State and Highway System*, US Department of Transportation, December 2004
- GangaRao HVS, Thippeswamy HK, Shekar V, and Craigo C, *Development of Glass Fiber Reinforced Polymer Composite Bridge Deck*, SAMPE Journal, 35 (4), 1999.
- Henry JA, *Deck Girders System for Highway Bridges Using Fiber Reinforced Plastics*, MS Thesis, North Carolina State University, 1985.
- Jeong HK, Sheno RA. *Reliability analysis of mid plane symmetric laminated plates using direct simulation method*. Composite Structures 1998;43:1-13
- Keelor, D.C., Luo V., , Earls, C.J., Yulismana, W. (2004) *Service Load Effective Compression Flange Width in FRP Deck Systems Acting Compositely with Steel Stringers*, Journal of Composites for Construction, American Society of Civil Engineers, Vol. 8 No. 4, Reston, Virginia, pp. 289-297.
- Kumar, P., Nanni, A, Chandrashekhara, K., “*Testing and evaluation of component for a composite bridge deck*”, Journal of Reinforced Plastics and Composites, v. 22, n. 5, 2003
- Lopez-Anido, R., Davalos, JF., Barbero, EJ., “*Experimental evaluation of stiffness of laminated composite beam elements under flexure.*”, Journal of Reinforced Plastics and Composites, v. 14, n. 4, April 1995
- Luo, Y., Keelor, C., Yulismana, W., Earls, C.J. (2002) “*Field Monitoring of the Boyer Bridge Fiber Reinforced Polymer Deck Installation,*” Proceedings of the International Bridge Conference, Pittsburgh, Pennsylvania, paper IBC-02-52, CD-ROM.
- Martin Marieta Composites, “*DuraSpan Fiber Reinforced Polymer (FRP) Bridge Deck*”, 2001

- Moon, FL., Eckel, DA., Gillespie, JW. "Shear Stud Connection for the Development of Composite Action between Steel Girders and Fiber Reinforced Polymer Bridge Decks", *Journal of Structural Engineering*, Vol. 128, No. 6, June, 2002
- Moses F, *Class Note CEE 3350*, University of Pittsburgh, 2001
- Nowak AS, Collins KR. *Reliability of Structures*, 2000
- Reddy JN, Pandey AK. *A first ply failure analysis of composite laminates. Computers and Structures* 1987;25:371-93
- Reifsnider KL, Case SW, *Damage Tolerance and Durability of Material Systems*, Wiley Interscience, New York, NY, 2002
- Salim, Hani A., Davalos, Julio F., Qiao, Pizhong and Kiger, Sam., *Analysis and Design of Fiber Reinforced Plastic Composite Deck and Stringer Bridges*, Composite Structures, Vol. 38, 1997
- Scop PM, Argon AS. *Statistical theory of strength of laminated composites. Journal of Composite Materials* 1967;1:92-9
- Temeles AB, *Field and Laboratory Tests of a Proposed Bridge Deck Panel Fabricated from Pultruded Fiber Reinforced Polymer Component*, Virginia Polytechnic Institute and State University, Blackburg, VA.
- Tsai SW. *A survey of macroscopic failure criteria for composite materials*. Technical Report, AFWAL-TR-84-4025
- Turner, K., and Harries, K. A. (2002). "Tests of shear stud connections between GFRP bridge decks and steel girders." draft final report, *Rep. No. ST02-03-LD*, Dept. of Civil and Environmental Engineering, Univ. of South Carolina, Columbia, S.C.
- Tuttle, ME., *Fundamental Strain Gage Technology*, Society for Experimental Mechanics, Lilburn, GA, 1998
- Vishay Measurements Group, *Manual for Strain Gage Technology*, Bulletin 309D, Raleigh, North Carolina, 1992
- Whitney JM, Leissa AW. *Analysis of heterogeneous anisotropic plates. Journal of Applied Mechanics* 1969;28:261-66
- Wood, D., Wipf, T., and Klaiber, FW., "Connection Tests of FRP Deck Specimens for Composite Construction.", Report of the Iowa State University, Civil and Construction Engineering, Structural Engineering Laboratory, 2001
- Zureick AH, Shih B, Munley E, *Fiber Reinforced Polymetric Bridge Deck*, *Struct. Eng. Rev.*, 1995;7(3):257-66